14 November 2017

Dear Dr. Tedesco,

Enclosed is the revised discussion paper tc-2017-160, formerly titled *"Characterization of Canadian High Arctic glacier surface albedo from MODIS data, 2001-2016",* now titled *"Spatiotemporal variability of Canadian High Arctic glacier surface albedo from MODIS data, 2001-16",* for consideration for publication in *The Cryosphere*.

We use MODIS surface reflectance and albedo C6 data to present the first complete picture of mean summer surface albedo variations over all glaciated surfaces in the Queen Elizabeth Islands, Canada, during the period 2001-16. Black-sky shortwave broadband albedo (BSA) decreases were largest in July. The 16-year history of mean summer BSA changes is strongly tied to variations in the summer NAO index, except in the years 2006, 2010, and 2016 when changes in the mean summer BSA appear to be dominated by the effect of changes in the mean August (rather than July) BSA.

We confirm that this work is original and has not been published elsewhere nor is it currently under consideration for publication elsewhere. All authors have approved the manuscript and agree to submission to *The Cryosphere*. The authors have no conflicts to declare.

We thank the two anonymous reviewers for their comments. We have carefully considered the comments and suggestions from both reviewers, and have made every attempt to address all comments and concerns following closure of the public discussion on 19 October 2017.

The manuscript has been condensed and re-organized for clarity and flow. Sections 3.3 (now section 3.4) and 4.1 (now section 4) have been shortened and repetition between these sections has been removed. Sections 4.1 and 4.2 have been merged (now section 4). Other notable revisions include the use of MODIS MOD11A2 C6 data instead of the MOD11A2 C5 data for our LST analysis in response to comments from Reviewer #2. All tables and figures pertaining to LST, including re-calculation of correlations between LST and BSA, have been revised to reflect this change. The MOD11A2 C6 product has a larger amount of missing data than the C5 product. This resulted in a larger number of no-data pixels in our BSA/LST correlations (new: 46% versus old 80%) which limited our ability to confidently interpret some of the spatial patterns that were discussed in our initial submission.

Reviewer #2 inquired about our use of the combined albedo data product (MCD43A3) in light of the Terra sensor degradation issues and calibration uncertainty. We selected the combined product to ensure optimal spatial coverage of the QEI glacier cover. However, we do acknowledge that these data are affected by sensor degradation effects and we have provided a more detailed account of MODIS sensor degradation issues that affect the albedo product used in our study.

In addition to a revised manuscript (MortimerSharp_tc2017_160_revised.docx), a detailed list of all revisions has been provided (MortimerSharp_tc2017_160_reviwer_comments.pdf). A PDF of the MS word markup with corresponding reviewer comments has also been provided (MortimerSharp_tc2017_160_revised_markup.pdf). Correspondence concerning this manuscript should be directed to Colleen Mortimer at cmortime@ualberta.ca.

Sincerely,
Colleen Mortimer

Author contact information
Colleen Mortimer[1] [cmortime@ualberta.ca]
Martin Sharp[1] [msharp@ualberta.ca]

1: Department of Earth and Atmospheric Sciences
1-26 Earth Science Building,
University of Alberta
Edmonton, Alberta,
Canada, T6G 2E3

tc-2017-160: formerly titled "Characterization of Canadian High Arctic glacier surface albedo from MODIS data, 2001-2016"

Author's response to reviewers

Reviewer 1 (Anonymous Referee #1): Received and published 13 September 2017.

Reviewer 1's general comments:

In this paper, the albedo and surface temperature of the glaciers in the Queen Elizabeth Islands (QEI) are investigated using MODIS data products for 2001 – 2016. Over the study period BSA is shown to decrease significantly in the month of July, while LST increases during the summer months (JJA). This is a valuable paper and it is well written (though a bit long) and technically sound. My comments below are almost all optional.

I believe that the authors have not fully taken advantage of this opportunity to explore the relationship between albedo and LST. Though they point out that albedo and LST are negatively correlated for the QEI, they do not discuss that relationship as cause-and-effect in either the Abstract or the Conclusion. The relationship between albedo and LST is discussed in Section 4.2 but I would have liked that discussion to have been better integrated throughout the paper. Since there was quite a bit of information about LST in the paper, the authors might want to consider including LST in the title of the manuscript.

The authors say that only the month of July shows statistically-significant albedo decrease over the study period. Thus, they should consider stating that the July albedo is decreasing over the study period instead of saying mean summer (JJA) albedo is decreasing.

If the paper can be made more concise it would be easier to follow.

Author's response to R1 general comment:

We thank the reviewer for the thoughtful evaluation of our manuscript. We have reviewed and addressed both the major considerations and minor specific comments.

1. **RC** refers to reviewer's comment
2. **AR** refers to author's response
3. Revised sections of the manuscript are presented in *italics*.

RC: If the paper can be made more concise it would be easier to follow.

AR: The paper has been revised to make it more concise and easier to follow. Sections 3.3 (now section 3.4) and 4.1 (now section 4) have been shortened. Repetition in sections 3.3 and 4.1 has been removed. Sections 4.1 and 4.2 have been merged (now section 4).

Revised text:

Revised Section 3.4, Lines 365-392:

'3.4 Principal Components Analysis

To explore whether there are any other spatial patterns in the 16-year mean summer BSA record that differ from the long-term (linear) trend, we performed a Principal Components Analysis of the BSA record (Sect. 2.3). The first and second Principal Components (Fig. 8) explain 65% and 12% of the variance in the mean summer BSA record, respectively. The spatial pattern of the First Principal Component (PC1) scores (Fig. 8a) is generally consistent with the spatial patterns of summer (JJA, Fig 5a) and July (Fig. 5c) mean BSA change described previously (Sect. 3.3). PC1 scores are strongly negative (< -0.005) on western Axel Heiberg Island

2

(large BSA declines), and weakly negative (> -0.001) or even positive at high elevations in the interiors of the ice masses where there was no change in the mean summer BSA. Moderately negative (~ -0.002) component scores occur on the western (continental) side of eastern Ellesmere Island's ice masses as well as over much of Manson Icefield and the southeast portion of Prince of Wales Icefield, where large decreases were observed in both the summer (JJA) and the July BSA.

For PC1, the highest Empirical Orthogonal Functions (EOFs) (32.8 and 25.9) correspond to the years with the lowest mean summer BSA (2011 and 2012) (Fig. 9). The lowest EOFs (-31.7 and -24.6) correspond to the years with the highest mean summer BSA (2013 and 2004) (Fig. 9). In addition, the departure from zero is much larger for the minimum component scores than for the maximum component scores (Fig. 8a), suggesting that both positive and negative BSA anomalies are likely caused by forcings with the same spatial pattern, albeit with the opposite sign. Investigating possible relationships between surface albedo and known large-scale patterns of atmospheric variability (Arctic Oscillation, Pacific North American Pattern, North Atlantic Oscillation), we found the EOFs for PC1 to be well (negatively) correlated with the mean summer North Atlantic Oscillation (NAO) index (r = -0.84, p < 0.001, Fig. 9), derived by averaging the June–August monthly mean NAO indices for 2001 to 2016 (http:www.cpc.ncep.noaa.gov). This is consistent with the finding of Mortimer et al. (2016) that there was a good agreement between the mean summer LST record and the NAO index in the QEI over the 2000–15 period.

The second Principal Component (PC2) had the largest EOFs of any component in 2006, 2010, and 2016. In these years, there was poor correspondence between the PC1 EOFs and the JJA NAO index (Fig. 9). The spatial pattern of the PC2 scores (Fig. 8b) resembles that of the August BSA change (Fig. 5d). Large negative PC2 scores (< -0.004) were observed on eastern Devon Ice Cap and Manson Icefield, where large August BSA declines (< -0.0075 yr^{-1}) occurred. Positive PC2 scores (Fig. 8b) were observed in southwest Axel Heiberg Island and at lower elevations on northern Ellesmere Island's southwestern ice caps, where the mean August BSA increased (Fig. 5d). Unlike PC1, there were no significant correlations between the EOFs of PC2 and known large-scale patterns of atmospheric variability.'

Revised Section 4, Lines 411-462:

'4 Discussion

Between 2001 and 2016 the bulk of the measured mean summer BSA declines in the QEI occurred in July (Sect. 3.2). This finding is consistent with previous work (e.g. Alt, 1987; Gardner and Sharp, 2007) that found variability in July near-surface air temperatures to be the primary influence on inter-annual variability in annual QEI mass balance. Variability in July air temperatures has, in turn, been associated with variations in the strength, position, and geometry of the July circumpolar vortex (Gardner and Sharp, 2007). Extreme high melt years in the QEI are associated with the intrusion of a steep ridge at all levels in the troposphere and the absence of the North American trough, making the QEI thermally homogeneous with continental North America (Alt, 1987). Between 2001 and 2016, in years with low (e.g. 2007–12) or high (e.g. 2001–04) albedos, there was a persistent ridge (trough) in the 500 hPa geopotential height surface centered over the north and west of the QEI (Fig. 4; Sect. 3.1.1). This configuration appears to be tied to the increased warming and albedo declines observed in the central western part of the QEI from 2007 to 2012. For example, strong warming (Fig. 7b) and albedo declines (Fig. 5a) over Axel Heiberg Island and north-central Ellesmere Island coincided with a ridge of high pressure centered over the north and west of the QEI (Fig. 4) that was often observed in years when the NAO index was negative (Fig. 9).

Differences in the spatial patterns of the monthly BSA change (Fig. 5b–d) reflect the dominant atmospheric circulation patterns that occur over the QEI during the summer months. In the QEI, anticyclonic circulation tends to dominate in the months of June and July, while cyclonic circulation often occurs in August (Alt, 1987; Gascon et al., 2013). In June and July, the largest BSA declines occurred in the climatically continental interiors of the ice masses on Ellesmere and Devon Islands, as well as on Axel Heiberg Island (Fig. 5). In these months, the mountains on eastern Ellesmere and Devon Islands act as a barrier to moisture transport from the east limiting (solid) precipitation (which can temporarily raise the surface albedo) on the western (lee) side of the eastern ice masses (Koerner 1979). Adiabatic heating of descending air masses on the western (lee) side of the eastern ice masses results in warm dry air which promotes warming, melting, and enhanced

albedo declines. In contrast, in August, when cyclonic circulation is common (Sect. 3.2.1), BSA declines were largest at low elevations in the maritime regions of eastern Devon Ice Cap, Manson Icefield, and the southwestern Prince of Wales Icefield (Fig. 5d). Low pressure systems which track from the southwest to the north and northeast are common in August, and they advect warm moist air into the Arctic from the south (Alt, 1987; Gascon et al., 2013). In the eastern QEI, orographic uplift of air masses tracking from the southwest, and subsequent adiabatic heating of these air masses when they descend on the eastern sides of ice masses, would bring warm dry air to the eastern (lee) side of the mountains in the eastern QEI, promoting both warming and albedo decline in these regions in August.

During the 2001–16 period, the mean summer QEI-wide BSA record was strongly tied to the summer NAO index (Sect. 2.4). -Anticyclonic circulation was shown to co-vary with the NAO index over the Greenland Ice Sheet, immediately to the east of the QEI, since ~2001 (Rajewicz and Marshall, 2014). On the Greenland Ice Sheet, clear sky conditions and the advection of warm air form the south that accompany anticyclonic ridging (Rajewicz and Marshall, 2014), similar to that observed in the QEI in June and July (Alt, 1987; Gascon et al., 2013; Bezeau et al., 2015), were found to enhance the strength of the ice-albedo feedback between 2009 and 2011 which resulted in higher rates of melt and glacier mass loss (Box et al., 2012). Although a similar phenomenon is likely to have occurred in the QEI, we find that in some years (2006, 2010, 2016) there was poor correspondence between the mean summer BSA record and the NAO index (Fig. 9), suggesting that an additional forcing may be influencing the spatial and temporal variability of glacier surface albedo in the QEI.

The spatial pattern of both the QEI snow accumulation (Fig. 2 and 3 in Koerner 1979) and $\partial^{18}O$ values (Fig. 7 in Koerner 1979) were inferred by Koerner (1979) for the 1962-73 period from surface snow samples and shallow firn cores collected in spring 1974. These spatial patterns (of snow accumulation and $\partial^{18}O$) closely resemble the spatial pattern of PC2 scores (Fig. 8). Specifically, areas having large negative PC2 scores (< -0.002; Fig. 8b) of the 16-year mean summer BSA record (Sect. 3.4) were characterized by relatively high accumulation rates (Fig. 2 and 3 in Koerner (1979)) and snow that is isotopically warm (Fig. 7 in Koerner (1979)), while areas with positive PC2 scores had lower snow accumulation rates. This similarity points to a possible role of precipitation in affecting the mean summer BSA in some years. To investigate the relationship between the albedo record and variability in precipitation we examined the cumulative mass change record for the QEI from the Gravity Recovery and Climate Experiment (GRACE; Wolken et al. (2016), extended to 2016 (B. Wouters, personal communication, 2017)). The record shows that in 2006, 2010, and 2016 (the years when PC2 of the 16-year mean summer BSA record had the largest EOFs of any Principal Component, Sect. 3.4), once the annual minimum glacier mass was reached, there was a prolonged period of constant low mass (i.e. no melt or snowfall) before fall/winter accumulation began (inferred from an increase in mass). In other years, there was a sharp transition from the local end-of-summer mass minimum to the period of seasonally increasing mass. This could indicate that in some years during the 2001–16 period, variability in August snowfall may have influenced the mean summer BSA.'

RC: Though they point out that albedo and LST are negatively correlated for the QEI, they do not discuss that relationship as cause-and-effect in either the Abstract or the Conclusion. The relationship between albedo and LST is discussed in Section 4.2 but I would have liked that discussion to have been better integrated throughout the paper.

AR: Following a comment from an anonymous reviewer the LST analysis was revised to use MODIS C6 data instead of MODIS C5 data. The MOD11A2 C6 product has a larger amount of missing data than the C5 product. This resulted in a larger number of no-data pixels in our BSA/LST correlations (new: 46% versus old 80%) which limited our ability to confidently interpret some of the spatial patterns that were discussed in our initial submission. As such, the discussion of the relationship between albedo and temperature has been reduced compared to the original manuscript and the discussion of cause-and-effect is also reduced. However, we have tried to better integrate discussion of LST and albedo earlier in the manuscript.

Additional linkages between albedo and LST have been added earlier in the manuscript. For example, Section 3.2 has now been divided into two separate sub-sections and linkages between albedo, LST, and

glacier mass change (highlighted text) have been added to Section 3.2.1. Discussion of the links between albedo and temperature have also been added to the methods section (Sect. 2.2) where we describe the MODIS LST data and the reason for its inclusion in the manuscript, and in the results Section 3.5 (comparison of albedo and LST patterns and trends). For brevity, only a short mention of the effect that the negative ice-albedo feedback could have on the QEI ice mass is included in the Abstract. Due to the change in data set used (MOD11A2 C6) and the resulting increase in the number of cells without data, the discussion of cause and effect is reduced. Additional text regarding the relationship between temperature and albedo has been included in the conclusion.

Revised text

Section 2.2 MODIS LST (MOD11A2) added text (lines 161-168):

'Warmer surface temperatures increase the rates of grain metamorphism and snowmelt, resulting in larger snow grains which have a lower albedo than those of fresh snow (Wiscombe and Warren 1980; Colbeck 1982) (Sect. 1). Air and surface temperatures also affect the timing of removal of the seasonal snowpack, which exposes lower albedo firn or glacier ice. Additionally, the melt of glacier ice releases impurities that have a low albedo and thus change the surface albedo of both ice and snow (e.g. Clarke and Noone 1985; Doherty et al., 2010; Sect. 1). As such, analysis of the glacier surface temperature and comparison of these data with the albedo record is included to help understand the observed spatiotemporal patterns of glacier albedo change in the QEI.'

Section 3.2.1 (lines 244-256), highlighted text moved from later in the manuscript and text edited for clarity:

'Section 3.2.1 Mean summer (JJA) BSA anomalies

The mean summer BSA anomalies, relative to the 2001–16 mean, are presented in Figure 3 and Table 1. For consistency with the regression analysis (Sect. 3.3), BSA anomalies were only computed for pixels having mean summer BSA observations in 11 or more of the 16 years (Sect. 2.3). The period 2001–16 is characterised by a six-year period of positive BSA anomalies (2001–06) followed by a six-year period of negative BSA anomalies (2007–12) (Table 1). Positive BSA anomalies were also observed in 2013 (+0.060) and 2014 (+0.015), while 2015 (-0.022) and 2016 (-0.005) saw a return to negative anomalies (Table 1). Negative BSA anomalies during the period 2007–12, which indicate a larger absorbed fraction of incoming shortwave radiation relative to the 16-year mean, coincide, and are consistent with, positive summer air and glacier surface temperature anomalies from 2007 to 2012 (Mortimer et al., 2016). Higher temperatures increase the rate of snow grain metamorphism which lowers the surface albedo (Wiscombe and Warren, 1980; Colbeck, 1982; Warren 1982), and a lower albedo increases the proportion of solar radiation absorbed at the ice-air interface, providing more energy for surface warming and melt. This positive feedback mechanism may have contributed to the tripling of glacier mass loss from this region between 2004–06 and 2007–09 (Gardner et al., 2011).'

Section 3.5 Comparison with the mean summer LST, added text (lines 395-397):

'Owing to the positive feedback between albedo and surface temperature we would expect to observe strong increases in surface temperature where albedo declines were large. To investigate the relationship between temperature and albedo over the QEI, the 16-year mean summer LST record was compared with the 16-year mean summer BSA record (Sect. 2.3).'

Conclusion, added text (lines 476-485):

'Albedo declines increase the proportion of incoming solar radiation absorbed at the air-ice interface, and thus the energy available to drive melt, warming, and further surface albedo decline. Warmer temperatures, in turn, increase the rate of snow grain metamorphism which lowers the albedo. Air and surface temperatures affect the removal (timing and extent) of the seasonal snowpack which exposes lower albedo firn and/or glacier ice, while melting glacier ice releases impurities that further reduce its albedo. Given that surface temperature and albedo are inextricably linked, knowing where and when albedo changes are likely to occur in future is important for predicting future rates of mass loss from the QEI ice caps. Recent investigations of atmospheric circulation patterns over the QEI (e.g. Gardner and Sharp, 2007) focused on characterization of July temperature and atmospheric conditions, since July is usually the month when melt rates peak. Our results suggest, however, that changes occurring during the month of August are also important, especially as the length of the melt season continues to increase.'

RC: The authors say that only the month of July shows statistically-significant albedo decrease over the study period. Thus, they should consider stating that the July albedo is decreasing over the study period instead of saying mean summer (JJA) albedo is decreasing.

AR: There appears to have been some misinterpretation of our results. No measurable changes in the June or August QEI-wide (regionally-averaged) BSA were observed owing to the large amount of spatial variability in the sign and magnitude of BSA change in these months. Measurable changes were observed in the mean summer (JJA) and mean July QEI-wide BSA. These changes, however, were not statistically significant at the $p < 0.05$ level. Although there were statistically significant (at the $p < 0.05$ confidence level) decreases in the mean summer (JJA) and/or July BSA at the pixel scale, this was not the case for either the mean summer (JJA) or July QEI-wide (spatially averaged) BSA change. As such, our conclusions and abstract remain unchanged. Text in the results section 3.3.1 (lines 306-308) has been revised for clarity.

Revised text:
> **Results section 3.3.1 lines 318-320**: *'Although the measured change in the QEI-wide mean summer BSA (average correlation coefficient of all pixels) was not statistically significant ($r = 0.31$, $p = 0.24$), BSA declines that were significant at the $p \leq 0.05$ level were observed at the pixel scale on all ice masses (Fig. 6a).'*

Reviewer 1 specific comments:

RC 1 Title: consider removing "C6" from the title since it's not that different from C5 for the albedo and LST, and many people, before reading the paper, have no idea what C6 is. You have appropriately mentioned the fact that you've used C6 in the paper as needed. Also consider including LST in the title, especially if you decide to enhance the discussion about cause-and-effect between LST and albedo for the QEI.

AR 1: Reference to "C6" removed from the title. The title has also been modified to better reflect the content of the paper. Instead of 'Characterization of' we use 'Spatiotemporal variability of' to indicate that the paper investigates both the spatial and temporal patterns of glacier surface albedo in the Canadian High Arctic.

Revised title:
> *'Spatiotemporal variability of Canadian High Arctic glacier surface albedo from MODIS data, 2001-16'*

RC 2: Figure 1 caption: do you mean "Top-left inset" and "Bottom-right inset"?

AR 2: Bottom-left inset in Figure 1 removed and caption corrected.

Revised Figure 1 caption:

'*Figure 1: Glaciated regions of the Queen Elizabeth Islands. Background image: MODIS, 4 July 2011. Inset: red polygon shows location of Queen Elizabeth Islands, Arctic Canada.*'

RC 3: Figures 2,3,5,6,7&9: it should be mentioned in the caption that white (Figs 2 & 3) is not ice and brown is not ice (Figs 5,6,7, & 9).

AR 3: Mention of white areas (Fig. 2 & 3) and brown (Fig. 5, 6, 7, 9 (now Figure 8)) areas that are not ice has been added to the figure captions.

Revised Figure captions:

'*Figure 2: Mean summer clear-sky shortwave broadband black-sky albedo over the QEI ice caps. White areas outside of the ice caps indicate non-glaciated ice cover.*

Figure 3: Mean summer clear-sky shortwave broadband albedo anomaly over the QEI ice caps relative to the 2001-16 mean. White areas outside of the ice caps indicate non-glaciated ice cover.

Figure 5: Linear rate of change (yr^{-1}) in (a) mean summer (JJA), (b) June, (c) July, and (b) August, clear-sky shortwave broadband black-sky albedo for 2001-16 over the QEI ice caps. Background image: MODIS, 4 July 2011. Brown indicates non-glaciated land cover.

Figure 6: p-value of the linear regression (Fig. 4) of (a) mean summer (JJA), (b) June, (c) July, and (d) August, clear-sky shortwave broadband black-sky albedo for the period 2001-16 over the QEI ice caps. Background image: MODIS, 4 July 2011. Brown indicates non-glaciated land cover.

Figure 7: Component scores for the first two Principal Components of the mean summer clear-sky BSA (Fig. 2) over the QEI ice caps. Background image: MODIS, 4 July 2011. Brown indicates non-glaciated land cover.

Figure 8: (a) Pearson Correlation Coefficient (r) and (b) p-value for linear regression of the 16 year BSA and LST record over the QEI ice caps. Background image: MODIS, 4 July 2011. Brown indicates non-glaciated land cover.'

RC 4: Figure 8 – lower panel: I am confused about the point that you are trying to get across in this graph; please clarify.

AR 4: The lower panel of Figure 8 (which is now Figure 9) illustrates the correspondence between the Empirical Orthogonal Functions for the first and second Principal Components of the 16 year mean summer BSA record, respectively, and the mean summer NAO index. The graph presents the EOFs of PC1 and PC2 of both the mean summer (JJA) BSA record and the mean summer (JJA) NAO index for each year during the period 2001-16.

The original legend on the lower panel of Figure 8 (now Figure 9) did not include the NAO index. This may have been a source of confusion. The legend has been modified to include the NAO index (black line) and a reference to Section 3.4 where this graph is discussed, has been added.

Modified Figure 9 with figure caption:

7
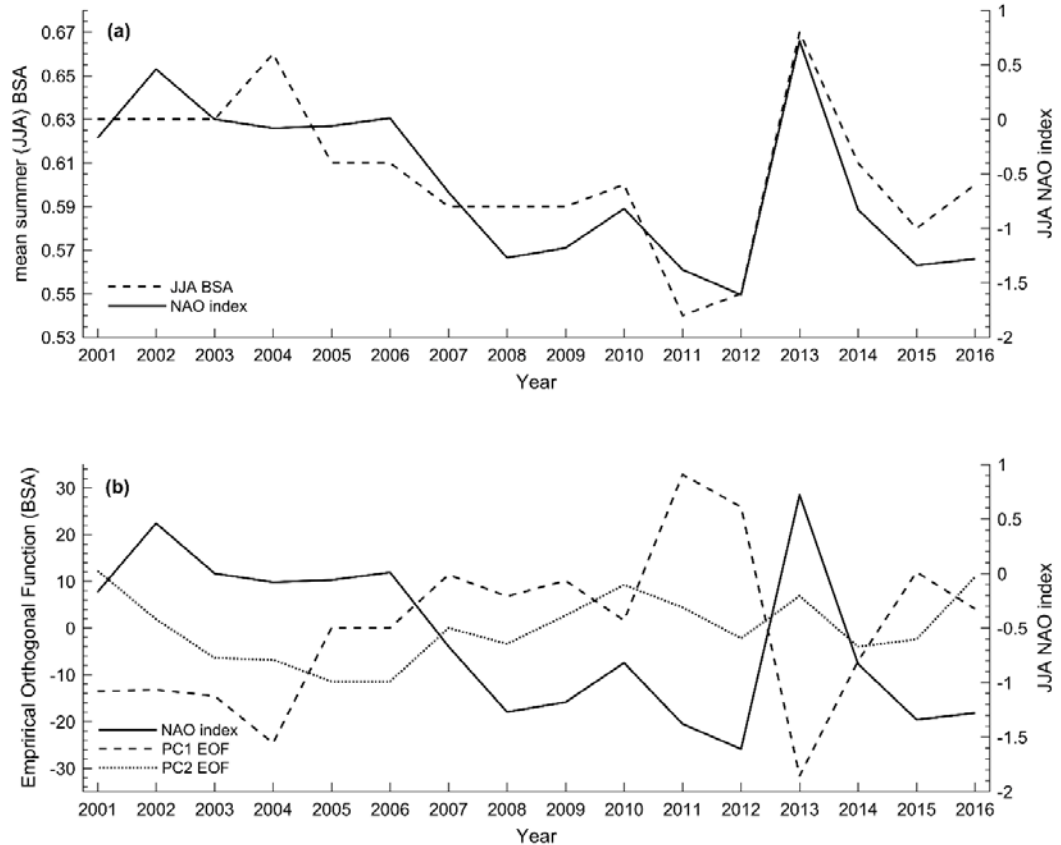
'Figure 9: (a) mean summer (JJA) clear-sky shortwave broadband black-sky albedo (left-hand axis) and the mean summer (JJA) NAO index (right-hand axis) for 2001-16. (b) Empirical Orthogonal Functions (EOF) for the First and Second Principal Components of the 16 year mean summer BSA record (left-hand axis), and the mean summer (JJA) NAO index (right-hand axis) for 2011-2016 (Sect. 3.4). '

RC 5: Line 14: note that the range of years says 2008-2012 on line 486

AR 5: Corrected to read 2007-12 throughout.

Revised text:

> **Line 12-14:** *'Most of the decrease in BSA, which was greatest at lower elevations around the margins of the ice masses, occurred between 2007 and 2012 when mean summer BSA was anomalously low.'*

> **Line247-248:** *'The period 2001–16 is characterised by a six-year period of positive BSA anomalies (2001–06) followed by a six-year period of negative BSA anomalies (2007–12) (Table 1).'*

> **Line 250-252:** *'Negative BSA anomalies during the period 2007–12, which indicate a larger absorbed fraction of incoming shortwave radiation relative to the 16-year mean, coincide, and are consistent with, positive summer air and glacier surface temperature anomalies from 2007 to 2012 (Mortimer et al., 2016).'*

> **Line 278-279:** *'… in years when the mean summer QEI-wide BSA anomaly was strongly negative (e.g. 2001–04) (or positive (e.g. 2007–12))'*

Line 418-420: *'Between 2001 and 2016, in years with low (e.g. 2007–12) or high (e.g. 2001–04)) albedos, there was a persistent ridge (trough) in the 500 hPa geopotential height surface centered over the north and west of the QEI (Fig. 4; Sect. 3.1.1).'*

Line 466-467: *'Strong negative BSA anomalies from 2007–12 suggest that the bulk of the observed albedo decline occurred during this six-year period.'*

RC 6 Line 60: MODIS has already been defined on lines 53 & 54

AR 6: Corrected.

Revised line 60 (now line 61):
'Observations from the MODIS sensors, aboard the Terra (2000 to present) and Aqua (2002 to present) satellites,…'

RC 7 Line 76 & 78: Lutch should be spelled Lucht

AR 7: Misspelled reference corrected in **lines 76 & 78 (now lines 77 & 79)**

Revised text:
Line 77: *'…kernel-driven BRDF model (Wanner et al., 1997; Lucht et al., 2000; Schaaf et al., 2002, 201b).'*
Line 79: '*…is used to estimate the surface albedo (Strugnell and Lucht, 2001; Schaaf et al., 2002; Jin et al., 2003; Liu et al., 2009).'*

RC 8 Line 99: perhaps the word "detectors" should be used instead of "instruments"?

AR 8: The word "instruments" replaced by "detectors".

Revised **Line 99 (now line 91-92:**
'*The MODIS sensors are currently operating well beyond their expected [productive] six year lifetimes (Barnes et al, 1998; Justice 1998) and the detectors are degrading (Xiong et al., 2001).'*

RC 9 Line 120-124: this discussion of MOD10A1 should be deleted; it is not relevant to this paper, and MOD10A1 is never mentioned again in the paper; it really isn't good validation for MCD43A3.

AR 9: Discussion of MOD10A1 has been deleted. Additionally, in response to an anonymous reviewer's comments, this section has been revised to be more informative regarding MODIS sensor design and capabilities.

Revised text, lines 90-138:

'2.1.1 MODIS sensor degradation

The MODIS sensors are currently operating well beyond their expected [productive] six year lifetimes (Barnes et al, 1998; Justice 1998) and the detectors are degrading (Xiong et al., 2001). For both the MODIS Terra and Aqua sensors, instruments were calibrated pre-launch (radiometric, spatial, specular calibration) (Gunther et al., 1996). On-orbit calibration procedures were included to monitor the sensor degradation that is expected as the instruments are exposed to solar radiation (Gunther et al., 1996). For the reflective solar bands (0.41–2.2 µm) the on-board calibration system includes a solar diffuser (SD) calibrated using the solar diffuser stability monitor (SDSM) (Gunther et al., 1998). Lunar and Earth view observations (for select desert sites) are also used to assess radiometric stability (Sun et al., 2003). Even so, long-term scan mirror and wavelength dependent degradation, which are not sufficiently accounted for by the on-board calibrators (SD/SDMS), have been observed (Xiong et al., 2001; Lyapustin et al., 2014 and references therein). Calibration degradation effects, which are largely confined to the MODIS Terra sensor, are greatest in the

blue band (B3) and decrease with increasing wavelength (Xiong and Barnes, 2006). An anomaly in the SD door operation (3 May 2003) and a decision to leave the door permanently open, exposing the SD to additional solar radiation, resulted in degradation of the SD on the MODIS Terra sensor that was faster than had originally been anticipated, and than was observed for the MODIS Aqua sensor (Xiong et al., 2005). Differences in the response versus scan angle (RVS) for the two side mirrors were also characterized pre-launch (Barnes et al., 1998). The RVS is important because it describes the scan mirror's response to different angles of incidence (AOI, for each band, detector and mirror side) (Sun et al., 2014). However, for the MODIS Terra sensor, following an overheating incident during pre-launch calibration, the RVS was not re-characterized and the exact pre-launch RVS characteristics are not known (Pan et al., 2007; Sun et al., 2014 and references therein). These issues have resulted in the performance of the MODIS Terra sensor being poorer than that of the MODIS Aqua sensor.

As a normal part of the operational procedure, the MODIS Characterization Support Team (http:mcst.gsfc.nasa.gov) periodically updates the calibration algorithms and approaches, during which time the entire L1B record (calibrated top of the atmosphere radiances) is re-processed to reflect improved understanding and characterization of changes to the instruments. Even so, non-physical trends in MODIS Terra data products, that result from calibration drift, have been observed and are well documented (e.g. Xiong et al., 2001; Xiong and Barnes, 2006; Franz et al., 2008; Kwiatkowski et al., 2008; Wang et al., 2012; Lyapustin et al., 2014; and references therein). The latest revision occurred with the C6 data and includes on-orbit calibration procedures to mitigate long-term calibration drift, particularly at the shorter wavelengths (Wenny et al., 2010; Toller et al., 2013; Sun et al., 2014; Lyapustin et al., 2014). The C6 dataset uses the on-board calibrators (e.g. SD/SDMS) and the mirror side ratios from lunar standard and Earth view observations (Toller et al, 2013; Sun et al., 2014). The C6 revision also includes an additional approach, aimed primarily at the short-wavelength bands, that uses observations of desert sites (pseudo-invariant targets) to derive instrument calibration coefficients and RVS at multiple AOIs (instead of the two AOIs provided by the SD and lunar standard) (Toller et al, 2013; Sun et al., 2014). Although this vicarious approach is less accurate than the one that uses the mirror-side ratios calibrated using a lunar standard, it has been found to provide a significant improvement to the L1B radiance measurements relative to the C5 data, prior to ~2013 (Toller 2013; Lyapustin et al., 2014). Updated L1B C6 radiances can be up to several percent higher than the C5 values (e.g. Band 3 and for most recent period ~2013 onward) (Toller et al., 2013; Lyapustin et al. 2014; Casey et al., 2017). However, evaluation of the L1B C6 Band 3 (0.46–0.48 μm) radiance over a desert site (Libya 4) identified residual errors (decadal trends on the order of several tenths of 1%; Lyapustin et al., 2014) that are within the product's stated accuracy (2% in absolute reflectance units for the reflective solar bands (Barnes et al., 1998; Justice et al., 1998)). The impact of the C6 updates on higher level MODIS science products is difficult to quantify because the corrections are time, mirror-side, angular, and detector dependent (Toller et al., 2013; Lyapustin et al. 2014; Sun et al., 2014). In addition, the C6 revision includes updates to algorithms (in addition to the calibration updates) used in the derivation of specific higher-level products (https://www.umb.edu/spectralmass/terra_aqua_modis/v006 outlines changes made to the MCD43A3 C6 data product). Important for the current study, however, is that recent analysis of surface albedo over the Greenland Ice Sheet, immediately to the east of the QEI, using MODIS C6 data (including the MCD43A3 product used in this study) identified statistically significant albedo declines over the wet snow zone (Casey et al., 2017). For the most part, these declines are thought to be physically real (Casey et al., 2017), which gives us confidence in the albedo trends presented here. There are no long-term, spatially distributed, in situ albedo records from the glaciers and ice caps in the QEI, so a comparison between the MCD43A3 records and ground observations is not possible. This is both a motivation for and a limitation of, the current study.

References added:

Barnes, W. L., Pagano, T.S., and Salomonson V.V.: Prelaunch characteristics of the Moderate Resolution Imaging Spectroradiometer (MODIS) on EOS-AM1, IEEE Transactions on Geoscience and Remote Sensing, 36(4), 1088-1100, doi: 10.1109/36.700993, 1998.

Franz, B.A., Kwiatkowska, E.J., Meister, G. and McClain, C.R.: Moderate Resolution Imaging Spectroradiometer on Terra: limitations for ocean color applications, Journal of Applied Remote Sensing, 2(1), 023525, doi: 10.1117/1.2957964, 2008.

Guenther, B., Barnes, W., Knight, E., Barker, J., Harnden, J., Weber, R., Roberto, M., Godden, G., Montgomery, H., and Abel, P.: MODIS calibration: a brief review of the strategy for the at-launch calibration approach, Journal of Atmospheric and Oceanic Technology, 13(2), 274-285. doi: 10.1175/1520-0426(1996)013<0274:MCABRO>2.0.CO;2, 1996

Guenther, B. Godden, G. D., Xiong, X., Knight, E.J., Qiu, S. Y., Montgomery, H., Hopkins, M. M., Khayat, M. G., and Zhidong Hao, Z.: Prelaunch algorithm and data format for the Level 1 calibration products for the EOS-AM1 Moderate Resolution Imaging Spectroradiometer (MODIS), IEEE Transactions on Geoscience and Remote Sensing, 36(4), 1142-1151, doi: 10.1109/36.701021, 1998.

Justice, C.O., Vermote, E., Townshend, J.R.G., Defries, R., Roy, D. P., Hall, D. K., Vincent V. Salomonson V. V. et al.: The Moderate Resolution Imaging Spectroradiometer (MODIS): Land remote sensing for global change research, IEEE Transactions on Geoscience and Remote Sensing, 36(4), 1228-1249, doi: 10.1109/36.701075, 1998.

Kwiatkowska, E. J., Franz, B. A., Meister, G., McClain, C. R., and Xiong, X.: Cross calibration of ocean-color bands from Moderate-Resolution Imaging Spectroradiometer on Terra platform, Applied Optics, 47(36), 6796–6810, doi:10.1364/AO.47.006796, 2008.

Pan C., Xiong, X., Che, N.: MODIS pre-launch characterization of reflective solar bands response vs. Scan angle, Proc. SPIE – Earth Observeing Systems XII, Optical Engineering Applications, 66770R, doi:10.117/12.730573, 2007.

Sun, J., Xiong, X., Guenther, B., and Barnes, W.: Radiometric stability monitoring of the MODIS reflective solar bands using the Moon, Metrologia, 40(1), S85, doi: 10.1088/0026-1394/40/1/319, 2003.

Sun, J., Xiong, X., Angal, A., Chen, H., Wu, A., and Geng, X.: Time-dependent response versus scan angle for MODIS reflective solar bands, IEEE Transactions on Geoscience and Remote Sensing, 52(6), 3159-3174, doi: 10.1109/TGRS.2013.2271448, 2014.

Wenny, B. N., Sun, J., Xiong, X., Wu, A., Chen, H., Angal, A., Choi, T., Madhavan, S., Geng, X., Kuyper, J., and Tan, L.: MODIS calibration algorithm improvements developed for Collection 6 Level-1B, Proc. SPIE – Earth Observing Systems XV, 78071F, doi: 10.1117/12.860892, 2010.

Xiong, X., Esposito, J., Sun, J., Pan, C., Guenther, B., and Barnes, W. L.: Degradation of MODIS optics and its reflective solar bands calibration, In Proc. SPIE – Sensors, Systems, and Next-Generation Satellites V, 4540, 62-70. Doi: 10.1117/12.450646, 2001.

Xiong, X., Eriyes, H., Xiong, S., Xie, X., Esposito, J., Sun, J., and Barnes, W.: Performance of Terra MODIS solar diffuser and solar diffuser stability monitor, In Proc. SPIE - Earth Observing Systems X, 58820S doi: 10.1117/12.615334, 2005.

Xiong, X., and Barnes, W.: An overview of MODIS radiometric calibration and characterization, Advances in Atmospheric Sciences, 23(1), 69-79, doi: 10.1007/s00376-006-0008-3, 2006.

RC 10 Line 151: This is misleading because, in Hall et al (2008a), the pixels when the temperature was >2 deg C were removed since it's impossible to have a temperature greater than zero and still be ice. Hall et al. (2008a) did not remove pixels with errors >2 deg C that were below zero, if I am recalling correctly.

RC 10.1: Hall et al. (2008a) did not remove pixels with errors >2 deg C that were below zero, if I am recalling correctly.

AR 10.1: You are correct in pointing out that Hall et al. 2008a did not remove pixels with errors >2°C that were below 0°C. Hall et al. (2008a) developed melt-frequency maps and identified any pixels with a LST >0°C as experiencing melt. The inclusion of Hall et al. (2008a) at the end of this sentence is, as you say, incorrect and misleading. As such, the reference to Hall et al. (2008a) has been removed and only the reference to Mortimer et al. (2016) is included.

Revised text, Line 151 (now line 177-179):

'Pixels for which the average LST error (QC_Day LST error flag) exceeded 2°C were removed from the analysis and any remaining pixels having a temperature >0°C were assigned a temperature of 0°C (Mortimer et al., 2016).'

RC 10.2: …'it's impossible to have a temperature greater than zero and still be ice.':

AR 10.2: Although the temperature of pure ice and snow cannot exceed 0°C, many pixels are not comprised solely of pure ice and snow. Rock, dust, impurities and ponded water (for which the maximum temperature can exceed 0°C) can exist on the snow/ice surface. The presence of these materials within the 1km x 1km pixel can result in an LST >0°C. Mortimer et al. (2016) found that pixels having an LST >0°C were mainly located on outlet glaciers and near the ice-cap margins and inferred that such pixels probably contained a mixture of exposed rock, ice, and meltwater during the melt season. The presence of materials other than pure ice and snow within a pixel can, therefore, result in an LST greater than the maximum temperature of pure ice and snow. To mitigate this effect, ice-covered pixels with an LST >0°C were reassigned a value of 0°C.

RC 11 Line 155: it should be stated that MOD11A2 Collection 6 data were downloaded

AR 11 Corrected

Revised Line 155 (now line 183-185):
>   *'MOD11A2 C6 data were downloaded from (https://lpdaac.usgs.gov/, accessed September– October 2017) and re-projected to a North America Albers Equal Area projection, WGS84 datum, 1 km resolution.'*

RC 12 Line 235: I would say "opposite from" instead of "opposite to"

AR 12 This text, as written, is not included in the revised manuscript.

RC 13 Line 319: I think sections 3.3 and 4.1 could be shortened and made to be more concise.

AR 13 Sections 3.3 (now section 3.4) and 4.1 (now section 4) have been shortened. Repetition in sections 3.3 and 4.1 has been removed. Sections 4.1 and 4.2 have been merged (now section 4).

Revised Section 3.4, Lines 365-392:

>   *'3.4 Principal Components Analysis*
>
>   *To explore whether there are any other spatial patterns in the 16-year mean summer BSA record that differ from the long-term (linear) trend, we performed a Principal Components Analysis of the BSA record (Sect. 2.3). The first and second Principal Components (Fig. 8) explain 65% and 12% of the variance in the mean summer BSA record, respectively. The spatial pattern of the First Principal Component (PC1) scores (Fig. 8a) is generally consistent with the spatial patterns of summer (JJA, Fig 5a) and July (Fig. 5c) mean BSA change described previously (Sect. 3.3). PC1 scores are strongly negative (< -0.005) on western Axel Heiberg Island (large BSA declines), and weakly negative (> -0.001) or even positive at high elevations in the interiors of the ice masses where there was no change in the mean summer BSA. Moderately negative (~ -0.002) component scores occur on the western (continental) side of eastern Ellesmere Island's ice masses as well as over much of Manson Icefield and the southeast portion of Prince of Wales Icefield, where large decreases were observed in both the summer (JJA) and the July BSA.*
>   *For PC1, the highest Empirical Orthogonal Functions (EOFs) (32.8 and 25.9) correspond to the years with the lowest mean summer BSA (2011 and 2012) (Fig. 9). The lowest EOFs (-31.7 and -24.6) correspond to the years with the highest mean summer BSA (2013 and 2004) (Fig. 9). In addition, the departure from zero is much larger for the minimum component scores than for the maximum component scores (Fig. 8a), suggesting that both positive and negative BSA anomalies are likely caused by forcings with the same spatial*

pattern, albeit with the opposite sign. Investigating possible relationships between surface albedo and known large-scale patterns of atmospheric variability (Arctic Oscillation, Pacific North American Pattern, North Atlantic Oscillation), we found the EOFs for PC1 to be well (negatively) correlated with the mean summer North Atlantic Oscillation (NAO) index (r = -0.84, p < 0.001, Fig. 9), derived by averaging the June–August monthly mean NAO indices for 2001 to 2016 (http:www.cpc.ncep.noaa.gov). This is consistent with the finding of Mortimer et al. (2016) that there was a good agreement between the mean summer LST record and the NAO index in the QEI over the 2000–15 period.

The second Principal Component (PC2) had the largest EOFs of any component in 2006, 2010, and 2016. In these years, there was poor correspondence between the PC1 EOFs and the JJA NAO index (Fig. 9). The spatial pattern of the PC2 scores (Fig. 8b) resembles that of the August BSA change (Fig. 5d). Large negative PC2 scores (< -0.004) were observed on eastern Devon Ice Cap and Manson Icefield, where large August BSA declines (< -0.0075 yr^{-1}) occurred. Positive PC2 scores (Fig. 8b) were observed in southwest Axel Heiberg Island and at lower elevations on northern Ellesmere Island's southwestern ice caps, where the mean August BSA increased (Fig. 5d). Unlike PC1, there were no significant correlations between the EOFs of PC2 and known large-scale patterns of atmospheric variability.'

Revised Section 4, Lines 411-462:

'4 Discussion

Between 2001 and 2016 the bulk of the measured mean summer BSA declines in the QEI occurred in July (Sect. 3.2). This finding is consistent with previous work (e.g. Alt, 1987; Gardner and Sharp, 2007) that found variability in July near-surface air temperatures to be the primary influence on inter-annual variability in annual QEI mass balance. Variability in July air temperatures has, in turn, been associated with variations in the strength, position, and geometry of the July circumpolar vortex (Gardner and Sharp, 2007). Extreme high melt years in the QEI are associated with the intrusion of a steep ridge at all levels in the troposphere and the absence of the North American trough, making the QEI thermally homogeneous with continental North America (Alt, 1987). Between 2001 and 2016, in years with low (e.g. 2007–12) or high (e.g. 2001–04)) albedos, there was a persistent ridge (trough) in the 500 hPa geopotential height surface centered over the north and west of the QEI (Fig. 4; Sect. 3.1.1). This configuration appears to be tied to the increased warming and albedo declines observed in the central western part of the QEI from 2007 to 2012. For example, strong warming (Fig. 7b) and albedo declines (Fig. 5a) over Axel Heiberg Island and north-central Ellesmere Island coincided with a ridge of high pressure centered over the north and west of the QEI (Fig. 4) that was often observed in years when the NAO index was negative (Fig. 9).

Differences in the spatial patterns of the monthly BSA change (Fig. 5b–d) reflect the dominant atmospheric circulation patterns that occur over the QEI during the summer months. In the QEI, anticyclonic circulation tends to dominate in the months of June and July, while cyclonic circulation often occurs in August (Alt, 1987; Gascon et al., 2013). In June and July, the largest BSA declines occurred in the climatically continental interiors of the ice masses on Ellesmere and Devon Islands, as well as on Axel Heiberg Island (Fig. 5). In these months, the mountains on eastern Ellesmere and Devon Islands act as a barrier to moisture transport from the east limiting (solid) precipitation (which can temporarily raise the surface albedo) on the western (lee) side of the eastern ice masses (Koerner 1979). Adiabatic heating of descending air masses on the western (lee) side of the eastern ice masses results in warm dry air which promotes warming, melting, and enhanced albedo declines. In contrast, in August, when cyclonic circulation is common (Sect. 3.2.1), BSA declines were largest at low elevations in the maritime regions of eastern Devon Ice Cap, Manson Icefield, and the southwestern Prince of Wales Icefield (Fig. 5d). Low pressure systems which track from the southwest to the north and northeast are common in August, and they advect warm moist air into the Arctic from the south (Alt, 1987; Gascon et al., 2013). In the eastern QEI, orographic uplift of air masses tracking from the southwest, and subsequent adiabatic heating of these air masses when they descend on the eastern sides of ice masses, would bring warm dry air to the eastern (lee) side of the mountains in the eastern QEI, promoting both warming and albedo decline in these regions in August.

During the 2001–16 period, the mean summer QEI-wide BSA record was strongly tied to the summer NAO index (Sect. 2.4). -Anticyclonic circulation was shown to co-vary with the NAO index over the Greenland Ice

Sheet, immediately to the east of the QEI, since ~2001 (Rajewicz and Marshall, 2014). On the Greenland Ice Sheet, clear sky conditions and the advection of warm air form the south that accompany anticyclonic ridging (Rajewicz and Marshall, 2014), similar to that observed in the QEI in June and July (Alt, 1987; Gascon et al., 2013; Bezeau et al., 2015), were found to enhance the strength of the ice-albedo feedback between 2009 and 2011 which resulted in higher rates of melt and glacier mass loss (Box et al., 2012). Although a similar phenomenon is likely to have occurred in the QEI, we find that in some years (2006, 2010, 2016) there was poor correspondence between the mean summer BSA record and the NAO index (Fig. 9), suggesting that an additional forcing may be influencing the spatial and temporal variability of glacier surface albedo in the QEI.

The spatial pattern of both the QEI snow accumulation (Fig. 2 and 3 in Koerner 1979) and $\partial^{18}O$ values (Fig. 7 in Koerner 1979) were inferred by Koerner (1979) for the 1962-73 period from surface snow samples and shallow firn cores collected in spring 1974. These spatial patterns (of snow accumulation and $\partial^{18}O$) closely resemble the spatial pattern of PC2 scores (Fig. 8). Specifically, areas having large negative PC2 scores (< -0.002; Fig. 8b) of the 16-year mean summer BSA record (Sect. 3.4) were characterized by relatively high accumulation rates (Fig. 2 and 3 in Koerner (1979)) and snow that is isotopically warm (Fig. 7 in Koerner (1979)), while areas with positive PC2 scores had lower snow accumulation rates. This similarity points to a possible role of precipitation in affecting the mean summer BSA in some years. To investigate the relationship between the albedo record and variability in precipitation we examined the cumulative mass change record for the QEI from the Gravity Recovery and Climate Experiment (GRACE; Wolken et al. (2016), extended to 2016 (B. Wouters, personal communication, 2017)). The record shows that in 2006, 2010, and 2016 (the years when PC2 of the 16-year mean summer BSA record had the largest EOFs of any Principal Component, Sect. 3.4), once the annual minimum glacier mass was reached, there was a prolonged period of constant low mass (i.e. no melt or snowfall) before fall/winter accumulation began (inferred from an increase in mass). In other years, there was a sharp transition from the local end-of-summer mass minimum to the period of seasonally increasing mass. This could indicate that in some years during the 2001–16 period, variability in August snowfall may have influenced the mean summer BSA.'

RC 14 Line 601: should read IEEE instead of IEE

AR 14 Reference corrected (IEEE instead of IEE)

Revised text:

'Salomon, J. G., Schaaf, C. B., Strahler, A. H., Gao, F., and Jin, Y.: Validation of the MODIS Bidirectional Reflectance Distribution Function and Albedo retrievals using combined observations from the Aqua and Terra platforms, IEEE Transactions on Geoscience and Remote Sensing, 44(6), 1555-1565, 2006.'

Reviewer 2 (Anonymous Referee #2): Received and published 23 September 2017

Reviewer 2's general comments:
The manuscript presents an important effort in understanding Canadian High Arctic glacier albedo and surface temperature. Change in Queen Elizabeth Islands (QEI) glacier surface albedo is presented from the combined Aqua and Terra MODIS Collection 6 albedo product and change in glacier surface temperature is presented from Terra MODIS Collection 5 Land Surface Temperature and Emissivity product. The temporal period of the analyses includes the QEI summer months (June, July, August) from 2001-2016. Albedo and land surface temperature changes are evaluated and presented as monthly and seasonal averages as well as spatial patterns. Satellite analysis is compared with reanalysis data, some complementary observation data and studies published to date.

AR: We thank the reviewer for the thoughtful evaluation of our manuscript. We have reviewed and addressed both the major considerations and minor specific comments. This is outlined below.

- RC refers to reviewer's comment
- AR refers to author's response
- Revised sections of the manuscript are presented in *italics*.

Reviewer 2's major considerations and author's responses

RC 1: "As written, the manuscript can be difficult to follow. The Data and Methods section provides appropriate content and detail. However, the manuscript may benefit from reorganization of content in the Introduction, Results, and Discussion sections. Content in the Discussion section could be moved to the beginning of the manuscript, with the option to provide a 'Background' section. Supporting details of complementary observations (e.g. snowfall, temperature) introduced in the Discussion might be better placed earlier in the manuscript, near results (see line by line suggestions below). In addition, there are grammatical errors and smaller ordering inconsistencies throughout the manuscript that deter from readability. Careful editing and attention to detail is needed in revising and ensuring the success of this manuscript."

AR 1: The manuscript has been revised to make it more concise and easier to follow. Specifically, Sections 3.3 (now section 3.4) and 4.1 (now section 4) have been shortened. Repetition in sections 3.3 and 4.1 has been removed. Sections 4.1 and 4.2 have been merged (now section 4). Additional attention has been paid to grammar and ordering inconsistencies throughout the manuscript to improve readability. While we appreciate the suggestion of a background section we chose not to include one here. We felt that, after revising and condensing the manuscript, the addition of a background section was not necessary (see **RC/AR 29**).

Revised text:

Revised Section 3.4, Lines 365-392:

> *'3.4 Principal Components Analysis*
>
> *To explore whether there are any other spatial patterns in the 16-year mean summer BSA record that differ from the long-term (linear) trend, we performed a Principal Components Analysis of the BSA record (Sect. 2.3). The first and second Principal Components (Fig. 8) explain 65% and 12% of the variance in the mean summer BSA record, respectively. The spatial pattern of the First Principal Component (PC1) scores (Fig. 8a) is generally consistent with the spatial patterns of summer (JJA, Fig 5a) and July (Fig. 5c) mean BSA change described previously (Sect. 3.3). PC1 scores are strongly negative (< -0.005) on western Axel Heiberg Island (large BSA declines), and weakly negative (> -0.001) or even positive at high elevations in the interiors of the*

15

ice masses where there was no change in the mean summer BSA. Moderately negative (~ -0.002) component scores occur on the western (continental) side of eastern Ellesmere Island's ice masses as well as over much of Manson Icefield and the southeast portion of Prince of Wales Icefield, where large decreases were observed in both the summer (JJA) and the July BSA.

For PC1, the highest Empirical Orthogonal Functions (EOFs) (32.8 and 25.9) correspond to the years with the lowest mean summer BSA (2011 and 2012) (Fig. 9). The lowest EOFs (-31.7 and -24.6) correspond to the years with the highest mean summer BSA (2013 and 2004) (Fig. 9). In addition, the departure from zero is much larger for the minimum component scores than for the maximum component scores (Fig. 8a), suggesting that both positive and negative BSA anomalies are likely caused by forcings with the same spatial pattern, albeit with the opposite sign. Investigating possible relationships between surface albedo and known large-scale patterns of atmospheric variability (Arctic Oscillation, Pacific North American Pattern, North Atlantic Oscillation), we found the EOFs for PC1 to be well (negatively) correlated with the mean summer North Atlantic Oscillation (NAO) index (r = -0.84, p < 0.001, Fig. 9), derived by averaging the June–August monthly mean NAO indices for 2001 to 2016 (http:www.cpc.ncep.noaa.gov). This is consistent with the finding of Mortimer et al. (2016) that there was a good agreement between the mean summer LST record and the NAO index in the QEI over the 2000–15 period.

The second Principal Component (PC2) had the largest EOFs of any component in 2006, 2010, and 2016. In these years, there was poor correspondence between the PC1 EOFs and the JJA NAO index (Fig. 9). The spatial pattern of the PC2 scores (Fig. 8b) resembles that of the August BSA change (Fig. 5d). Large negative PC2 scores (< -0.004) were observed on eastern Devon Ice Cap and Manson Icefield, where large August BSA declines (< -0.0075 yr^{-1}) occurred. Positive PC2 scores (Fig. 8b) were observed in southwest Axel Heiberg Island and at lower elevations on northern Ellesmere Island's southwestern ice caps, where the mean August BSA increased (Fig. 5d). Unlike PC1, there were no significant correlations between the EOFs of PC2 and known large-scale patterns of atmospheric variability.'

Revised Section 4, Lines 411-462:

'4 Discussion

Between 2001 and 2016 the bulk of the measured mean summer BSA declines in the QEI occurred in July (Sect. 3.2). This finding is consistent with previous work (e.g. Alt, 1987; Gardner and Sharp, 2007) that found variability in July near-surface air temperatures to be the primary influence on inter-annual variability in annual QEI mass balance. Variability in July air temperatures has, in turn, been associated with variations in the strength, position, and geometry of the July circumpolar vortex (Gardner and Sharp, 2007). Extreme high melt years in the QEI are associated with the intrusion of a steep ridge at all levels in the troposphere and the absence of the North American trough, making the QEI thermally homogeneous with continental North America (Alt, 1987). Between 2001 and 2016, in years with low (e.g. 2007–12) or high (e.g. 2001–04)) albedos, there was a persistent ridge (trough) in the 500 hPa geopotential height surface centered over the north and west of the QEI (Fig. 4; Sect. 3.1.1). This configuration appears to be tied to the increased warming and albedo declines observed in the central western part of the QEI from 2007 to 2012. For example, strong warming (Fig. 7b) and albedo declines (Fig. 5a) over Axel Heiberg Island and north-central Ellesmere Island coincided with a ridge of high pressure centered over the north and west of the QEI (Fig. 4) that was often observed in years when the NAO index was negative (Fig. 9).

Differences in the spatial patterns of the monthly BSA change (Fig. 5b–d) reflect the dominant atmospheric circulation patterns that occur over the QEI during the summer months. In the QEI, anticyclonic circulation tends to dominate in the months of June and July, while cyclonic circulation often occurs in August (Alt, 1987; Gascon et al., 2013). In June and July, the largest BSA declines occurred in the climatically continental interiors of the ice masses on Ellesmere and Devon Islands, as well as on Axel Heiberg Island (Fig. 5). In these months, the mountains on eastern Ellesmere and Devon Islands act as a barrier to moisture transport from the east limiting (solid) precipitation (which can temporarily raise the surface albedo) on the western (lee) side of the eastern ice masses (Koerner 1979). Adiabatic heating of descending air masses on the western (lee) side of the eastern ice masses results in warm dry air which promotes warming, melting, and enhanced albedo declines. In contrast, in August, when cyclonic circulation is common (Sect. 3.2.1), BSA declines were

16

largest at low elevations in the maritime regions of eastern Devon Ice Cap, Manson Icefield, and the southwestern Prince of Wales Icefield (Fig. 5d). Low pressure systems which track from the southwest to the north and northeast are common in August, and they advect warm moist air into the Arctic from the south (Alt, 1987; Gascon et al., 2013). In the eastern QEI, orographic uplift of air masses tracking from the southwest, and subsequent adiabatic heating of these air masses when they descend on the eastern sides of ice masses, would bring warm dry air to the eastern (lee) side of the mountains in the eastern QEI, promoting both warming and albedo decline in these regions in August.

During the 2001–16 period, the mean summer QEI-wide BSA record was strongly tied to the summer NAO index (Sect. 2.4). -Anticyclonic circulation was shown to co-vary with the NAO index over the Greenland Ice Sheet, immediately to the east of the QEI, since ~2001 (Rajewicz and Marshall, 2014). On the Greenland Ice Sheet, clear sky conditions and the advection of warm air form the south that accompany anticyclonic ridging (Rajewicz and Marshall, 2014), similar to that observed in the QEI in June and July (Alt, 1987; Gascon et al., 2013; Bezeau et al., 2015), were found to enhance the strength of the ice-albedo feedback between 2009 and 2011 which resulted in higher rates of melt and glacier mass loss (Box et al., 2012). Although a similar phenomenon is likely to have occurred in the QEI, we find that in some years (2006, 2010, 2016) there was poor correspondence between the mean summer BSA record and the NAO index (Fig. 9), suggesting that an additional forcing may be influencing the spatial and temporal variability of glacier surface albedo in the QEI.

The spatial pattern of both the QEI snow accumulation (Fig. 2 and 3 in Koerner 1979) and $∂^{18}O$ values (Fig. 7 in Koerner 1979) were inferred by Koerner (1979) for the 1962-73 period from surface snow samples and shallow firn cores collected in spring 1974. These spatial patterns (of snow accumulation and $∂^{18}O$) closely resemble the spatial pattern of PC2 scores (Fig. 8). Specifically, areas having large negative PC2 scores (< -0.002; Fig. 8b) of the 16-year mean summer BSA record (Sect. 3.4) were characterized by relatively high accumulation rates (Fig. 2 and 3 in Koerner (1979)) and snow that is isotopically warm (Fig. 7 in Koerner (1979)), while areas with positive PC2 scores had lower snow accumulation rates. This similarity points to a possible role of precipitation in affecting the mean summer BSA in some years. To investigate the relationship between the albedo record and variability in precipitation we examined the cumulative mass change record for the QEI from the Gravity Recovery and Climate Experiment (GRACE; Wolken et al. (2016), extended to 2016 (B. Wouters, personal communication, 2017)). The record shows that in 2006, 2010, and 2016 (the years when PC2 of the 16-year mean summer BSA record had the largest EOFs of any Principal Component, Sect. 3.4), once the annual minimum glacier mass was reached, there was a prolonged period of constant low mass (i.e. no melt or snowfall) before fall/winter accumulation began (inferred from an increase in mass). In other years, there was a sharp transition from the local end-of-summer mass minimum to the period of seasonally increasing mass. This could indicate that in some years during the 2001–16 period, variability in August snowfall may have influenced the mean summer BSA.'

RC 2: "In the data and methods section (Page 4, line 122) MOD10A1 data was mentioned "to be a reasonable representation of the true surface albedo". Does this refer to analysis conducted by the authors for this manuscript or to Box et al., 2017? Please clarify. If MOD10A1 data was not inspected by the authors for this manuscript, why not?"

AC 2: The reference to the MOD10A1 data has been removed and the methods section (section 2.1 MODIS sensor degradation) detailing MODIS sensor calibration issues has been revised.

Revised text, lines 90-138:

'2.1.1 MODIS sensor degradation

The MODIS sensors are currently operating well beyond their expected [productive] six year lifetimes (Barnes et al, 1998; Justice 1998) and the detectors are degrading (Xiong et al., 2001). For both the MODIS Terra and Aqua sensors, instruments were calibrated pre-launch (radiometric, spatial, specular calibration) (Gunther et al., 1996). On-orbit calibration procedures were included to monitor the sensor degradation that

is expected as the instruments are exposed to solar radiation (Gunther et al., 1996). For the reflective solar bands (0.41–2.2 μm) the on-board calibration system includes a solar diffuser (SD) calibrated using the solar diffuser stability monitor (SDSM) (Gunther et al., 1998). Lunar and Earth view observations (for select desert sites) are also used to assess radiometric stability (Sun et al., 2003). Even so, long-term scan mirror and wavelength dependent degradation, which are not sufficiently accounted for by the on-board calibrators (SD/SDMS), have been observed (Xiong et al., 2001; Lyapustin et al., 2014 and references therein). Calibration degradation effects, which are largely confined to the MODIS Terra sensor, are greatest in the blue band (B3) and decrease with increasing wavelength (Xiong and Barnes, 2006). An anomaly in the SD door operation (3 May 2003) and a decision to leave the door permanently open, exposing the SD to additional solar radiation, resulted in degradation of the SD on the MODIS Terra sensor that was faster than had originally been anticipated, and than was observed for the MODIS Aqua sensor (Xiong et al., 2005). Differences in the response versus scan angle (RVS) for the two side mirrors were also characterized pre-launch (Barnes et al., 1998). The RVS is important because it describes the scan mirror's response to different angles of incidence (AOI, for each band, detector and mirror side) (Sun et al., 2014). However, for the MODIS Terra sensor, following an overheating incident during pre-launch calibration, the RVS was not re-characterized and the exact pre-launch RVS characteristics are not known (Pan et al., 2007; Sun et al., 2014 and references therein). These issues have resulted in the performance of the MODIS Terra sensor being poorer than that of the MODIS Aqua sensor.

As a normal part of the operational procedure, the MODIS Characterization Support Team (http:mcst.gsfc.nasa.gov) periodically updates the calibration algorithms and approaches, during which time the entire L1B record (calibrated top of the atmosphere radiances) is re-processed to reflect improved understanding and characterization of changes to the instruments. Even so, non-physical trends in MODIS Terra data products, that result from calibration drift, have been observed and are well documented (e.g. Xiong et al., 2001; Xiong and Barnes, 2006; Franz et al., 2008; Kwiatkowski et al., 2008; Wang et al., 2012; Lyapustin et al., 2014; and references therein). The latest revision occurred with the C6 data and includes on-orbit calibration procedures to mitigate long-term calibration drift, particularly at the shorter wavelengths (Wenny et al., 2010; Toller et al., 2013; Sun et al., 2014; Lyapustin et al., 2014). The C6 dataset uses the on-board calibrators (e.g. SD/SDMS) and the mirror side ratios from lunar standard and Earth view observations (Toller et al, 2013; Sun et al., 2014). The C6 revision also includes an additional approach, aimed primarily at the short-wavelength bands, that uses observations of desert sites (pseudo-invariant targets) to derive instrument calibration coefficients and RVS at multiple AOIs (instead of the two AOIs provided by the SD and lunar standard) (Toller et al, 2013; Sun et al., 2014). Although this vicarious approach is less accurate than the one that uses the mirror-side ratios calibrated using a lunar standard, it has been found to provide a significant improvement to the L1B radiance measurements relative to the C5 data, prior to ~2013 (Toller 2013; Lyapustin et al., 2014). Updated L1B C6 radiances can be up to several percent higher than the C5 values (e.g. Band 3 and for most recent period ~2013 onward) (Toller et al., 2013; Lyapustin et al. 2014; Casey et al., 2017). However, evaluation of the L1B C6 Band 3 (0.46–0.48 μm) radiance over a desert site (Libya 4) identified residual errors (decadal trends on the order of several tenths of 1%; Lyapustin et al., 2014) that are within the product's stated accuracy (2% in absolute reflectance units for the reflective solar bands (Barnes et al., 1998; Justice et al., 1998)). The impact of the C6 updates on higher level MODIS science products is difficult to quantify because the corrections are time, mirror-side, angular, and detector dependent (Toller et al., 2013; Lyapustin et al. 2014; Sun et al., 2014). In addition, the C6 revision includes updates to algorithms (in addition to the calibration updates) used in the derivation of specific higher-level products (https://www.umb.edu/spectralmass/terra_aqua_modis/v006 outlines changes made to the MCD43A3 C6 data product). Important for the current study, however, is that recent analysis of surface albedo over the Greenland Ice Sheet, immediately to the east of the QEI, using MODIS C6 data (including the MCD43A3 product used in this study) identified statistically significant albedo declines over the wet snow zone (Casey et al., 2017). For the most part, these declines are thought to be physically real (Casey et al., 2017), which gives us confidence in the albedo trends presented here. There are no long-term, spatially distributed, in situ albedo records from the glaciers and ice caps in the QEI, so a comparison between the MCD43A3 records and ground observations is not possible. This is both a motivation for and a limitation of, the current study.

References added:

Barnes, W. L., Pagano, T.S., and Salomonson V.V.: Prelaunch characteristics of the Moderate Resolution Imaging Spectroradiometer (MODIS) on EOS-AM1, IEEE Transactions on Geoscience and Remote Sensing, 36(4), 1088-1100, doi: 10.1109/36.700993, 1998.

Franz, B.A., Kwiatkowska, E.J., Meister, G. and McClain, C.R.: Moderate Resolution Imaging Spectroradiometer on Terra: limitations for ocean color applications, Journal of Applied Remote Sensing, 2(1), 023525, doi: 10.1117/1.2957964, 2008.

Guenther, B., Barnes, W., Knight, E., Barker, J., Harnden, J., Weber, R., Roberto, M., Godden, G., Montgomery, H., and Abel, P.: MODIS calibration: a brief review of the strategy for the at-launch calibration approach, Journal of Atmospheric and Oceanic Technology, 13(2), 274-285. doi: 10.1175/1520-0426(1996)013<0274:MCABRO>2.0.CO;2, 1996

Guenther, B. Godden, G. D., Xiong, X., Knight, E.J., Qiu, S. Y., Montgomery, H., Hopkins, M. M., Khayat, M. G., and Zhidong Hao, Z.: Prelaunch algorithm and data format for the Level 1 calibration products for the EOS-AM1 Moderate Resolution Imaging Spectroradiometer (MODIS), IEEE Transactions on Geoscience and Remote Sensing, 36(4), 1142-1151, doi: 10.1109/36.701021, 1998.

Justice, C.O., Vermote, E., Townshend, J.R.G., Defries, R., Roy, D. P., Hall, D. K., Vincent V. Salomonson V. V. et al.: The Moderate Resolution Imaging Spectroradiometer (MODIS): Land remote sensing for global change research, IEEE Transactions on Geoscience and Remote Sensing, 36(4), 1228-1249, doi: 10.1109/36.701075, 1998.

Kwiatkowska, E. J., Franz, B. A., Meister, G., McClain, C. R., and Xiong, X.: Cross calibration of ocean-color bands from Moderate-Resolution Imaging Spectroradiometer on Terra platform, Applied Optics, 47(36), 6796–6810, doi:10.1364/AO.47.006796, 2008.

Pan C., Xiong, X., Che, N.: MODIS pre-launch characterization of reflective solar bands response vs. Scan angle, Proc. SPIE – Earth Observeing Systems XII, Optical Engineering Applications, 66770R, doi:10.117/12.730573, 2007.

Sun, J., Xiong, X., Guenther, B., and Barnes, W.: Radiometric stability monitoring of the MODIS reflective solar bands using the Moon, Metrologia, 40(1), S85, doi: 10.1088/0026-1394/40/1/319, 2003.

Sun, J., Xiong, X., Angal, A., Chen, H., Wu, A., and Geng, X.: Time-dependent response versus scan angle for MODIS reflective solar bands, IEEE Transactions on Geoscience and Remote Sensing, 52(6), 3159-3174, doi: 10.1109/TGRS.2013.2271448, 2014.

Wenny, B. N., Sun, J., Xiong, X., Wu, A., Chen, H., Angal, A., Choi, T., Madhavan, S., Geng, X., Kuyper, J., and Tan, L.: MODIS calibration algorithm improvements developed for Collection 6 Level-1B, Proc. SPIE – Earth Observing Systems XV, 78071F, doi: 10.1117/12.860892, 2010.

Xiong, X., Esposito, J., Sun, J., Pan, C., Guenther, B., and Barnes, W. L.: Degradation of MODIS optics and its reflective solar bands calibration, In Proc. SPIE – Sensors, Systems, and Next-Generation Satellites V, 4540, 62-70. Doi: 10.1117/12.450646, 2001.

Xiong, X., Eriyes, H., Xiong, S., Xie, X., Esposito, J., Sun, J., and Barnes, W.: Performance of Terra MODIS solar diffuser and solar diffuser stability monitor, In Proc. SPIE - Earth Observing Systems X, 58820S doi: 10.1117/12.615334, 2005.

Xiong, X., and Barnes, W.: An overview of MODIS radiometric calibration and characterization, Advances in Atmospheric Sciences, 23(1), 69-79, doi: 10.1007/s00376-006-0008-3, 2006.

RC 3: "Additionally, is there a reason the authors have focused on Terra data? The manuscript may be strengthened by analysis of MODIS Aqua MYD10A1 and Terra MOD10A1 data. As stated, the MCD43A3 data represents data acquired from both Terra and Aqua sensors. Calibration challenges which have primarily impacted Terra data may be teased apart by analysis of Aqua MYD10A1 data, Terra MOD10A1 data, and combined sensor MCD43A3 data."

AR 3: The combined MCD43A3 data product was selected for this study (instead of the Terra or Aqua only) to ensure optimal spatial coverage of the QEI ice cover. The study is meant as a first assessment of QEI surface albedo and is just as concerned with the spatial patterns in albedo just as it is with the temporal patterns

of albedo change. We acknowledge that these data include observations from both the Aqua and Terra sensors, and are therefore affected by calibration challenges that impact the Terra data more than the Aqua data. The methods section (Section 2.1 MODIS sensor degradation) has been re-written to provide a better account of the issues relating to sensor degradation.

Revised text, lines 90-138:

'2.1.1 MODIS sensor degradation

The MODIS sensors are currently operating well beyond their expected [productive] six year lifetimes (Barnes et al, 1998; Justice 1998) and the detectors are degrading (Xiong et al., 2001). For both the MODIS Terra and Aqua sensors, instruments were calibrated pre-launch (radiometric, spatial, specular calibration) (Gunther et al., 1996). On-orbit calibration procedures were included to monitor the sensor degradation that is expected as the instruments are exposed to solar radiation (Gunther et al., 1996). For the reflective solar bands (0.41–2.2 µm) the on-board calibration system includes a solar diffuser (SD) calibrated using the solar diffuser stability monitor (SDSM) (Gunther et al., 1998). Lunar and Earth view observations (for select desert sites) are also used to assess radiometric stability (Sun et al., 2003). Even so, long-term scan mirror and wavelength dependent degradation, which are not sufficiently accounted for by the on-board calibrators (SD/SDMS), have been observed (Xiong et al., 2001; Lyapustin et al., 2014 and references therein). Calibration degradation effects, which are largely confined to the MODIS Terra sensor, are greatest in the blue band (B3) and decrease with increasing wavelength (Xiong and Barnes, 2006). An anomaly in the SD door operation (3 May 2003) and a decision to leave the door permanently open, exposing the SD to additional solar radiation, resulted in degradation of the SD on the MODIS Terra sensor that was faster than had originally been anticipated, and than was observed for the MODIS Aqua sensor (Xiong et al., 2005). Differences in the response versus scan angle (RVS) for the two side mirrors were also characterized pre-launch (Barnes et al., 1998). The RVS is important because it describes the scan mirror's response to different angles of incidence (AOI, for each band, detector and mirror side) (Sun et al., 2014). However, for the MODIS Terra sensor, following an overheating incident during pre-launch calibration, the RVS was not re-characterized and the exact pre-launch RVS characteristics are not known (Pan et al., 2007; Sun et al., 2014 and references therein). These issues have resulted in the performance of the MODIS Terra sensor being poorer than that of the MODIS Aqua sensor.

As a normal part of the operational procedure, the MODIS Characterization Support Team (http:mcst.gsfc.nasa.gov) periodically updates the calibration algorithms and approaches, during which time the entire L1B record (calibrated top of the atmosphere radiances) is re-processed to reflect improved understanding and characterization of changes to the instruments. Even so, non-physical trends in MODIS Terra data products, that result from calibration drift, have been observed and are well documented (e.g. Xiong et al., 2001; Xiong and Barnes, 2006; Franz et al., 2008; Kwiatkowski et al., 2008; Wang et al., 2012; Lyapustin et al., 2014; and references therein). The latest revision occurred with the C6 data and includes on-orbit calibration procedures to mitigate long-term calibration drift, particularly at the shorter wavelengths (Wenny et al., 2010; Toller et al., 2013; Sun et al., 2014; Lyapustin et al., 2014). The C6 dataset uses the on-board calibrators (e.g. SD/SDMS) and the mirror side ratios from lunar standard and Earth view observations (Toller et al, 2013; Sun et al., 2014). The C6 revision also includes an additional approach, aimed primarily at the short-wavelength bands, that uses observations of desert sites (pseudo-invariant targets) to derive instrument calibration coefficients and RVS at multiple AOIs (instead of the two AOIs provided by the SD and lunar standard) (Toller et al, 2013; Sun et al., 2014). Although this vicarious approach is less accurate than the one that uses the mirror-side ratios calibrated using a lunar standard, it has been found to provide a significant improvement to the L1B radiance measurements relative to the C5 data, prior to ~2013 (Toller 2013; Lyapustin et al., 2014). Updated L1B C6 radiances can be up to several percent higher than the C5 values (e.g. Band 3 and for most recent period ~2013 onward) (Toller et al., 2013; Lyapustin et al. 2014; Casey et al., 2017). However, evaluation of the L1B C6 Band 3 (0.46–0.48 µm) radiance over a desert site (Libya 4) identified residual errors (decadal trends on the order of several tenths of 1%; Lyapustin et al., 2014) that are within the product's stated accuracy (2% in absolute reflectance units for the reflective solar bands (Barnes et al., 1998; Justice et al., 1998)). The impact of the C6 updates on higher level MODIS

science products is difficult to quantify because the corrections are time, mirror-side, angular, and detector dependent (Toller et al., 2013; Lyapustin et al. 2014; Sun et al., 2014). In addition, the C6 revision includes updates to algorithms (in addition to the calibration updates) used in the derivation of specific higher-level products (https://www.umb.edu/spectralmass/terra_aqua_modis/v006 outlines changes made to the MCD43A3 C6 data product). Important for the current study, however, is that recent analysis of surface albedo over the Greenland Ice Sheet, immediately to the east of the QEI, using MODIS C6 data (including the MCD43A3 product used in this study) identified statistically significant albedo declines over the wet snow zone (Casey et al., 2017). For the most part, these declines are thought to be physically real (Casey et al., 2017), which gives us confidence in the albedo trends presented here. There are no long-term, spatially distributed, in situ albedo records from the glaciers and ice caps in the QEI, so a comparison between the MCD43A3 records and ground observations is not possible. This is both a motivation for and a limitation of, the current study.'

RC 4: "Section 2.2 discusses MODIS LST data. Why was Collection 5 MOD11A2 data used? (Page 5, lines 155-157) Communication with the MODIS data distributor, LP DAAC, revealed that MOD11A2 and MYD11A2 Collection 6 data have been available since mid-2015. Additionally, with the discussion of the Terra sensor degradation, it seems short-sighted to use Terra data only. Why was Terra data used? Was Aqua data used (i.e. MYD11A2)? If not, why not? Recommendation to add MYD11A2 data analysis."

AR 4: The manuscript has been revised and now uses the C6 MOD11A2 data instead of the C5 product. Terra data were used because of the time-period under investigation (2001-16). Terra data are available since 2000 while Aqua data are only available after 2002. Use of the Terra LST data (MOD11A2) allowed comparison with the albedo record for the full 2001-16 time period.

RC 5: "Reorganization of content is advised toward readability. There are several cases where content is difficult to follow. Example, Results Section, 3.1 Suggestion to add sentences clarifying and further detailing results. As written, parts of the section are terse and non-intuitive."

AR 5: Section 3.1 has been re-ordered and additional text has been added for readability.

Revised text, Section 3.1 (now lines 224-242):

'3.1 Mean summer albedo
Annual maps of the mean summer clear-sky broadband shortwave black-sky MCD43A3 albedo for all glacier-covered surfaces in the QEI for the 2001–16 period are presented in Figure 2. The QEI-wide mean summer BSA, averaged across all 16 years, was 0.550 ± 0.115 (mean ± 1 standard deviation; Table 1). The lowest QEI-wide mean summer BSA (0.539 ± 0.127) was recorded in 2011 while the highest (0.668 ± 0.089) was recorded in 2013 (Table 1).
In general, mean summer BSA is lower around the margins of the ice masses, where glacier ice is exposed in the summer, than it is in the higher elevation interior regions where snow or firn are exposed year-round (Fig. 2). During years when the QEI-wide mean summer BSA was low (e.g. 2011), we observed a broad zone of low albedo values (< 0.4) around the margins of the major ice masses (Fig. 2). Conversely, in years when the mean summer BSA was high (e.g. 2013), this zone was much less obvious. High data dropout at high elevations on Axel Heiberg Island, and over the summit of the Devon Ice Cap in 2014 and 2006 (Table S1), may have produced a negative albedo bias for these regions, since the albedo is typically greater at higher elevations. Aggregating the 2001–16 average mean summer BSA into 50 m elevation bins, we observed a linear rate of BSA increase with elevation (0.0085 per 50 m elevation bin, r^2 = 0.99).
In addition to the mean summer (JJA) BSA, the monthly mean BSA values for June, July, and August, were also investigated (Sect. 2.3) (Table 2, Fig. S1–S3). July had the lowest 16-year monthly mean BSA (0.551 ± 0.131), followed closely by August (0.579 ± 0.127) (Table 2). In each year during the 2001–16 period, the highest summer monthly BSA was always recorded in June while the lowest monthly BSA was recorded in either July or August. The lowest monthly mean BSA values for June and August were recorded in 2011, while

the lowest July mean BSA occurred in 2012. The highest monthly mean BSA for both June and July occurred in 2013; for August, it occurred in 2003.'

RC 6: Lines 196-197 Why does Table 1 2001-2016 average differ from manuscript stated average (i.e. Table 1 states 0.599, manuscript states 0.550)?

AR 6: The value of 0.599 in Table 1 refers to the mean summer (JJA) BSA. The value of 0.551 on line 196-107 refers to the July mean BSA which is 0.551 ± 0.0131 and is presented in Table 2. As such, line 196-197 (**now lines 238-239**): *'July had the lowest 16-year monthly mean BSA (0.551 ± 0.131), followed closely by August (0.579 ± 0.127) (Table 2).'* remains unchanged except for addition of reference to appropriate Table (Table 2).

RC 7: For example, readers may appreciate a sentence stating that in addition to the JJA averages, monthly mean albedo was also calculated (Table 2, see Section 2.3).

AR 7: Section 3.1 has been re-ordered to make it easier to follow and a sentence (Line 209, highlighted) regarding the monthly mean BSA albedo has been added, with reference to the appropriate Table, Figures, and methods section.

Revised text, section 3.1 (**now lines 224-242**): Line 209 highlighted

> *'**3.1 Mean summer albedo***
> *Annual maps of the mean summer clear-sky broadband shortwave black-sky MCD43A3 albedo for all glacier-covered surfaces in the QEI for the 2001–16 period are presented in Figure 2. The QEI-wide mean summer BSA, averaged across all 16 years, was 0.550 ± 0.115 (mean ± 1 standard deviation; Table 1). The lowest QEI-wide mean summer BSA (0.539 ± 0.127) was recorded in 2011 while the highest (0.668 ± 0.089) was recorded in 2013 (Table 1).*
> *In general, mean summer BSA is lower around the margins of the ice masses, where glacier ice is exposed in the summer, than it is in the higher elevation interior regions where snow or firn are exposed year-round (Fig. 2). During years when the QEI-wide mean summer BSA was low (e.g. 2011), we observed a broad zone of low albedo values (< 0.4) around the margins of the major ice masses (Fig. 2). Conversely, in years when the mean summer BSA was high (e.g. 2013), this zone was much less obvious. High data dropout at high elevations on Axel Heiberg Island, and over the summit of the Devon Ice Cap in 2014 and 2006 (Table S1), may have produced a negative albedo bias for these regions, since the albedo is typically greater at higher elevations. Aggregating the 2001–16 average mean summer BSA into 50 m elevation bins, we observed a linear rate of BSA increase with elevation (0.0085 per 50 m elevation bin, $r^2 = 0.99$).*
> *In addition to the mean summer (JJA) BSA, the monthly mean BSA values for June, July, and August, were also investigated (Sect. 2.3) (Table 2, Fig. S1–S3). July had the lowest 16-year monthly mean BSA (0.551 ± 0.131), followed closely by August (0.579 ± 0.127) (Table 2). In each year during the 2001–16 period, the highest summer monthly BSA was always recorded in June while the lowest monthly BSA was recorded in either July or August. The lowest monthly mean BSA values for June and August were recorded in 2011, while the lowest July mean BSA occurred in 2012. The highest monthly mean BSA for both June and July occurred in 2013; for August, it occurred in 2003.'*

RC 8: Include references to Tables, methods as appropriate.

AR 8: Additional references to Tables, Figures, and methods have been added throughout These are identified on the markup copy, some examples are provided below.

Examples:

> **Results Section 3.1, lines 225-239:**

'Annual maps of the mean summer clear-sky broadband shortwave black-sky MCD43A3 albedo for all glacier-covered surfaces in the QEI for the 2001–16 period are presented in Figure 2. The QEI-wide mean summer BSA, averaged across all 16 years, was 0.550 ± 0.115 (mean ± 1 standard deviation; Table 1). The lowest QEI-wide mean summer BSA (0.539 ± 0.127) was recorded in 2011 while the highest (0.668 ± 0.089) was recorded in 2013 (Table 1).

In general, mean summer BSA is lower around the margins of the ice masses, where glacier ice is exposed in the summer, than it is in the higher elevation interior regions where snow or firn are exposed year-round (Fig. 2). During years when the QEI-wide mean summer BSA was low (e.g. 2011), we observed a broad zone of low albedo values (< 0.4) around the margins of the major ice masses (Fig. 2). Conversely, in years when the mean summer BSA was high (e.g. 2013), this zone was much less obvious. High data dropout at high elevations on Axel Heiberg Island, and over the summit of the Devon Ice Cap in 2014 and 2006 (Table S1), may have produced a negative albedo bias for these regions, since the albedo is typically greater at higher elevations. Aggregating the 2001–16 average mean summer BSA into 50 m elevation bins, we observed a linear rate of BSA increase with elevation (0.0085 per 50 m elevation bin, r^2 = 0.99).

In addition to the mean summer (JJA) BSA, the monthly mean BSA values for June, July, and August, were also investigated (Sect. 2.3) (Table 2, Fig. S1–S3). July had the lowest 16-year monthly mean BSA (0.551 ± 0.131), followed closely by August (0.579 ± 0.127) (Table 2).'

Results Section 3.2.1, lines 245-250:

'The mean summer BSA anomalies, relative to the 2001–16 mean, are presented in Figure 3 and Table 1. For consistency with the regression analysis (Sect. 3.3), BSA anomalies were only computed for pixels having mean summer BSA observations in 11 or more of the 16 years (Sect. 2.3). The period 2001–16 is characterised by a six-year period of positive BSA anomalies (2001–06) followed by a six-year period of negative BSA anomalies (2007–12) (Table 1).'

Results Section 3.2.2, lines 285-287:

'In addition to the mean summer (JJA) BSA anomalies, the mean June, July, and August BSA anomalies were also examined (Fig. S4–S6) (Sect. 2.3). The sign of the mean July BSA anomaly (Table 2) was always consistent with that of the mean summer (JJA) BSA anomaly (Table 1).'

RC 9: Similarly, in the Discussion section, it is stated that "delayed snowfall onset and limited melt in August were inferred from the GRACE mass change record". However, earlier in the manuscript, speculative statements are made on snowfall patterns, implying there are no quantitative data nor analyses to cite for QEI. Use of a specific snowfall proxy data (i.e. GRACE, reanalysis) or other observational datasets would be more quantitative than speculative remarks currently in the Results and Discussions sections.

AR 9: While we agree that quantified data based statements are preferred over speculation where possible, in the case of the QEI ice cover, spatially-distributed in-situ precipitation measurements do not exist for this time-period. Where appropriate, speculative comments have been removed from the text (**see RC/AR 28**). A reference to recent modeled precipitation changes (Vincent et al. 2015) (**RC/AR 14**) was added to the introduction. Vincent et al. (2015) found an increase in precipitation and an increase in the ratio of snowfall to total precipitation over the Canadian Arctic during the period 1948-2012. However, it is important to note that these trends were calculated by gridding climate station data (50km x 50km grid). There are only three such stations (Resolute Bay, Eureka, Alert) in the QEI and none of these are located over ice. Because of the coarse spatial resolution of the modelled data and the caveat that these trends were not validated over the permanent ice cover, the modelled data were not useful for validating trends at the scale of the individual ice caps which are the focus of our study.

We did consider using other modeled climate data in our study. The CanRCM4 (0.44°; 0.22° up to 2009) and MARv3.5.2 20 km monthly data forced with ERA Interim were investigated. However, we found the

spatial resolution of these data to be too coarse to discern spatial patterns in precipitation, and MAR results only covered a part of the QEI. Similar issues of spatial resolution were encountered with the NCEP/NCAR Reanalysis R1 temperature and precipitation data (2.5°x2.5° grid). Additionally, the absence of in-situ measurements on ice means that we are unable to validate these datasets. For the temperature record, it was possible to use in-situ climate records from stations located on the ice (Agassiz and Devon Ice Caps) to validate the NCEP/NCAR Reanalysis R1 data and MODIS LST records (Sharp et al., 2011). Sharp et al. (2011) found upper-air (700hPa) air temperatures from NCEP/NCAR Reanalysis R1 data to be well correlated with on-ice air temperature records, available for the Devon (1997-2009) and Agassiz (1988-2009) Ice Caps. Both Sharp et al. 2011 (2000-06) and Mortimer et al. 2016 (2000-15) found the 700hPa air temperatures to be strongly correlated with the MODIS LST record. A similar comparison is not possible for precipitation due to the absence of in situ measurements on ice, and caution was taken not to over-interpret precipitation trends.

The GRACE data do not provide detailed spatial information about snowfall patterns. However, when combined with existing knowledge of the accumulation and ablation seasons in the region these data can provide information about the relative timing of the transition from summer mass loss (which ends when the minimum annual glacier mass is reached) to the winter period of mass gain (inferred from the onset of mass increase) which occurs in autumn. This is described in **lines 454-461** of the revised manuscript.

Revised text, lines 454-461:

> *'To investigate the relationship between the albedo record and variability in precipitation we examined the cumulative mass change record for the QEI from the Gravity Recovery and Climate Experiment (GRACE; Wolken et al. (2016), extended to 2016 (B. Wouters, personal communication, 2017)). The record shows that in 2006, 2010, and 2016 (the years when PC2 of the 16-year mean summer BSA record had the largest EOFs of any Principal Component, Sect. 3.4), once the annual minimum glacier mass was reached, there was a prolonged period of constant low mass (i.e. no melt or snowfall) before fall/winter accumulation began (inferred from an increase in mass). In other years, there was a sharp transition from the local end-of-summer mass minimum to the period of seasonally increasing mass.'*

RC 10: Two specific areas of speculation are: (1) Results Section 3.1, line 203, 'may indicate early onset of snowfall that fall' and (2) Results Section 3.2, lines 290-292 snowfall patterns may be changing in QEI). Quantified data based statements are preferred over speculation where possible.

AC 10: Again, while we agree that quantitative statements are preferred over speculation, the absence of in-situ precipitation data limits our ability to provide them. The specific areas of concern noted in RC 10 have been removed from the manuscript.

RC 11: Recommendation for the authors to clearly state the additional QEI LST analysis provided in this manuscript as compared to Mortimer et al., 2016. (See some line by line comments below.) I recommend considering the role of the QEI LST analysis in this manuscript.

RC11a: Recommendation for the authors to clearly state the additional QEI LST analysis provided in this manuscript as compared to Mortimer et al., 2016. (See some line by line comments below.)

AR 11a: Following your recommendations, the manuscript has been revised and now uses the MOD11A2 C6 data instead of the C5 data. Text has been added to the Methods (Section 2.2) to clearly state the differences in the QEI LST analysis provided in this manuscript compared to Mortimer et al., 2016.

Revised additional text, lines 175-177:

'The LST analyses presented here are an update of those presented by Mortimer et al. (2016) which used MODIS C5 data. The two analyses also differ in the time period used (we use 2001–16 instead of 2000–15 to coincide with the BSA analysis).'

RC 11b: I recommend considering the role of the QEI LST analysis in this manuscript.

AR 11b: Temperature changes drive the snow grain metamorphism and melt of snow which both affect its albedo. In addition, the removal of the seasonal snowpack (which exposes lower albedo firn or glacier ice), and the melt of glacier ice (which releases impurities which have low albedo and thus changes the surface albedo of both ice and snow) are driven by changing air and surface temperatures. Hence comparison of the LST and albedo datasets provides insight into the mechanisms driving albedo change in different regions of the QEI. As such, analyses of the LST dataset are included in this manuscript to help understand the observed spatiotemporal patterns of albedo change in the QEI. Additional text clarifying the reason for inclusion of the LST data has been added to both the methods (Section 2.2) and results (Section 3.5) sections, as well as to the conclusion.

Revised text:

Methods Section 2.2 lines 161-167 added text:

'Warmer surface temperatures increase the rates of grain metamorphism and snowmelt, resulting in larger snow grains which have a lower albedo than those of fresh snow (Wiscombe and Warren 1980; Colbeck 1982) (Sect. 1). Air and surface temperatures also affect the timing of removal of the seasonal snowpack, which exposes lower albedo firn or glacier ice. Additionally, the melt of glacier ice releases impurities that have a low albedo and thus change the surface albedo of both ice and snow (e.g. Clarke and Noone 1985; Doherty et al., 2010; Sect. 1). As such, analysis of the glacier surface temperature and comparison of these data with the albedo record is included to help understand the observed spatiotemporal patterns of glacier albedo change in the QEI.'

Results section 3.5 lines 394-396 added text:

'Owing to the positive feedback between albedo and surface temperature we would expect to observe strong increases in surface temperature where albedo declines were large. To investigate the relationship between temperature and albedo over the QEI, the 16-year mean summer LST record was compared with the 16-year mean summer BSA record (Sect. 2.3).'

Conclusion, added text (lines 476-485):

'Albedo declines increase the proportion of incoming solar radiation absorbed at the air-ice interface, and thus the energy available to drive melt, warming, and further surface albedo decline. Warmer temperatures, in turn, increase the rate of snow grain metamorphism which lowers the albedo. Air and surface temperatures affect the removal (timing and extent) of the seasonal snowpack which exposes lower albedo firn and/or glacier ice, while melting glacier ice releases impurities that further reduce its albedo. Given that surface temperature and albedo are inextricably linked, knowing where and when albedo changes are likely to occur in future is important for predicting future rates of mass loss from the QEI ice caps. Recent investigations of atmospheric circulation patterns over the QEI (e.g. Gardner and Sharp, 2007) focused on characterization of July temperature and atmospheric conditions, since July is usually the month when melt rates peak. Our results suggest, however, that changes occurring during the month of August are also important, especially as the length of the melt season continues to increase.'

RC 12: Was the Randolph Glacier Inventory used to delineate QEI glacier analysis areas? If so, please state clearly where appropriate (i.e. manuscript text, figure captions) and cite.

AR 12: The Randolph Glacier Inventory was used to delineate QEI glacier areas throughout the analysis. This was stated in **Line 186 (now line 220-222)** of the original manuscript: *'To ensure that only data for glaciated surfaces were retained, all BSA and LST outputs used in this analysis were clipped to the Randolph Glacier Inventory v3.2 region 32 (Arctic Canada North) reference polygons (Arendt et al., 2012; Pfeffer et al., 2014).'*

RC 13: Page 2, line 38 – What is meant by 'accelerated release'? Suggestion to reword, clarify intent.

AR 13: Sentence reworded.

Revised text, Line 36-38 (now lines 37-40):
> *'Albedo decreases can also be caused by aerosol deposition (Warren and Wiscombe, 1980), biological activity on glacier surfaces (Fountain et al., 2004), and the release of impurities contained within melting snow and ice, which become concentrated at the snow/ice surface (Clarke and Noone, 1985; Conway et al., 1996; Flanner et al., 2007; Doherty et al., 2010).'*

RC 14: Page 2, lines 40-42 – The authors are correct to state fresh snow would raise surface albedo. Suggestion to include QEI precipitation data quantifying the suggestion, or reference precipitation studies.

AR 14: Reference to Vincent et al. (2015), who reported both an increase in total precipitation and an increase in the ratio of snowfall to total precipitation over the Canadian Arctic during the period 1948-2012, has been added. These trends were calculated by gridding climate station data. In the QEI, there are only three such stations (Resolute Bay, Eureka, Alert) and none of them are located on glacier ice (see **RC/AR 9**). Reference to Box et al. (2012) who found a second-order negative albedo feedback (defined by a positive correlation between albedo and surface air temperature anomalies) in the accumulation area of the nearby Greenland Ice Sheet has also been added to the end of this sentence.

Revised text:
> **Lines 39-42 (now lines 40-43)**
> *'Given the observed increases in air and glacier surface temperatures across the QEI (Mortimer et al., 2016) we anticipate a reduction in the surface albedo in this region, unless warming has also been accompanied by an increase in solid precipitation (Vincent et al., 2015) that is large enough to raise the surface albedo (e.g. Box et al., 2012).'*
> **Reference added**
> *Vincent, L. A., Zhang, X., Brown, R. D., Feng, Y., Mekis, E., Milewska, E. J., Wan, H., and Wang, X. L.: Observed trends in Canada's climate and influence of low-frequency variability modes, Journal of Climate, 28, 4545-4560, doi: 10.1175/JCLI-D-14-00697.1, 2015.*

RC 15: Page 2, line 49 – Suggestion to clarify for readers the source of the temperature analysis used in referenced studies.

AR 15: Text revised for clarity.

Revised line 49 (now lines 49-52):
> *'Between 2000 and 2015, increases in QEI summer 700 hPa air temperatures derived from the NCEP/NCAR R1 Reanalysis (Kalnay and others, 1996) and glacier surface temperatures from the Moderate Resolution Imaging Spectroradiometer (MODIS) were greatest in the north and west of the QEI (Sharp et al., 2011; Mortimer et al., 2016). We do not know whether there is a similar spatial pattern in the albedo record.'*

RC 16: Page 3, lines 89-91 – Suggestion to edit sentences. As written, one could glean that it is difficult to discriminate between surface snow and ice vs cloud spectral visible-thermal infrared response. This is not

always difficult to do spectrally. If the authors intend to discuss cloud remote sensing only, please clarify this. A more appropriate reference than Hall 2008a, may be Hall et al., 2002, MODIS snow-cover products, Remote Sensing of Environment, 83, 181-194.

AR 16: Text moved and re-written for clarity. Reference to Hall et al. (2002) has been added. The issue of concern here is the presence of clouds which can potentially introduce additional variability in the dataset (due to the removal of data when clouds are detected) that is not representative of physical changes on the surface.

Revised text (now lines 139-144):

'Furthermore, the MCD43A3 data used here were produced only under clear sky conditions (Hall et al., 2002; 2012). A conservative cloud mask is applied to remove observations made when clouds are detected (Ackerman et al., 1998). The resulting data gaps may introduce variability in the albedo record that is not representative of true physical change. Despite this, the MCD43A3 albedo product has been found to provide a reasonable representation of the seasonal albedo cycle over glaciers and ice caps (e.g. Stroeve et al., 2006). Hence, in the absence of long-term ground measurements of glacier surface albedo in the QEI, we made the assumption that this is also the case in the QEI.'

Reference added: *Hall, D. K., Riggs, G. A., Salomonson V. V. DiGirolamo N. E., Bayr K. J.: MODIS snow-cover products, Remote Sens. Environ., 83(1), 181-194, doi: 10.1016/S0034-4257(02)00095-0, 2002.*

RC 16: Page 4, line 98 – Delete 'some of'.

AR 16: Deleted 'some of'

Revised text Line 98 (now lines 91-92):

'The MODIS sensors are currently operating well beyond their expected [productive] six year lifetimes (Barnes et al, 1998; Justice 1998) and the detectors are degrading (Xiong et al., 2001).'

RC 17: Page 4, line 102 – Lyapustin et al. was not the first to report on Terra's band degradation. Recommendation to additionally read and cite early / appropriate work, e.g. Xiong et al., 2001, Degradation of MODIS optics and its reflective solar bands calibration, doi: 10.1117/12.450646
Xiong and Barnes, 2006, An overview of MODIS radiometric calibration and characterization, doi: 10.1007/s00376-006-0008-3
Sun et al., 2014 Time-dependent response versus scan angle for MODIS reflective solar bands, IEEE TGRS, doi: 10.1109/TGRS.2013.2271448

AR 17: References to earlier studies have been added following additional review of the relevant literature (see **RC/AR 18**). References to Sun et al. (2014) and Xiong and Barnes (2006) are included in a revised section on MODIS sensor degradation (**lines 90-138).**

Revised text:

Line 102 (now line 91-92):
'The MODIS sensors are currently operating well beyond their expected [productive] six year lifetimes (Barnes et al, 1998; Justice 1998) and the detectors are degrading (Xiong et al., 2001).'

Revised methods section 2.1 (lines 90-138) text with references to Xiong et al. (2001), Xiong and Barnes (2006) and Sun et al. (2014) are highlighted:

'2.1.1 MODIS sensor degradation

The MODIS sensors are currently operating well beyond their expected [productive] six year lifetimes (Barnes et al, 1998; Justice 1998) and the detectors are degrading (Xiong et al., 2001). For both the MODIS Terra and Aqua sensors, instruments were calibrated pre-launch (radiometric, spatial, specular calibration) (Gunther et al., 1996). On-orbit calibration procedures were included to monitor the sensor degradation that is expected as the instruments are exposed to solar radiation (Gunther et al., 1996). For the reflective solar bands (0.41–2.2 µm) the on-board calibration system includes a solar diffuser (SD) calibrated using the solar diffuser stability monitor (SDSM) (Gunther et al., 1998). Lunar and Earth view observations (for select desert sites) are also used to assess radiometric stability (Sun et al., 2003). Even so, long-term scan mirror and wavelength dependent degradation, which are not sufficiently accounted for by the on-board calibrators (SD/SDMS), have been observed (Xiong et al., 2001; Lyapustin et al., 2014 and references therein). Calibration degradation effects, which are largely confined to the MODIS Terra sensor, are greatest in the blue band (B3) and decrease with increasing wavelength (Xiong and Barnes, 2006). An anomaly in the SD door operation (3 May 2003) and a decision to leave the door permanently open, exposing the SD to additional solar radiation, resulted in degradation of the SD on the MODIS Terra sensor that was faster than had originally been anticipated, and than was observed for the MODIS Aqua sensor (Xiong et al., 2005). Differences in the response versus scan angle (RVS) for the two side mirrors were also characterized pre-launch (Barnes et al., 1998). The RVS is important because it describes the scan mirror's response to different angles of incidence (AOI, for each band, detector and mirror side) (Sun et al., 2014). However, for the MODIS Terra sensor, following an overheating incident during pre-launch calibration, the RVS was not re-characterized and the exact pre-launch RVS characteristics are not known (Pan et al., 2007; Sun et al., 2014 and references therein). These issues have resulted in the performance of the MODIS Terra sensor being poorer than that of the MODIS Aqua sensor.

As a normal part of the operational procedure, the MODIS Characterization Support Team (http:mcst.gsfc.nasa.gov) periodically updates the calibration algorithms and approaches, during which time the entire L1B record (calibrated top of the atmosphere radiances) is re-processed to reflect improved understanding and characterization of changes to the instruments. Even so, non-physical trends in MODIS Terra data products, that result from calibration drift, have been observed and are well documented (e.g. Xiong et al., 2001; Xiong and Barnes, 2006; Franz et al., 2008; Kwiatkowski et al., 2008; Wang et al., 2012; Lyapustin et al., 2014; and references therein). The latest revision occurred with the C6 data and includes on-orbit calibration procedures to mitigate long-term calibration drift, particularly at the shorter wavelengths (Wenny et al., 2010; Toller et al., 2013; Sun et al., 2014; Lyapustin et al., 2014). The C6 dataset uses the on-board calibrators (e.g. SD/SDMS) and the mirror side ratios from lunar standard and Earth view observations (Toller et al, 2013; Sun et al., 2014). The C6 revision also includes an additional approach, aimed primarily at the short-wavelength bands, that uses observations of desert sites (pseudo-invariant targets) to derive instrument calibration coefficients and RVS at multiple AOIs (instead of the two AOIs provided by the SD and lunar standard) (Toller et al, 2013; Sun et al., 2014). Although this vicarious approach is less accurate than the one that uses the mirror-side ratios calibrated using a lunar standard, it has been found to provide a significant improvement to the L1B radiance measurements relative to the C5 data, prior to ~2013 (Toller 2013; Lyapustin et al., 2014). Updated L1B C6 radiances can be up to several percent higher than the C5 values (e.g. Band 3 and for most recent period ~2013 onward) (Toller et al., 2013; Lyapustin et al. 2014; Casey et al., 2017). However, evaluation of the L1B C6 Band 3 (0.46–0.48 µm) radiance over a desert site (Libya 4) identified residual errors (decadal trends on the order of several tenths of 1%; Lyapustin et al., 2014) that are within the product's stated accuracy (2% in absolute reflectance units for the reflective solar bands (Barnes et al., 1998; Justice et al., 1998)). The impact of the C6 updates on higher level MODIS science products is difficult to quantify because the corrections are time, mirror-side, angular, and detector dependent (Toller et al., 2013; Lyapustin et al. 2014; Sun et al., 2014). In addition, the C6 revision includes updates to algorithms (in addition to the calibration updates) used in the derivation of specific higher-level products (https://www.umb.edu/spectralmass/terra_aqua_modis/v006 outlines changes made to the MCD43A3 C6 data product). Important for the current study, however, is that recent analysis of surface albedo over the Greenland Ice Sheet, immediately to the east of the QEI, using MODIS C6 data (including the MCD43A3 product used in this study) identified statistically significant albedo declines over the wet snow

zone (Casey et al., 2017). For the most part, these declines are thought to be physically real (Casey et al., 2017), which gives us confidence in the albedo trends presented here. There are no long-term, spatially distributed, in situ albedo records from the glaciers and ice caps in the QEI, so a comparison between the MCD43A3 records and ground observations is not possible. This is both a motivation for and a limitation of, the current study.'

References added:

Barnes, W. L., Pagano, T.S., and Salomonson V.V.: Prelaunch characteristics of the Moderate Resolution Imaging Spectroradiometer (MODIS) on EOS-AM1, IEEE Transactions on Geoscience and Remote Sensing, 36(4), 1088-1100, doi: 10.1109/36.700993, 1998.

Franz, B.A., Kwiatkowska, E.J., Meister, G. and McClain, C.R.: Moderate Resolution Imaging Spectroradiometer on Terra: limitations for ocean color applications, Journal of Applied Remote Sensing, 2(1), 023525, doi: 10.1117/1.2957964, 2008.

Guenther, B., Barnes, W., Knight, E., Barker, J., Harnden, J., Weber, R., Roberto, M., Godden, G., Montgomery, H., and Abel, P.: MODIS calibration: a brief review of the strategy for the at-launch calibration approach, Journal of Atmospheric and Oceanic Technology, 13(2), 274-285. doi: 10.1175/1520-0426(1996)013<0274:MCABRO>2.0.CO;2, 1996

Guenther, B. Godden, G. D., Xiong, X., Knight, E.J., Qiu, S. Y., Montgomery, H., Hopkins, M. M., Khayat, M. G., and Zhidong Hao, Z.: Prelaunch algorithm and data format for the Level 1 calibration products for the EOS-AM1 Moderate Resolution Imaging Spectroradiometer (MODIS), IEEE Transactions on Geoscience and Remote Sensing, 36(4), 1142-1151, doi: 10.1109/36.701021, 1998.

Justice, C.O., Vermote, E., Townshend, J.R.G., Defries, R., Roy, D. P., Hall, D. K., Vincent V. Salomonson V. V. et al.: The Moderate Resolution Imaging Spectroradiometer (MODIS): Land remote sensing for global change research, IEEE Transactions on Geoscience and Remote Sensing, 36(4), 1228-1249, doi: 10.1109/36.701075, 1998.

Kwiatkowska, E. J., Franz, B. A., Meister, G., McClain, C. R., and Xiong, X.: Cross calibration of ocean-color bands from Moderate-Resolution Imaging Spectroradiometer on Terra platform, Applied Optics, 47(36), 6796–6810, doi:10.1364/AO.47.006796, 2008.

Pan C., Xiong, X., Che, N.: MODIS pre-launch characterization of reflective solar bands response vs. Scan angle, Proc. SPIE − Earth Observeing Systems XII, Optical Engineering Applications, 66770R, doi:10.117/12.730573, 2007.

Sun, J., Xiong, X., Guenther, B., and Barnes, W.: Radiometric stability monitoring of the MODIS reflective solar bands using the Moon, Metrologia, 40(1), S85, doi: 10.1088/0026-1394/40/1/319, 2003.

Sun, J., Xiong, X., Angal, A., Chen, H., Wu, A., and Geng, X.: Time-dependent response versus scan angle for MODIS reflective solar bands, IEEE Transactions on Geoscience and Remote Sensing, 52(6), 3159-3174, doi: 10.1109/TGRS.2013.2271448, 2014.

Wenny, B. N., Sun, J., Xiong, X., Wu, A., Chen, H., Angal, A., Choi, T., Madhavan, S., Geng, X., Kuyper, J., and Tan, L.: MODIS calibration algorithm improvements developed for Collection 6 Level-1B, Proc. SPIE − Earth Observing Systems XV, 78071F, doi: 10.1117/12.860892, 2010.

Xiong, X., Esposito, J., Sun, J., Pan, C., Guenther, B., and Barnes, W. L.: Degradation of MODIS optics and its reflective solar bands calibration, In Proc. SPIE − Sensors, Systems, and Next-Generation Satellites V, 4540, 62-70. Doi: 10.1117/12.450646, 2001.

Xiong, X., Eriyes, H., Xiong, S., Xie, X., Esposito, J., Sun, J., and Barnes, W.: Performance of Terra MODIS solar diffuser and solar diffuser stability monitor, In Proc. SPIE - Earth Observing Systems X, 58820S doi: 10.1117/12.615334, 2005.

Xiong, X., and Barnes, W.: An overview of MODIS radiometric calibration and characterization, Advances in Atmospheric Sciences, 23(1), 69-79, doi: 10.1007/s00376-006-0008-3, 2006.

RC 18: Page 4, paragraph 3. Suggestion for authors to reread literature on MODIS sensor calibration, degradation and capabilities. Line 110, more correct to state that C6 did improve radiance measurements from launch to ~2013. It remains to be assessed how accurate and reliable MODIS C6 data will be moving

forward from C6 implementation (~2013 to present). Line 110: Recommendation to check the MODIS Characterization Support Team literature https://mcst.gsfc.nasa.gov/publications?f%5Btype%5D=102 .

AR 18: Literature has been reviewed and have been included in the revised methods section (Section 2.1.1) presented above. Specific mention of the improved radiances up until ~2013 has been added.

Revised text, Line 110 (now lines 121-123):

> *'Although this vicarious approach is less accurate than the one that uses the mirror-side ratios calibrated using a lunar standard, it has been found to provide a significant improvement to the L1B radiance measurements relative to the C5 data, prior to ~2013 (Toller 2013; Lyapustin et al., 2014).'*

RC 19: For lines 113-114, it is not that the sensor is capable of identifying trends greater than 0.01, so much as +/- 0.01 is the limit of MODIS sensor accuracy and precision. The paragraph could be rewritten to be more informative and clear regarding MODIS sensor design and capabilities.

AC 19: This paragraph has been re-written to be more informative and accurate regarding MODIS sensor design and capabilities. The text *'is capable of identifying trends greater than 0.01'* has been removed.

Revised methods text is included with RC/AR 20, below.

RC 20: The paragraph (Page 4, Paragraph 3) could be rewritten to be more informative and clear regarding MODIS sensor design and capabilities.

AR 20: MODIS Characterization Support Team literature has been reviewed and this section has been re-written to be more informative.

Revised text, lines 90-138:

> *'2.1.1 MODIS sensor degradation*
>
> *The MODIS sensors are currently operating well beyond their expected [productive] six year lifetimes (Barnes et al, 1998; Justice 1998) and the detectors are degrading (Xiong et al., 2001). For both the MODIS Terra and Aqua sensors, instruments were calibrated pre-launch (radiometric, spatial, specular calibration) (Gunther et al., 1996). On-orbit calibration procedures were included to monitor the sensor degradation that is expected as the instruments are exposed to solar radiation (Gunther et al., 1996). For the reflective solar bands (0.41–2.2 µm) the on-board calibration system includes a solar diffuser (SD) calibrated using the solar diffuser stability monitor (SDSM) (Gunther et al., 1998). Lunar and Earth view observations (for select desert sites) are also used to assess radiometric stability (Sun et al., 2003). Even so, long-term scan mirror and wavelength dependent degradation, which are not sufficiently accounted for by the on-board calibrators (SD/SDMS), have been observed (Xiong et al., 2001; Lyapustin et al., 2014 and references therein). Calibration degradation effects, which are largely confined to the MODIS Terra sensor, are greatest in the blue band (B3) and decrease with increasing wavelength (Xiong and Barnes, 2006). An anomaly in the SD door operation (3 May 2003) and a decision to leave the door permanently open, exposing the SD to additional solar radiation, resulted in degradation of the SD on the MODIS Terra sensor that was faster than had originally been anticipated, and than was observed for the MODIS Aqua sensor (Xiong et al., 2005). Differences in the response versus scan angle (RVS) for the two side mirrors were also characterized pre-launch (Barnes et al., 1998). The RVS is important because it describes the scan mirror's response to different angles of incidence (AOI, for each band, detector and mirror side) (Sun et al., 2014). However, for the MODIS Terra sensor, following an overheating incident during pre-launch calibration, the RVS was not re-characterized and the exact pre-launch RVS characteristics are not known (Pan et al., 2007; Sun et al., 2014 and references therein). These issues have resulted in the performance of the MODIS Terra sensor being poorer than that of the MODIS Aqua sensor.*

As a normal part of the operational procedure, the MODIS Characterization Support Team (http:mcst.gsfc.nasa.gov) periodically updates the calibration algorithms and approaches, during which time the entire L1B record (calibrated top of the atmosphere radiances) is re-processed to reflect improved understanding and characterization of changes to the instruments. Even so, non-physical trends in MODIS Terra data products, that result from calibration drift, have been observed and are well documented (e.g. Xiong et al., 2001; Xiong and Barnes, 2006; Franz et al., 2008; Kwiatkowski et al., 2008; Wang et al., 2012; Lyapustin et al., 2014; and references therein). The latest revision occurred with the C6 data and includes on-orbit calibration procedures to mitigate long-term calibration drift, particularly at the shorter wavelengths (Wenny et al., 2010; Toller et al., 2013; Sun et al., 2014; Lyapustin et al., 2014). The C6 dataset uses the on-board calibrators (e.g. SD/SDMS) and the mirror side ratios from lunar standard and Earth view observations (Toller et al, 2013; Sun et al., 2014). The C6 revision also includes an additional approach, aimed primarily at the short-wavelength bands, that uses observations of desert sites (pseudo-invariant targets) to derive instrument calibration coefficients and RVS at multiple AOIs (instead of the two AOIs provided by the SD and lunar standard) (Toller et al, 2013; Sun et al., 2014). Although this vicarious approach is less accurate than the one that uses the mirror-side ratios calibrated using a lunar standard, it has been found to provide a significant improvement to the L1B radiance measurements relative to the C5 data, prior to ~2013 (Toller 2013; Lyapustin et al., 2014). Updated L1B C6 radiances can be up to several percent higher than the C5 values (e.g. Band 3 and for most recent period ~2013 onward) (Toller et al., 2013; Lyapustin et al. 2014; Casey et al., 2017). However, evaluation of the L1B C6 Band 3 (0.46–0.48 µm) radiance over a desert site (Libya 4) identified residual errors (decadal trends on the order of several tenths of 1%; Lyapustin et al., 2014) that are within the product's stated accuracy (2% in absolute reflectance units for the reflective solar bands (Barnes et al., 1998; Justice et al., 1998)). The impact of the C6 updates on higher level MODIS science products is difficult to quantify because the corrections are time, mirror-side, angular, and detector dependent (Toller et al., 2013; Lyapustin et al. 2014; Sun et al., 2014). In addition, the C6 revision includes updates to algorithms (in addition to the calibration updates) used in the derivation of specific higher-level products (https://www.umb.edu/spectralmass/terra_aqua_modis/v006 outlines changes made to the MCD43A3 C6 data product). Important for the current study, however, is that recent analysis of surface albedo over the Greenland Ice Sheet, immediately to the east of the QEI, using MODIS C6 data (including the MCD43A3 product used in this study) identified statistically significant albedo declines over the wet snow zone (Casey et al., 2017). For the most part, these declines are thought to be physically real (Casey et al., 2017), which gives us confidence in the albedo trends presented here. There are no long-term, spatially distributed, in situ albedo records from the glaciers and ice caps in the QEI, so a comparison between the MCD43A3 records and ground observations is not possible. This is both a motivation for and a limitation of, the current study.

References added:

Barnes, W. L., Pagano, T.S., and Salomonson V.V.: Prelaunch characteristics of the Moderate Resolution Imaging Spectroradiometer (MODIS) on EOS-AM1, IEEE Transactions on Geoscience and Remote Sensing, 36(4), 1088-1100, doi: 10.1109/36.700993, 1998.

Franz, B.A., Kwiatkowska, E.J., Meister, G. and McClain, C.R.: Moderate Resolution Imaging Spectroradiometer on Terra: limitations for ocean color applications, Journal of Applied Remote Sensing, 2(1), 023525, doi: 10.1117/1.2957964, 2008.

Guenther, B., Barnes, W., Knight, E., Barker, J., Harnden, J., Weber, R., Roberto, M., Godden, G., Montgomery, H., and Abel, P.: MODIS calibration: a brief review of the strategy for the at-launch calibration approach, Journal of Atmospheric and Oceanic Technology, 13(2), 274-285. doi: 10.1175/1520-0426(1996)013<0274:MCABRO>2.0.CO;2, 1996

Guenther, B. Godden, G. D., Xiong, X., Knight, E.J., Qiu, S. Y., Montgomery, H., Hopkins, M. M., Khayat, M. G., and Zhidong Hao, Z.: Prelaunch algorithm and data format for the Level 1 calibration products for the EOS-AM1 Moderate Resolution Imaging Spectroradiometer (MODIS), IEEE Transactions on Geoscience and Remote Sensing, 36(4), 1142-1151, doi: 10.1109/36.701021, 1998.

Justice, C.O., Vermote, E., Townshend, J.R.G., Defries, R., Roy, D. P., Hall, D. K., Vincent V. Salomonson V. V. et al.: The Moderate Resolution Imaging Spectroradiometer (MODIS): Land remote sensing for global

change research, IEEE Transactions on Geoscience and Remote Sensing, 36(4), 1228-1249, doi: 10.1109/36.701075, 1998.

Kwiatkowska, E. J., Franz, B. A., Meister, G., McClain, C. R., and Xiong, X.: Cross calibration of ocean-color bands from Moderate-Resolution Imaging Spectroradiometer on Terra platform, Applied Optics, 47(36), 6796–6810, doi:10.1364/AO.47.006796, 2008.

Pan C., Xiong, X., Che, N.: MODIS pre-launch characterization of reflective solar bands response vs. Scan angle, Proc. SPIE – Earth Observeing Systems XII, Optical Engineering Applications, 66770R, doi:10.117/12.730573, 2007.

Sun, J., Xiong, X., Guenther, B., and Barnes, W.: Radiometric stability monitoring of the MODIS reflective solar bands using the Moon, Metrologia, 40(1), S85, doi: 10.1088/0026-1394/40/1/319, 2003.

Sun, J., Xiong, X., Angal, A., Chen, H., Wu, A., and Geng, X.: Time-dependent response versus scan angle for MODIS reflective solar bands, IEEE Transactions on Geoscience and Remote Sensing, 52(6), 3159-3174, doi: 10.1109/TGRS.2013.2271448, 2014.

Wenny, B. N., Sun, J., Xiong, X., Wu, A., Chen, H., Angal, A., Choi, T., Madhavan, S., Geng, X., Kuyper, J., and Tan, L.: MODIS calibration algorithm improvements developed for Collection 6 Level-1B, Proc. SPIE – Earth Observing Systems XV, 78071F, doi: 10.1117/12.860892, 2010.

Xiong, X., Esposito, J., Sun, J., Pan, C., Guenther, B., and Barnes, W. L.: Degradation of MODIS optics and its reflective solar bands calibration, In Proc. SPIE – Sensors, Systems, and Next-Generation Satellites V, 4540, 62-70, doi: 10.1117/12.450646, 2001.

Xiong, X., Eriyes, H., Xiong, S., Xie, X., Esposito, J., Sun, J., and Barnes, W.: Performance of Terra MODIS solar diffuser and solar diffuser stability monitor, In Proc. SPIE - Earth Observing Systems X, 58820S doi: 10.1117/12.615334, 2005.

Xiong, X., and Barnes, W.: An overview of MODIS radiometric calibration and characterization, Advances in Atmospheric Sciences, 23(1), 69-79, doi: 10.1007/s00376-006-0008-3, 2006.'

RC 21: Page 5, line 129 – Suggestion to move citation to correct location in the sentence, i.e. Schaaf and Wang 2015 reference should immediately follow MCD43 product mention.

AR 21: Citation moved to earlier in the sentence.

Revised Line 129 (now lines 147-149):

> *'Summer (1-2 June (day 152) to 30-31 August (day 243)) MODIS MCD43A3 and MCD43A2 C6 (Schaaf and Wang, 2015) data for MODIS tiles h17v00, h16v00, h16v01, and h15v01 for the period 2001-2016 were obtained from the NASA/USGS Land Processes Distributed Active Archive Center (http://lpdaac.usgs.gov/accessed November 2016).'*

RC 22: Page 5, line 141 – Awkward as written, suggestion to reword to clarify further use of BSA term e.g. 'henceforth BSA refers to the black sky albedo MODIS shortwave broadband data.'

AR 22: Line no longer included in manuscript.

RC 23: Page 5, lines 151-152 – The authors seem to generalize in that "uncertainties in the MOD11A2 LSTs arise mainly from cloud contamination". Suggestion to reread relevant literature and present accurately. Does the sentence refer to over snow only?

AR 23: This sentence referred to uncertainties in the trends derived from the MOD11A2 data and not in the MOD11A2 data itself. The text has been revised for clarity.

Revised text, lines 151-152 (now lines 179-183):

> *'Uncertainties in trends derived from the MOD11A2 LST data arise mainly from cloud contamination (Box et al., 2012; Hall et al., 2012) and the removal of observations for periods when clouds are detected (Ackerman et al., 1998; Hall et al., 2008b). Variability in the number of clear-sky days within each observation period and from one year to the next was not found to*

introduce significant variability in the MODIS-derived LST relative to the true near-surface air temperature in the QEI (see Mortimer et al., 2016).'

RC 24: Page 6, line 159 – Is there a reference from precipitation records/data in QEI? i.e. what station, record or data is 400 mm/yr derived from?

AR 24: The reference for the 400 mm/yr should be Braithwaite, 2005. In the original manuscript, this reference, which refers to both the temperature and precipitation ranges, was included at the end of the following sentence. The text has been revised to clarify this omission.

Revised text line 159 (now lines 187-188):

> *'Annual precipitation in the QEI is low (<400 mm yr^{-1}) and varies little from one year to the next; in contrast, the annual temperature range is large (> 40°C) (Braithwaite, 2005).'*

RC 25: Page 7, line 195 – Suggestion to include MCD43A3 for clarity and completeness.

AR 25: Mention of MCD43A3 included for clarity and completeness, as suggested.

Revised text line 195 (now line 225-226):

> *'Annual maps of the mean summer clear-sky broadband shortwave black-sky MCD43A3 albedo for all glacier-covered surfaces in the QEI for the 2001–16 period are presented in Figure 2.'*

RC 26: Page 9, line 272 – Note that it is not only the calibration accuracy that limits the capability to measure trends, but also the sensor design. Please add reference to sensor capabilities (e.g. Justice et al., 1998, doi: 10.1109/36.701075 and/or similar on MODIS instrument design and post-launch capabilities, see https://mcst.gsfc.nasa.gov/publications?f%5Btype%5D=102).

AR 26: Sentence revised for accuracy in both the methods (Section #, line 202-205) and results (Section 3.3.1, line 315) sections. Additional references to literature discussing sensor capabilities (Barnes et al., 1998; Justice et al., 1998) have been added. References to the appropriate methods section have been included in the results.

Revised text:

> **Line 125-128 (Section 2.1.1):**
>
> *'…evaluation of the L1B C6 Band 3 (0.46–0.48 μm) radiance over a desert site (Libya 4) identified residual errors (decadal trends on the order of several tenths of 1%; Lyapustin et al., 2014) that are within the product's stated accuracy (2% in absolute reflectance units for the reflective solar bands (Barnes et al., 1998; Justice et al., 1998)).*
>
> **Lines 192-195 (now lines 202-205, Section 2.3):**
> *'Following Casey et al. (2017), BSA trends between -0.001 yr^{-1} and +0.001 yr^{-1} are considered to be negligible. Negligible trends were defined by Casey et al. (2017) on the basis of the magnitude of the residual calibration uncertainties in the C6 data (on the order of several tenths of one percent in TOA reflectance (Lyaputsin et al., 2014)) over pseudo-invariant desert sites (Sect. 2.1.1).'*
>
> **Lines 298-299 (now Results Section 3.3.1 line 315):**
> *'More than 95% of pixels experienced a non-negligible (> |0.001| yr^{-1}, Sect. 2.3) decrease in summer BSA…'*
>
> **References added:**
> *Barnes, W. L., Pagano, T.S., and Salomonson V.V.: Prelaunch characteristics of the Moderate Resolution Imaging Spectroradiometer (MODIS) on EOS-AM1, IEEE Transactions on Geoscience and Remote Sensing, 36(4), 1088-1100, doi: 10.1109/36.700993, 1998.*

Justice, C.O., Vermote, E., Townshend, J.R.G., Defries, R., Roy, D. P., Hall, D. K., Vincent V. Salomonson V. V. et al.: The Moderate Resolution Imaging Spectroradiometer (MODIS): Land remote sensing for global change research, IEEE Transactions on Geoscience and Remote Sensing, 36(4), 1228-1249, doi: 10.1109/36.701075, 1998.

RC 27: Page 12, lines 365-366, Suggestion to reword sentence, avoiding use of "positive (negative)" words side by side.

AR 27: This line, as written, is no longer included in the revised manuscript.

RC 28: Page 12, lines 376-377 It is stated that "delayed snowfall onset and limited melt in August were inferred from the GRACE mass change record". Did the authors process GRACE data, or does this reference a study? If it references a study, please include the citation. If the authors processed GRACE data, please include mention of in Data and Methods.

AR 28: Text has been re-organized for clarity. The above-mentioned delayed snowfall onset and limited melt in August were inferred from the GRACE mass change record data presented in Wolken et al. (2016), extended to 2016. The explanation of this was originally included in Section 3.3 (now section 3.4). The more detailed explanation has now been moved to the discussion and has replaced the general comment to better describe how we used the GRACE data.

Revised text (lines 454-462):
> *'To investigate the relationship between the albedo record and variability in precipitation we examined the cumulative mass change record for the QEI from the Gravity Recovery and Climate Experiment (GRACE; Wolken et al. (2016), extended to 2016 (B. Wouters, personal communication, 2017)). The record shows that in 2006, 2010, and 2016 (the years when PC2 of the 16-year mean summer BSA record had the largest EOFs of any Principal Component, Sect. 3.4), once the annual minimum glacier mass was reached, there was a prolonged period of constant low mass (i.e. no melt or snowfall) before fall/winter accumulation began (inferred from an increase in mass). In other years, there was a sharp transition from the local end-of-summer mass minimum to the period of seasonally increasing mass. This could indicate that in some years during the 2001–16 period, variability in August snowfall may have influenced the mean summer BSA.'*

RC 29: Page 13, lines 407-409 Example of content that may be better placed in the beginning of the manuscript.

AR 29: We appreciate your recommendation to include a background section or to include some of this material at the beginning of the manuscript. In revising the manuscript, however, we found that this particular point fitted better towards the end as it helps to place the importance and relevance of the August BSA change in the context of existing literature.

RC 30: Page 15, lines 465-466 Example of sentence where it is difficult to assess what is new in this manuscript vs. Mortimer et al., 2016.

AR 30: The text from Lines 465-466 is no longer included in the revised manuscript. However, in response to this comment we reviewed the existing text to ensure that it was clear as to whether we were referring to the current study or to Mortimer et al. 2016. Specifically, in response to your comment regarding C5 vs C6 (**RC 4**), LST anomalies were recalculated and are presented in Figure S7. Additional text has been included to specify differences between Mortimer et al. 2016 and this study. Where possible, references to figures in the current text (i.e. Figure 7 and Figure S7) are used instead of referring to the earlier Mortimer et al. 2016 study.

Revised text and figures:

Added text lines 176-179:
'The LST analyses presented here are an update of those presented by Mortimer et al. (2016) which used MODIS C5 data. The two analyses also differ in the time-period used (we use 2001-16 instead of 2000-15 to coincide with the BSA analysis).'

Figure S7 (added Figure):
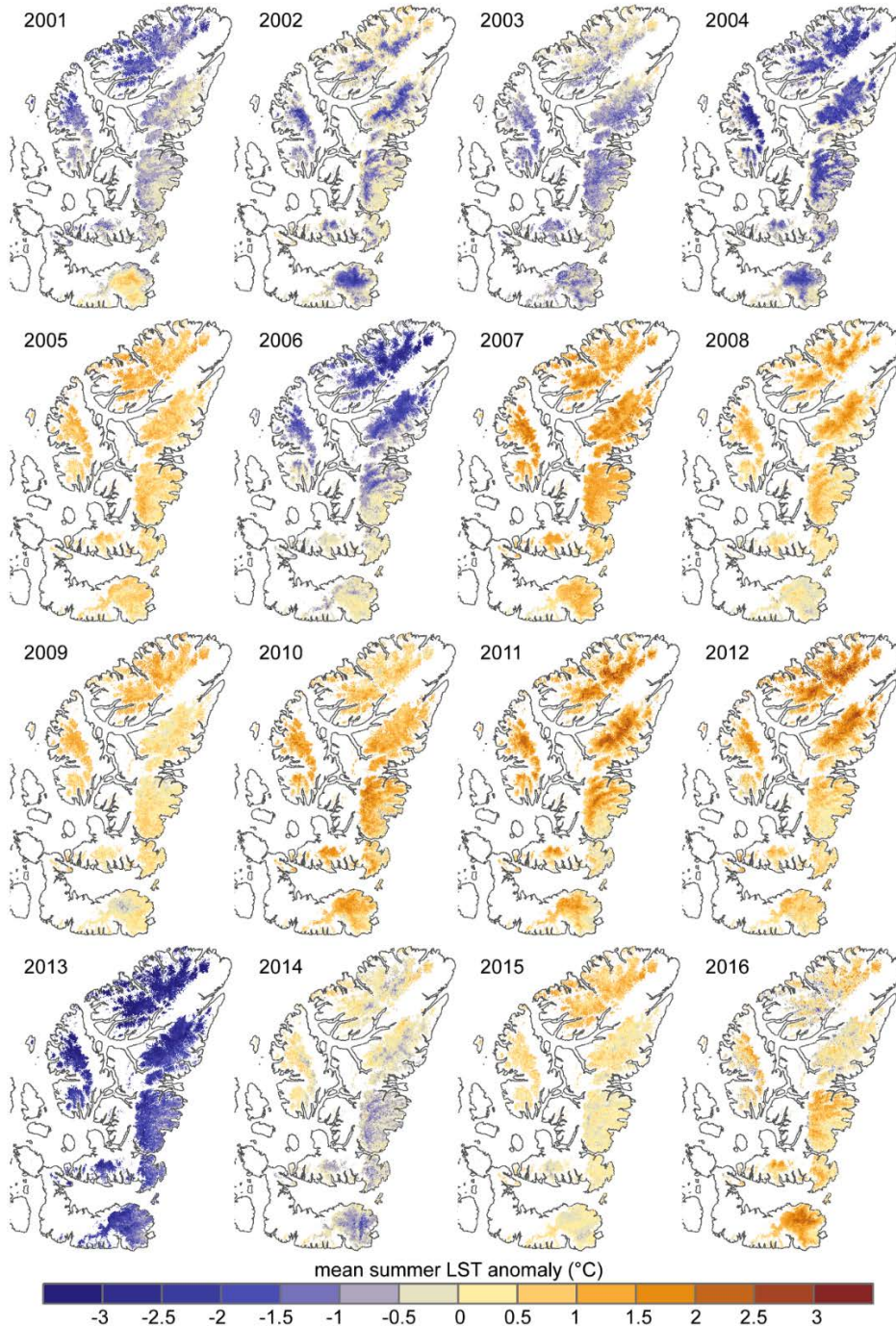
Figure S7: Mean August clear-sky BSA anomaly relative to the 2001–16 mean for the QEI ice caps relative to the 2001–16 mean. White areas outside of the ice caps indicate non-glaciated ice cover.

Where possible, references to figures in the current text (i.e. Figure 7 and Figure S7) are used instead of referring to the earlier Mortimer et al. 2016 study.

> **Revised line 273-276:**
> *'In 2005 and 2006 (years when the mean summer QEI-wide BSA anomaly was near zero and there was a large amount of spatial variability in the mean summer BSA), BSA anomalies on the western-most part of Axel Heiberg Island (Fig. 3) were double the magnitude of the QEI-wide BSA anomaly (Table 1) and of the same sign. A similar feature (large anomaly values of the same sign as the QEI-wide anomaly) was also observed in the LST anomaly record in 2005 (Fig. S7).'*
> **Revised line 339-340:**
> *'...even though strong increases in LST ($>0.1°C \, yr^{-1}$) were observed in these locations between 2001 and 2016 (Fig. 7).'*

RC 31: Figure 1 caption – Do the authors intend to reference Moderate Resolution Imaging Spectroradiometer instead of "Moderate Resolution Spectroradiometer"?

AR 31: Figure 1 Correct, it should read Moderate Resolution Imaging Spectroradiometer instead of Moderate Resolution Spectroradiometer. In revised manuscript, MODIS is used in the figure caption instead of used instead of Moderate Resolution Imaging Spectroradiometer.

Revised Figure 1 caption:
> *'Figure 1: Glaciated regions of the Queen Elizabeth Islands. Background image: MODIS 4 July 2011. Inset: red polygon shows location of Queen Elizabeth Islands, Arctic Canada.'*

RC 32: Figure 1 image – In some formats, it is difficult to differentiate the thematic colours used in the figure. Consider if there may be other colours to use. For reader friendliness, it may also help to move the legend and increase the font size of the legend text. Also, consider adding a label to the 8 regions. This may help readers in interpretation of Supplemental Table S2

AR 32: Figure 1 revised. Bottom-right inset no longer included because regional BSA values are no longer referred to in text. Labels for the major ice masses have been included on the main map. Supplemental Table 2 has been removed.

Revised Figure 1:
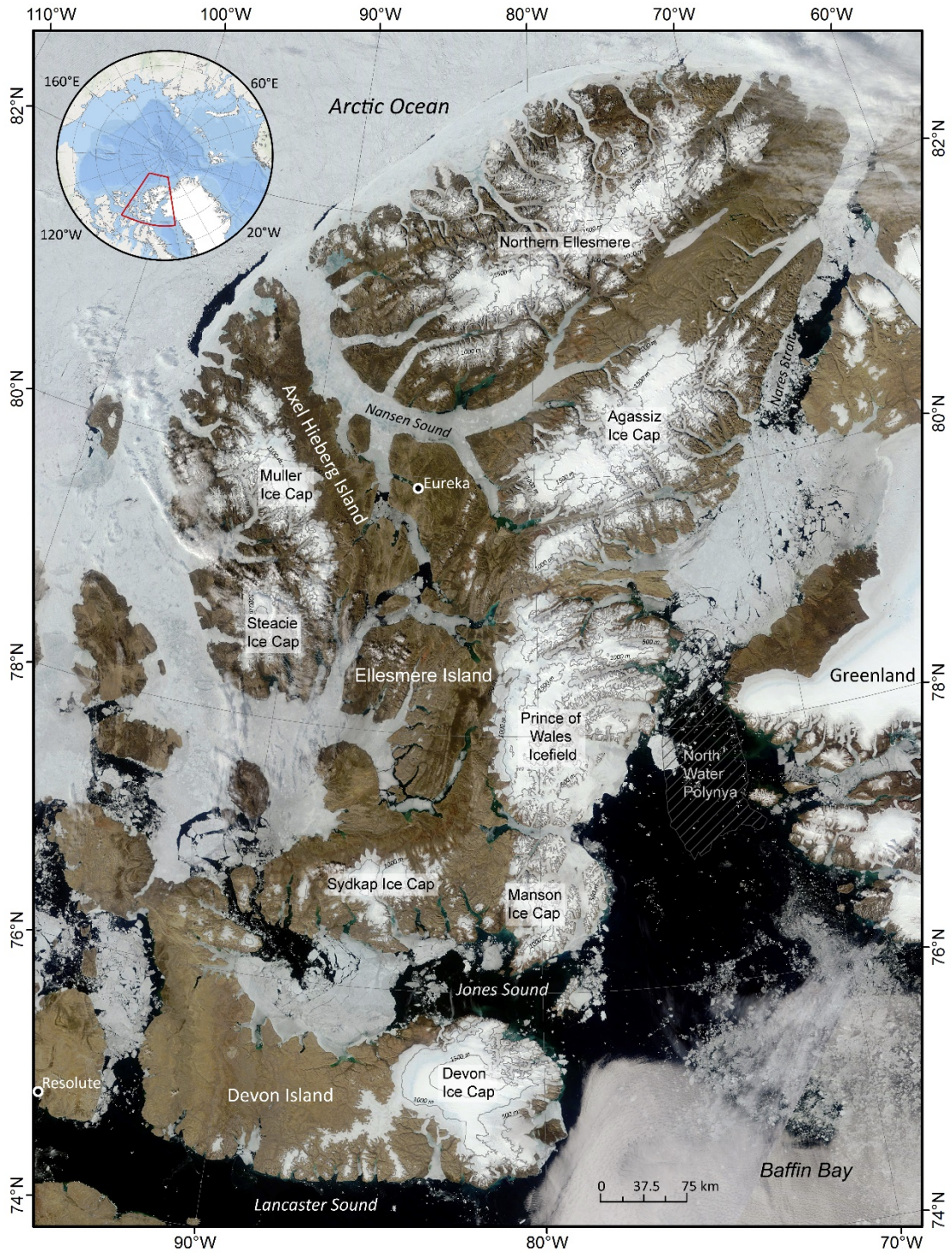
Figure 1: Glaciated regions of the Queen Elizabeth Islands. Background image: MODIS 4 July 2011. Inset: red polygon shows location of Queen Elizabeth Islands, Arctic Canada.

RC 33: Figure 4 – Figure text, misspelled word 'anomaly' in two locations, please correct.

AR 33: Figure 4 corrected for two erroneous spellings of 'anomaly'

Revised Figure 4:
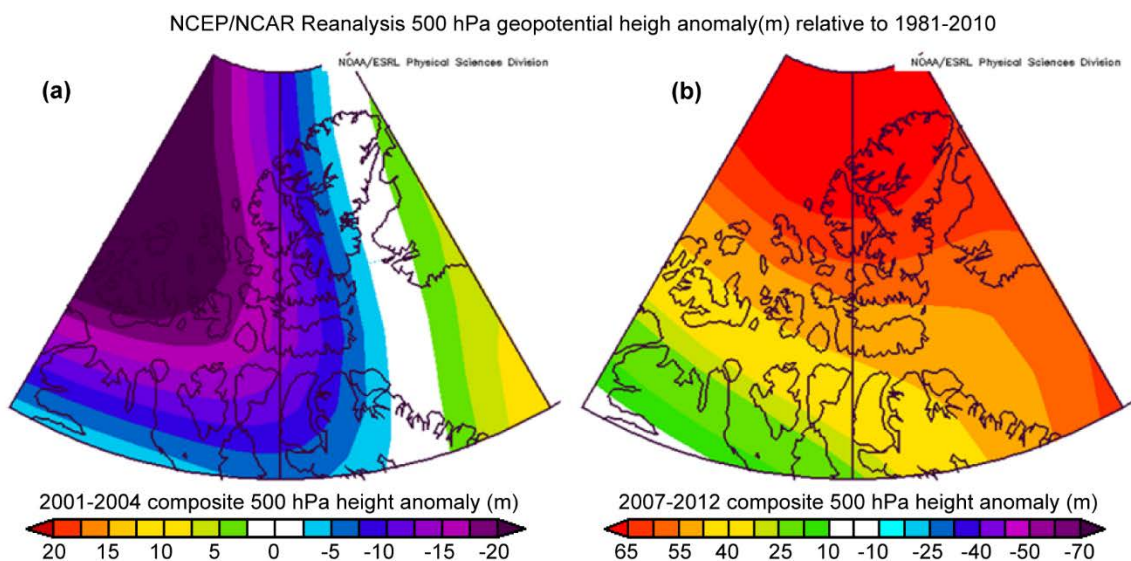
NCEP/NCAR Reanalysis 500 hPa geopotential heigh anomaly(m) relative to 1981-2010

(a)

(b)

2001-2004 composite 500 hPa height anomaly (m)

20 15 10 5 0 -5 -10 -15 -20

2007-2012 composite 500 hPa height anomaly (m)

65 55 40 25 10 -10 -25 -40 -50 -70

Figure 4: Mean summer (JJA) composite NCEP/NCAR Reanalysis 500 hPa geopotential height anomaly for (a) a period of large negative BSA anomalies (2001–04) and (b) a period of large positive BSA anomalies (2007–12). Source: https://www.esrl.noaa.gov/psd.

RC 34: Figure 5 – Why there is no data (white in figure) for the period 2001-2016 in some locations of QEI ice?

AR 34: Cloud cover results in an absence of data. The amount of missing data, presented in Table S1, varies between months and from one year to the next. Because of this variability, thresholds were set to ensure consistency between years in calculating the mean summer and mean monthly BSA. This was outlined in Section 2.3 **lines 191-194**: *'For each year during the 2001–16 period, mean summer (JJA) BSA was calculated for pixels having at least 10 BSA observations in each month (June, July, August) and at least 45 of a possible 92 observations during the JJA period. These monthly thresholds ensure both an even distribution of BSA data throughout the summer season and consistency between different years.'*

Further, to ensure the trend in BSA was not biased towards extremely warm or cold years, regressions were only computed for pixels having at least 11 mean summer BSA observations. This was outlined in **lines 197-202:** *'The mean summer (JJA) BSA and LST and the mean monthly (June, July, August) BSA, as well as the BSA and LST anomalies, were calculated on a pixel-by-pixel basis relative to the 2001–16 mean for pixels having mean summer observations in 11 or more years. These constituted ~87% and ~98% of possible BSA and LST pixels, respectively. Long-term rates of change in BSA and LST over the period 2001–16 were determined by linear regression between the 16 year records of mean summer LST/BSA and time. Consistent with the BSA and LST anomalies, regressions were computed on a pixel-by-pixel basis for all pixels having mean summer observations for 11 or more years.'*

RC 35: Figure S7 – Example of important, interesting QEI LST content for the authors to consider moving from the supplemental material to the main manuscript.

AR 35: Figure S7, which was revised to use the C6 instead of the C5 data (see **RC/AR 3**), has been moved from supplemental material to the main text and is now Figure 7.

Figure 7 (revised and moved):
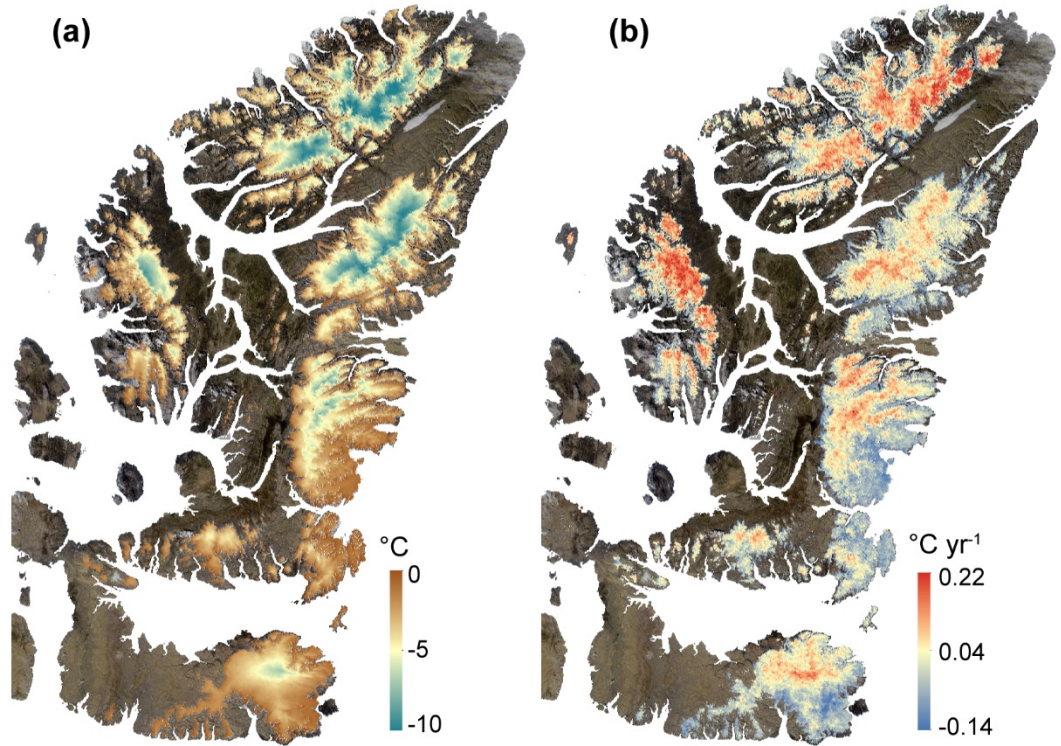
Figure 7: QEI (a) 16 year average mean summer land surface temperature (°C) and (b) linear rate of change of mean summer LST (°C yr^{-1}) for the period 2001-16 over the QEI ice caps. Background image: MODIS, 4 July 2011. Brown indicates non-glaciated land cover.

Spatiotemporal variability of Canadian High Arctic glacier surface albedo from MODIS data, 2001-16

Colleen A. Mortimer[1] and Martin Sharp[1]

[1]Department of Earth and Atmospheric Sciences, University of Alberta, Edmonton, T6G 2E3, Canada

5   *Correspondence to*: Colleen A. Mortimer (cmortime@ualberta.ca)

Abstract. Inter-annual variations and longer-term trends in the annual mass balance of glaciers in Canada's Queen Elizabeth Islands (QEI) are largely attributable to changes in summer melt. The largest source of melt energy in the QEI in summer is net shortwave radiation, which is modulated by changes in glacier surface albedo. We used measurements from the Moderate Resolution Imaging Spectroradiometer (MODIS) sensors to investigate large large-scale spatial patterns, and temporal trends,

10   and variability in the summer surface albedo of QEI glaciers and their relationship to observed changes in glacier surface temperature from 2001 to 2016. Mean summer black-sky shortwave broadband albedo (BSA) decreased at a rate of 0.029 ± 0.025 decade^{-1} over that period. Larger reductions in BSA occurred in July (-0.050 ± 0.031 decade^{-1}). No change in BSA was observed in either June or August. Most of the decrease in BSA, which was greatest at lower elevations around the margins of the ice masses, occurred between 2007 and 2012 when mean summer BSA was anomalously low. The First Principal

15   Component of the 16-year record of mean summer BSA was well correlated with the mean summer North Atlantic Oscillation Index, except in 2006, 2010, and 2016 when the mean summer BSA appears to be dominated by the August BSA. During the period 2001–16, this 16-year period, the mean summer LST increased by 0.046 049 ± 0.036 038 °C yr^{-1} and the BSA record was negatively correlated (r: -0.64 86, p<0.01) with the LST record, indicative of a positive ice-albedo feedback that would increase rates of mass loss from the QEI glaciers.

20   **1 Introduction**

The area of glaciers and ice caps in the Queen Elizabeth Islands (QEI, Fig. 1), Arctic Canada, in 2000 was ~104,000 km^2 (Arendt et al., 2013 2012). From 2000 to 2015, the summer mean surface temperature of glaciers in this region increased at a rate of 0.06 ± 0.04°C yr^{-1}, and summer mean air temperatures from 2005-20 12 were > 1.0°C warmer than the 1948-2015 mean (Mortimer et al., 2016). QEI summer mean air and glacier surface temperatures are strongly correlated with the annual and

25   summer glacier mass balances, which have become increasingly negative since at least 2003 (Gardner et al., 2013; Lenaerts et al., 2013; Wolken et al., 2016). Inter-annual variations and longer-term trends in annual glacier mass balance in the QEI are dominated by changes in summer melt (Koerner, 2005), and net shortwave radiation is the largest source of melt energy on

Commented [CM1]: Rev 1
RC 1 Title: consider removing "C6" from the title since it's not t different from C5 for the albedo and LST, and many people, befo reading the paper, have no idea what C6 is. You have appropriate mentioned the fact that you've used C6 in the paper as needed. Also consider including LST in the title, especially if you decide enhance the discussion about cause-and-effect between LST and albedo for the QEI.
AR 1: Reference to "C6" removed from the title.

Commented [m2]: Rev. 1
RC 5: Line 14: note that the range of years says 2008-2012 on li 486
AR 5: Corrected to read 2007-2012 throughout.

the QEI ice caps (Gascon et al., 2013). Variability in net shortwave radiation, in turn, is strongly modulated by changes in the surface albedo (van den Broeke et al., 2011; Tedesco et al., 2016), the ratio of reflected to incoming solar radiation.

30 The high albedo of fresh snow declines naturally over time due to settling and grain growth (Warren, 1982). This initial decrease in albedo raises the shortwave energy absorption, leading to warming and/or melt, and a further lowering of the surface albedo. Warmer temperatures and increased snowpack water content further accelerate grain growth, causing more rapid albedo decline that enhances surface warming and/or melt (Wiscombe and Warren, 1980; Colbeck, 1982). A positive snow/ice albedo feedback has been linked to accelerating high-latitude warming, and is increasingly recognized as an important

35 factor in explaining recent increases in rates of mass loss from the Greenland Ice Sheet (e.g. Tedesco et al., 2016), which lies immediately to the east of the QEI.

On glaciers and ice caps, surface warming and increased melt in summer can lead to earlier and more widespread removal of the previous winter's snowpack, and earlier and more prolonged exposure of underlying low-albedo glacier ice. Albedo decreases can also be caused by aerosol deposition (Warren and Wiscombe, 1980), ~~enhanced~~ biological activity on glacier

40 surfaces (Fountain et al., 2004), and ~~accelerated~~ the release of impurities from melting snow and ice, which become concentrated at the snow/ice surface (Clarke and Noone, 1985; Conway et al., 1996; Flanner et al., 2007; Doherty et al., 2010). Given the observed increases in air and glacier surface temperatures across the QEI (Mortimer et al., 2016) we anticipate a reduction in the surface albedo in this region, unless warming has also been accompanied by an increase in solid precipitation (Vincent et al., 2015) that is large enough to raise the surface albedo (e.g. Box et al., 2012). The expected albedo reduction

45 has, however, yet to be documented or quantified.

Decadal-scale declines in the surface albedo of the Greenland Ice Sheet~~, which lies immediately to the east of the QEI,~~ have been simulated using regional climate models, and documented using remote sensing data validated by in situ measurements (e.g. Stroeve et al., 2005, 2013; Box et al., 2012; 2017; Alexander et al., 2014; Tedesco et al., 2016; Casey et al. 2017~~Stroeve et al., 2005, 2013; Casey et al. 2017; Box et al., 2012; 2017; Alexander et al., 2014; Tedesco et al., 2016)~~. Global assessments

50 of land surface albedo (e.g. He et al., 2014) have included the QEI, but these analyses were extremely broad in nature and the detailed spatial pattern of glacier albedo change and its variation over time are unknown. Between 2000 and 2015, measured increases in both QEI summer 700 hPa air from the NCEP/NCAR R1 Reanalysis (Kalnay and others, 1996) and glacier surface temperatures from the Moderate Resolution Imaging Spectroradiometer (MODIS) ~~and glacier surface temperatures in the QEI~~ were greatest in the north and west of the ~~region~~ QEI (Sharp et al., 2011; Mortimer et al., 2016). ~~but w~~We do not know whether

55 there is a similar spatial pattern in the albedo record.

Field-based measurements provide information about the surface albedo at specific locations, but there are no long-term spatially distributed in-situ records of the surface radiation budget of glaciers and ice caps in the QEI.

Remote sensing methods enable monitoring of the surface albedo and its spatial and temporal variability at the scale of both individual ice caps and the regional glacier cover. Here, we use measurements of surface albedo from the ~~Moderate Resolution~~

60 ~~Imaging Spectroradiometer (~~MODIS~~)~~ sensors to present the first near-complete picture of variations in the summer surface albedo of QEI glaciers and ice caps from 2001 to 2016. We characterize the spatial and temporal variability in summer albedo,

2

and quantify the rate of albedo change across the QEI~~, and investigate spatial patterns in the relationship between the mean summer albedo and mean summer land surface temperature (LST) records over the QEI ice caps and glaciers from 2001 to 2016~~.

2 Data and methods

2.1 MCD43A3 data

Observations from the ~~Moderate Resolution Imaging Spectroradiometers (~~MODIS ~~sensors)~~, aboard the Terra (2000 to present) and Aqua (2002 to present) satellites (Barnes et al., 1998), are used to assess the spatial and temporal evolution of the surface albedo over the QEI glaciers and ice caps in summer (June-August). We use the MODIS/Terra and Aqua BRDF/Albedo Daily L3 Global – 500m Collection 06 (C6) product (MCD43A3, Schaaf and Wang (2015)), which provides both white-sky (bi-hemispherical reflectance under isotropic conditions) and black-sky (directional hemispherical reflectance) shortwave broadband surface albedo (Schaaf et al., 2011; https://www.umb.edu/spectralmass/terra_aqua_modis/v006, and references therein). MCD43A3 albedo is calculated daily for local solar noon ~~from~~ using atmospherically corrected surface reflectance measurements ~~from~~ made by sensors on both the Terra and Aqua satellites over a 16-day period that is centered on the ninth day of each 16-day moving window (https://www.umb.edu/spectralmass/terra_aqua_modis/v006). A semi-empirical Bidirectional Reflectance Distribution Function (BRDF) model, which describes the surface scattering/reflectance of a target as a function of illumination, is used to estimate surface albedo from directional surface reflectance information recorded by the MODIS sensors (Schaaf et al., 2002, 2011; Jin et al., 2003; Salomon et al., 2006). MCD43A3 white- and black-sky albedos are estimated from Level 2G-lite surface reflectances (MOD/MYD 09) for seven visible and near-infrared bands (spanning 0.4 to 2.4 µm) and three broad bands (shortwave (0.3-5.0 µm), visible (0.3-0.7 µm) and near infrared (0.7-5.0 µm)) in one of two ways.

If sufficient (>7) multi-date cloud-free observations with angular sampling sufficient to fully characterize the viewing/illumination geometry are acquired during a ~~16~~ 16-day period, a high quality *full inversion* is run using a semi-empirical RossThick LiSparse Reciprocal (RTSLR) kernel-driven BRDF model (Wanner et al., 1997; ~~Lutch~~ Lucht et al., 2000; Schaaf et al., 2002~~,~~; ~~201b~~ 2011). If insufficient observations (<7) are available, then a lower quality *magnitude inversion*, which relies on a priori knowledge to scale an archetypal BRDF, is used to estimate the surface albedo (Strugnell and Lutch, 2001; Schaaf et al., 2002; Jin et al., 2003; Liu et al., 2009). Data quality flags, provided in the MCD43A2 data quality assessment product, indicate whether albedo values [for each pixel] were obtained using the *full* or *magnitude inversion*. Since this study aims to generate an initial assessment of the spatio-temporal variability of the surface albedo of glaciers and ice caps in the QEI with good spatial coverage, both *full* and *magnitude inversion* data are used. Although *magnitude inversions* produce lower quality albedo estimates than the *full inversion* method, previous work using the C5 data showed that the *magnitude*

3

inversion data provide a good representation of the seasonal and spatial patterns ~~in~~ of glacier surface albedo (Schaaf et al., 2011; Stroeve et al., 2013). To our knowledge, no recent research comparing the *magnitude* and *full inversion* retrievals over glaciers and ice caps has been published for the MCD43A3 C6 data. Comparison of the MODIS C5 and C6 *full inversion* albedo data from the Greenland Ice Sheet confirmed many of the broad spatial patterns in surface albedo identified in the C5 data, but the magnitude of the C6 albedo change was much smaller (Casey et al., 2017).

2.1.1 MODIS sensor degradation

The MODIS sensors are currently operating well beyond their expected [productive] six year lifetimes (Barnes et al, 1998; Justice 1998) and the detectors are degrading (Xiong et al., 2001). For both the MODIS Terra and Aqua sensors, instruments were calibrated pre-launch (radiometric, spatial, specular calibration) (Gunther et al., 1996). On-orbit calibration procedures were included to monitor the sensor degradation that is expected as the instruments are exposed to solar radiation (Gunther et al., 1996). For the reflective solar bands (0.41–2.2 µm) the onboard calibration system includes a solar diffuser (SD) calibrated using the solar diffuser stability monitor (SDSM) (Gunther et al., 1998). Lunar and Earth view observations (select desert sites) are also used to assess radiometric stability (Sun et al. 2003). Even so, long-term scan mirror and wavelength dependent degradation which are not sufficiently accounted for by the on-board calibrators (SD/SDMS) have been observed (Xiong et al., 2001; Lyapustin et al., 2014 and references therein). Calibration degradation effects, which are largely confined to the MODIS Terra sensor, are greatest in the blue band (B3) and decrease with increasing wavelength (Xiong and Barnes 2006). An anomaly in the SD door operation (3 May 2003) and a decision to leave the door permanently open, exposing the SD to additional solar radiation, resulted in degradation of the SD on the MODIS Terra sensor that was faster than had originally been anticipated, and than was observed for the MODIS Aqua sensor (Xiong et al., 2005). Differences in the response versus scan angle (RVS) for the two side mirrors were also characterized pre-launch (Barnes et al., 1998). The RVS is important because it describes the scan mirror's response to different angles of incidence (AOI, for each band, detector and mirror side) (Sun et al., 2014). However, for the MODIS Terra sensor, following an overheating incident during pre-launch calibration, the RVS was not re-characterized and the exact pre-launch RVS characteristics are not known (Pan et al., 2007; Sun et al., 2014 and references therein). These issues have resulted in the performance of the MODIS Terra sensor being poorer than that of the MODIS Aqua sensor.

As a normal part of the operational procedure, the MODIS Characterization Support Team (http:mcst.gsfc.nasa.gov) periodically updates the calibration algorithms and approaches, during which time the entire L1B record (calibrated top of the atmosphere radiances) is re-processed to reflect improved understanding and characterization of changes to the instruments. Even so, non-physical trends in MODIS Terra data products, that result from calibration drift, have been observed and are well documented (e.g. Xiong et al., 2001; Xiong and Barnes, 2006; Franz et al., 2008; Kwiatkowski et al., 2008; Wang et al., 2012; Lyapustin et al., 2014; and references therein). The latest revision occurred with the C6 data and includes on-orbit calibration procedures to mitigate long-term calibration drift, particularly at the shorter wavelengths (Wenny et al., 2010; Toller et al.,

95

100

105

110

115

120

Commented [m8]: Rev. 2
RC 20: The paragraph (Page 4, Paragraph 3) could be rewritten t more informative and clear regarding MODIS sensor design and capabilities.
AR 20: MODIS Characterization Support Team literature has bee reviewed and this section has been re-written to be more informa

Commented [m9]: Rev. 2
RC 16: Page 4, line 98 – Delete 'some of'.
AR 16: Deleted 'some of'

Commented [m10]: Rev. 1
RC 8 Line 99: perhaps the word "detectors" should be used inste of "instruments"??
AR 8: The word "instruments" replaced by "detectors".

Commented [m11]: Rev. 2
RC 17: Page 4, line 102 – Lyapustin et al. was not the first to rep on Terra's band degradation. Recommendation to additionally rea and cite early / appropriate work, e.g. Xiong et al., 2001, Degrada of MODIS optics and its reflective solar bands calibration, doi: 10.1117/12.450646
AR 17: References to earlier studies have been added.

Commented [m12]: R2: Page 4, line 102 – Lyapustin et al. v not the first to report on Terra's band degradation. Recommendat to additionally read and cite early / appropriate work, e.g. Xiong al., 2001, Degradation of MODIS optics and its reflective solar b calibration, doi: 10.1117/12.450646
Xiong and Barnes, 2006, An overview of MODIS radiometric calibration and characterization, doi: 10.1007/s00376-006-0008-
Sun et al., 2014 Time-dependent response versus scan angle for MODIS reflective solar bands, IEEE TGRS, doi: 10.1109/TGRS.2013.2271448

2013; Sun et al., 2014; Lyapustin et al., 2014). The C6 dataset uses the on-board calibrators (e.g. SD/SDMS) and the mirror side ratios from lunar standard and Earth view observations (Toller et al, 2013; Sun et al., 2014). The C6 revision also includes an additional approach, aimed primarily at the short-wavelength bands, that uses observations of desert sites (pseudo-invariant targets) to derive instrument calibration coefficients and RVS at multiple AOIs (instead of the two AOIs provided by the SD and lunar standard) (Toller et al, 2013; Sun et al., 2014). Although this vicarious approach is less accurate than the one that uses the mirror-side ratios calibrated using a lunar standard, it has been found to provide a significant improvement to the L1B radiance measurements relative to the C5 data, prior to ~2013 (Toller 2013; Lyapustin et al., 2014). Updated L1B C6 radiances can be up to several percent higher than the C5 values (e.g. Band 3 and for most recent period ~2013 onward) (Toller et al., 2013; Lyapustin et al. 2014; Casey et al., 2017). However, evaluation of the L1B C6 Band 3 (0.46-0.48 µm) radiance over a desert site (Libya 4) identified residual errors (decadal trends on the order of several tenths of 1%; Lyapustin et al., 2014) that are within the product's stated accuracy (2% in absolute reflectance units for the reflective solar bands (Barnes et al., 1998; Justice et al., 1998)). The impact of the C6 updates on higher level MODIS science products is difficult to quantify because the corrections are time, mirror-side, angular, and detector dependent (Toller et al., 2013; Lyapustin et al. 2014; Sun et al., 2014). In addition, the C6 revision includes updates to algorithms (in addition to the calibration updates) used in the derivation of specific higher-level products (https://www.umb.edu/spectralmass/terra_aqua_modis/v006 outlines changes made to the MCD43A3 C6 data product). Important for the current study, however, is that recent analysis of surface albedo over the Greenland Ice Sheet, immediately to the east of the QEI, using MODIS C6 data (including the MCD43A3 product used in this study) identified statistically significant albedo declines over the wet snow zone (Casey et al., 2017). For the most part, these declines are thought to be physically real (Casey et al., 2017), which gives us confidence in the albedo trends presented here. There are no long-term, spatially distributed, in situ albedo records from the glaciers and ice caps in the QEI, so a comparison. This is both a motivation for, and a limitation of, the current study.

Furthermore, the MCD43A3 data used here were produced only under clear sky conditions (Hall et al., 2002; 2012). A conservative cloud mask is applied to remove observations made when clouds are detected (Ackerman et al., 1998). The resulting data gaps may introduce variability in the albedo record that is not representative of true physical change. Despite this, the MCD43A3 albedo product has been found to provide a reasonable representation of the seasonal albedo cycle over glaciers and ice caps (e.g. Stroeve et al., 2006). Hence, in the absence of long-term ground measurements of glacier surface albedo in the QEI, we made the assumption that this is also the case in the QEI.

The principal uncertainties in MODIS-derived surface albedo data arise from cloud contamination and sensor degradation. Similarity in the spectral signatures of snow, ice, and thin cloud makes it difficult to discriminate between these surface types (Strabala et al., 1994; King et al., 2004), and the conservative MODIS cloud mask tends to detect more clouds than actually occur over snow and ice (Ackerman et al., 1998; Hall et al., 2008a). Thus, the absence of observations for periods when clouds are present and the removal of data for periods when clouds are detected may introduce variability in the albedo record that is not representative of true physical change. Despite this, the MCD43A3 albedo product has been found to provide a reasonable representation of the seasonal albedo cycle over glaciers and ice caps (e.g. Stroeve et al., 2006). Hence, in the absence of long-

Commented [m13]: Rev. 2
RC 18: Page 4, paragraph 3. Suggestion for authors to reread literature on MODIS sensor calibration, degradation and capabilities. Line 110, more correct to state that C6 did improve radiance measurements from launch to ~2013. It remains to be assessed how accurate and reliable MODIS C6 data will be moving forward from C6 implementation (~2013 to present). Line 110: Recommendation to check the MODIS Characterization Support Team literature https://mcst.gsfc.nasa.gov/publications?f%5Btype%5D=102 .
AC 18: Literature has been reviewed and note about improved radiances up until ~2013 has been added.

Commented [m14]: Rev. 2
RC 19: For lines 113-114, it is not that the sensor is capable of identifying trends greater than 0.01, so much as +/- 0.01 is the limit of MODIS sensor accuracy and precision. The paragraph could be rewritten to be more informative and clear regarding MODIS sensor design and capabilities.
AC 19: This paragraph has been re-written to be more informative and accurate regarding MODIS sensor design and capabilities. The text 'is capable of identifying trends greater than 0.01' has been removed.

Commented [m15]: Rev. 2
RC 16: Page 3, lines 89-91 – Suggestion to edit sentences. As written, one could glean that it is difficult to discriminate between surface snow and ice vs cloud spectral visible-thermal infrared response. This is not always difficult to do spectrally. If the authors intend to discuss cloud remote sensing only, please clarify this. A more appropriate reference than Hall 2008a, may be Hall et al., 2 MODIS snow-cover products, Remote Sensing of Environment, 181-194.
AR 16: text moved and re-written for clarity. Reference to Hall 2 has been added. The issue of concern here is the absence of cloud, which can potentially introduce additional variability in the dataset that is not representative of physical changes on the surface.

term ground measurements of glacier surface albedo in the QEI, we made the assumption that this is also the case in that region.

160 The MODIS sensors are currently operating well beyond their expected [productive] six year lifetimes and some of the instruments are degrading (Wang et al., 2012; Toller et al., 2013). Systematic (decreasing) temporal trends are present in measurements in the visible and NIR (bands 1-7) of the MODIS C5 data (Lyapustin et al., 2014). Calibration degradation effects, which are largely confined to the Terra sensor, are greatest in the blue band (B3) and decrease with increasing wavelength (Lyapustin et al., 2014). Over time, un-corrected sensor degradation gives rise to decreasing measured surface

165 radiances, which may result in apparent MODIS-derived albedo declines that differ from the true physical change. Contrary to the findings of earlier work that identified strong albedo declines over the dry snow zone of the Greenland Ice Sheet from 2001-2013 using the C5 data (e.g. Stroeve et al., 2005, 2013; Box et al., 2012; Alexander et al., 2014), a recent investigation concluded that much of the observed decline in broadband albedo from Terra-only data resulted from sensor degradation (Polashenski et al., 2015).

170 Long-term drifts in sensor calibration are addressed in the C6 data used in this study. A new calibration technique that uses in-orbit data from pseudo time-invariant desert site targets is in the calculation of C6 surface reflectances (Toller et al., 2013). This vicarious calibration approach has improved the precision of C6 reflectances, and it also mitigates long-term sensor drift, particularly at the shorter wavelengths. The C6 post-calibration residual error is on the order of several tenths of one percent for top of the atmosphere (TOA) reflectance (Lyapustin et al., 2014), but larger discrepancies between calibrated Aqua and

175 Terra measurements have been observed in the most recent data (post 2014) (Casey et al., 2017). MODIS C6 data have been shown to be capable of identifying trends in surface albedo >0.01 decade^{-1} (Lyapustin et al., 2014). A recent analysis of summer (June-August) ice surface albedo changes from MODIS C6 data identified statistically significant declines in surface albedo over the wet snow zone of the Greenland Ice Sheet during the period 2001-2016. For the most part, these decreases in surface albedo are thought to be physically real (Casey et al., 2017).

180 There are no long-term, spatially distributed, in situ albedo records from the glaciers and ice caps in the QEI, so a comparison between the MCD43A3 records and ground observations is not possible, and this is a limitation of this study. Ground-truthing of the MOD10A1 C6 albedo product over the Greenland Ice Sheet, immediately adjacent to the QEI, has been undertaken using in situ measurements from the Greenland Climate Network (GC-Net) and the Programme for Monitoring of the Greenland Ice Sheet (PROMICE) (Box et al., 2017). This study found the MOD10A1 C6 data to be a reasonable representation

185 of the true surface albedo. In the absence of quality spatially distributed field measurements of surface albedo from our study area, we assume that this is also the case on the QEI ice caps.

Commented [m16]: Rev. 2
RC 2: "In the data and methods section (Page 4, line 122) MOD10A1 data was mentioned "to be a reasonable representatio the true surface albedo". Does this refer to analysis conducted by authors for this manuscript or to Box et al., 2017? Please clarify. MOD10A1 data was not inspected by the authors for this manusc why not?"
AC 2: The reference to the MOD10A1 data has been removed an the methods section detailing MODIS sensor calibration issues ha been revised.

Commented [m17]: Rev 1
RC 9 Line 120-124: this discussion of MOD10A1 should be dele it is not relevant to this paper, and MOD10A1 is never mentioned again in the paper; it really isn't good validation for MCD43A3
AR 9: Discussion of MOD10A1 has been deleted. Additionally, response to an anonymous reviewer's comments, this section has been revised to be more informative regarding MODIS sensor de and capabilities.

2.1 1.2 MCD43A3 data processing

Summer (1-2 June (day 152) to 30-31 August (day 243)) MODIS MCD43A3 and MCD43A2 Collection 6 (Schaaf and Wang, 2015) data for MODIS tiles h17v00, h16v00, h16v01, and h15v01 for the period 2001-2016 were obtained from the NASA/USGS Land Processes Distributed Active Archive Center (Schaaf and Wang (2015), http://lpdaac.usgs.gov/ accessed November 2016). Daytime clear-sky white- and black-sky shortwave broadband and visible albedo data (MCD43A3) and accompanying quality assessment information (MCD43A2) were extracted from the hierarchical data format files and re-projected from the standard MODIS sinusoidal projection to a North America Albers Equal Area projection, WGS84 datum, 500 m resolution, using the MODIS re-projection tool version 4.1 (https://lpdaac.usgs.gov/tools/modis_reprojection_tool). The maximum summer (June-August) solar zenith angle over our study area (74°) was below the product's stated accuracy (<75°, Vermote et al., 2011; Wang et al., 2012), so no additional filtering was performed to remove data with high solar zenith angles. The white- and black sky albedos (representing completely diffuse and completely direct illumination, respectively) represent extreme estimates of the actual (blue-sky) bi-hemispheric surface albedo. To avoid redundancy, only results for the black-sky albedo (BSA) (which are fully consistent with those obtained using the white-sky albedo (WSA)) are presented here. The BSA was selected because our analysis focuses on albedo retrieved under clear-sky conditions. This approach is consistent with previous work using MCD43A3 data (e.g. Alexander et al., 2014; Tedesco et al., 2016; Casey et al., 2017). Unless otherwise specified, henceforth BSA refers to the shortwave broadband black-sky albedo.

2.2 MODIS LST (MOD11A2)

Warmer surface temperatures increase the rates grain metamorphism and snowmelt, resulting in larger snow grains which have a lower albedo than those of fresh snow (Wiscombe and Warren 1980; Colbeck 1982) (Sect. 1.0). Air and surface temperatures also affect the timing of removal of the seasonal snowpack, which exposes lower albedo firn or glacier ice. Additionally, the melt of glacier ice releases impurities that have a low albedo and thus change the surface albedo of both ice and snow (e.g. Clarke and Noone 1985; Doherty et al., 2010; Sect. 1.0). As such, analysis of the glacier surface temperature and comparison of these data with the albedo record is included to help understand the observed spatiotemporal patterns of glacier albedo change in the QEI.

We use tThe Eight-Day L3 Global Land Surface Temperature and Emissivity product (MOD11A2) C5C6, which has been found to be a reasonable proxy for the duration and/or intensity of summer melting in the QEI (Sharp et al., 2011; Mortimer et al., 2016), was used to investigate the relationship between glacier surface temperature and albedo. Only the 'daytime' LST data, generated with the day/night algorithm of Wan and Li (1997), is evaluated here. This is consistent with previous work in this region (e.g. Sharp et al., 2011, Mortimer et al. 2016). MOD11A2 daytime and night-time LSTs are computed from MODIS channels 31 (11 µm) and 32 (12 µm) using a split-window technique and all available daytime clear-sky scenes from the Terra satellite for sequential eight day periods (Wan et al., 2002). These data have a spatial resolution of 1 km and nominal product accuracy of ± 1°C but the accuracy over snow and ice surfaces can be as low as ±2°C (Hall et al., 2008zb; Koenig and Hall,

Commented [m18]: Rev. 2
RC 21: Page 5, line 129 – Suggestion to move citation to correct location in the sentence, i.e. Schaaf and Wang 2015 reference should immediately follow MCD43 product mention.
AR: citation moved.

Commented [m19]: Rev. 2
RC 22: Page 5, line 141 – Awkward as written, suggestion to revise to clarify further use of BSA term e.g. 'henceforth BSA refers to black sky albedo MODIS shortwave broadband data.'
AR 22: Line no longer included in manuscript.

Commented [CM20]: Rev 1.
RC: Though they point out that albedo and LST are negatively correlated for the QEI, they do not discuss that relationship as cause-and-effect in either the Abstract or the Conclusion. The relationship between albedo and LST is discussed in Section 4.2 but I would liked that discussion to have been better integrated throughout the paper.

Commented [m21]: Rev. 2
RC 4: "Section 2.2 discusses MODIS LST data. Why was Collection 5 MOD11A2 data used? (Page 5, lines 155-157) Communication with the MODIS data distributor, LP DAAC, revealed that MOD11A2 and MYD11A2 Collection 6 data have been available since mid-2015. Additionally, with the discussion of the Terra sensor degradation, it seems short-sighted to use Terra data only. Why was Terra data used? Was Aqua data used (i.e. MYD11A2)? If not, why not? Recommendation to add MYD11A2 data analysis."
AR 4: The manuscript has been revised and now uses the C6 MOD11A2 data instead of the C5 product. Terra data was used because of the time period under investigation with Terra data being since 2000 and Aqua data only being available since 2002. The Terra data allowed comparison with the albedo record for the full time period (2001-16).

220 2010). The LST analyses presented here are an update of those presented by Mortimer et al. (2016) which used the MODIS C5 data. The two analyses also differ in the time period used (we use 2001-16 instead of 2000-15 to coincide with the BSA analysis). Pixels for which the average LST error (QC_Day LST error flag) exceeded 2°C were removed from the analysis and any remaining pixels having a temperature >0°C were assigned a temperature of 0°C (e.g. Hall et al., 2008a; Mortimer et al., 2016). Uncertainties in trends derived from the MOD11A2 LST data in the MOD11A2 LSTs arise mainly from cloud

225 contamination (Box et al., 2012; Hall et al., 2012) and the removal of observations for periods when clouds are detected (Ackerman et al., 1998; Hall et al., 2008ba). Variability in the number of clear-sky days within each observation period and from one year to the next was not found to introduce significant variability in the MODIS-derived LST relative to the true near-surface air temperature in the QEI (see Mortimer et al., 2016). MOD11A2 C6 data were downloaded from (https://lpdaac.usgs.gov/, accessed September 2014 - October 2015 and June 2017) and re-projected to a North America Albers

230 Equal Area projection, WGS84 datum, 1 km resolution.

2.3 Mean summer BSA and LST

Annual precipitation in the QEI is low (<400 mm yr^{-1}) and varies little from one year to the next; iIn contrast, the annual temperature range is large (> 40°C) (Braithwaite, 2005). Inter-annual variability in QEI annual mass balance is dominated by changes in the summer mass balance (Koerner, 2005), which, in turn, is strongly correlated with summer air temperature

235 (Sharp et al., 2011). Spatial and temporal patterns in BSA and LST were, therefore, evaluated for the summer months (June-August). For each year during the 2001-2016 period, mean summer (JJA) BSA was calculated for pixels having at least 10 BSA observations in each month (June, July, August) and at least 45 of a possible 92 observations during the JJA period. These monthly thresholds ensure both an even distribution of BSA data throughout the summer season and consistency between different years. Mean summer LST was calculated following the methods of Mortimer et al. (2016) where the mean

240 summer LST is calculated for pixels having at least 7 of a possible 12 observations between 1-2 June (day 153) and 28-29 August (day 241).

The mMean summer (JJA) BSA and LST and the mean monthly (June, July, August) BSA, as well as the BSA and LST anomalies, anomalies were calculated on a pixel-by-pixel basis relative to the 2001-2016 mean for pixels having mean summer observations in 11 or more years. This These constituted ~87% and ~9398% of possible BSA and LST pixels, respectively.

245 Long-term rates of change in BSA and LST over the period 2001-2016 were determined by linear regression between the 16 year records of mean summer LST and / BSA and time. Consistent with the BSA and LST anomalies, regressions were computed on a pixel-by-pixel basis for all pixels having mean summer observations for 11 or more years. Following Casey et al. (2017), BSA trends between -0.001 yr^{-1} and +0.001 yr^{-1} are considered to be negligible. Negligible trends were defined by Casey et al. (2017) on the basis of the magnitude of the residual calibration uncertainties in the C6 data (on the order of several

250 tenths of one percent in TOA reflectance (Lyaputsin et al., 2014)) over pseudo-invariant desert sites (Sect. 2.1.1). albedo trends below the detection limit of the C6 data (0.01 decade^{-1} (Lyapustin et al., 2014)) are considered to be negligible.

8

Commented [m22]: Rev. 2
RC 11: Recommendation for the authors to clearly state the additional QEI LST analysis provided in this manuscript as comp[...] to Mortimer et al., 2016.
AR 11: Following your recommendations, the manuscript has be[...] revised and now includes the MOD11A2 C6 data instead of the C[...] data. Text has been added to the Methods (Section 2.2) to clearly state the differences in the QEI LST analysis provided in this manuscript compared to Mortimer et al., 2016.

Commented [m23]: Rev. 1
RC 10.1: Hall et al. (2008a) did not remove pixels with errors >2[...] C that were below zero, if I am recalling correctly.
AR 10.1: You are correct in pointing out that Hall et al. 2008a di[...] not remove pixels with errors >2°C that were below 0°C. Hall et [...] (2008a) developed melt-frequency maps and identified any pixels[...] with a LST >0°C as experiencing melt. The inclusion of Hall et a[...] (2008a) at the end of this sentence is, as you say, incorrect and misleading. As such, the reference to Hall et 2(008a) has been removed and only the reference to Mortimer et al. (2016) is inclu[...]
RC 10.2: …'it's impossible to have a temperature greater than ze[...] and still be ice.':
AR 10.2: Although the temperature of pure ice and snow cannot [...] exceed 0°C, many pixels are not comprised solely of pure ice and[...] snow. Rock, dust, impurities and ponded water (for which the maximum temperature can exceed 0°C) can exist on the snow/ice surface. The presence of these materials within the 1km x 1km pi[...] can result in an LST >0°C. Mortimer et al. (2016) found that pixe[...] having an LST >0°C were mainly located on outlet glaciers and [...] the ice-cap margins and inferred that such pixels probably contain[...] a mixture of exposed rock, ice, and meltwater during the melt sea[...] The presence of materials other than pure ice and snow within a p[...] can, therefore, result in an LST greater than maximum temperatu[...] pure ice and snow. To mitigate this effect, ice-covered pixels wit[...] LST >0°C were reassigned a value of 0°C.

Commented [m24]: Rev. 2
RC 23: Page 5, lines 151-152 – The authors seem to generalize i[...] that "uncertainties in the MOD11A2 LSTs arise mainly from clou[...] contamination". Suggestion to reread relevant literature and prese[...] accurately. Does the sentence refer to over snow only?
AR 23: This sentence referred to uncertainties in the trends deriv[...] from the MOD11A2 data and not in the MOD11A2 data itself. T[...] text has been revised for clarity.

Commented [m25]: Rev. 1
RC 11 Line 155: it should be stated that MOD11A2 Collection 6[...] were downloaded
AR 11: C6 added.

Commented [m26]: Rev. 2
RC 24: Page 6, line 159 – Is there a reference from precipitation [...] records/data in QEI? i.e. what station, record or data is 400 mm/y[...] derived from?
AR 24: The reference for the 400 mm/yr should be Braithwaite [...] 2005. This reference, included at the end of the following senten[...] refers to both the temperature and precipitation ranges. Omitted reference now included.

To explore whether there were data contained any other spatial patterns that differed from the long-term (linear) trend, a Principal Components Analysis of the 16 year mean summer BSA record was performed using data from all pixels with mean summer BSA observations in every year (50% of pixels).

To investigate the spatial pattern of the relationship between surface temperature (LST) and albedo (BSA), linear correlations between the 16 year LST and BSA records were computed. The MCD43A3 C6 albedo data are produced daily whereas the MOD11A2 LST data are produced only every eight days. For this direct comparison between the LST and BSA data, eight day BSA averages were computed from the daily data for the same eight day periods as the MOD11A2 LST product, and resampled to a 1 km spatial resolution (nearest neighbour resampling). For each year, mean summer BSAs were computed from these eight day averages for all pixels having at least seven 7 of a possible twelve 12 observations, consistent with the computation of mean summer LST. (Sect. 2.2). The difference between the mean summer BSA values derived from these 8-day averages and those computed from the daily data (0.008) is within the uncertainty of MODIS reflectance products (0.05 for solar zenith angle <75°; Vermote et al., (2011)). Linear correlations between the 16 year BSA (eight day averaged) and LST records were then computed on a pixel-by-pixel basis for all pixels having LST and BSA observations in all years (~8046% of all possible pixels).

To ensure that only data for glaciated surfaces were retained, all BSA and LST outputs used in this analysis were clipped to the Randolph Glacier Inventory v3.2 region 32 (Arctic Canada North) reference polygons (Arendt et al., 20132012; Pfeffer et al., 2014). Surface elevations were obtained from the Canadian Digital Elevation Dataset (CDED) edition 3.0, scale 1:50 k, re-sampled to a 500 m resolution.

3 Results

3.1 Mean summer albedo

Annual maps of the mean summer clear-sky broadband shortwave black-sky MCD43A3 albedo for all glacier-covered surfaces in the QEI for the 2001-2016 period are presented in Fig. ure 2. The QEI-wide mean summer BSA, averaged across all 16 years, was 0.550 ± 0.115 (mean $\pm$ 1 standard deviation; Table 1). The lowest QEI-wide mean summer BSA (0.539 ± 0.127) was recorded in 2011 while the highest (0.668 ± 0.089) was recorded in 2013 (Table 1).

In general, mean summer BSA is lower around the margins of the ice masses, where glacier ice is exposed in the summer, than it is in the higher elevation interior regions where snow or firn are exposed year-round (Fig. 2). During years when the QEI-wide mean summer BSA was low (e.g. 2011), we observed a broad zone of low albedo values (< 0.4) around the margins of the major ice masses (Fig. 2). Conversely, in years when the mean summer BSA was high (e.g. 2013), this zone was much less obvious. High data dropout at high elevations on Axel Heiberg Island, and over the summit of the Devon Ice Cap in 2014 and 2006 (Table S1), may have produced a negative albedo bias for these regions, since the albedo is typically greater at higher

Commented [m27]: Rev. 2
RC 8: Include references to Tables, methods as appropriate.
AR 8: Additional references to Tables, Figures, and methods have been added throughout.

Commented [m28]: Rev. 2
RC 5: "Reorganization of content is advised toward readability. There are several cases where content is difficult to follow. Exam Results Section, 3.1 Suggestion to add sentences clarifying and further detailing results. As written, parts of the section are terse non-intuitive."
AR 5: Section 3.1 has been re-ordered and additional text has be added for readability.

Commented [m29]: Rev. 2
RC 25: Page 7, line 195 – Suggestion to include MCD43A3 for clarity and completeness.
AR 25: Mention of MCD43A3 included for clarity and complete as suggested.

elevations. Aggregating the 2001-16 average mean summer BSA into 50 m elevation bins, we observed a linear rate of BSA increase with elevation (0.0085 per 50 m elevation bin, $r^2 = 0.99$).

In addition to the mean summer (JJA) BSA, the monthly mean BSA values for June, July, and August, were also investigated
285 (Sect. 2.3) (Table 2, Fig. S1-S3). July had the lowest 16-year monthly mean BSA (0.551 ± 0.131), followed closely by August (0.579 ± 0.127) (Table 2, ~~Fig. S1-S3~~). In each year during the 2001-~~20~~16 period, the highest summer monthly BSA was always recorded in June while the lowest monthly BSA was recorded in either July or August. The lowest monthly mean BSA values for June and August were recorded in 2011, while the lowest~~; for~~ July, ~~the lowest monthly~~ mean BSA occurred in 2012. The highest monthly mean BSA for both June and July occurred in 2013; for August, it occurred in 2003. ~~and may indicate early~~
290 ~~onset of snowfall that fall.~~

~~In general, mean summer BSA is lower around the margins of the ice masses than in the higher elevation interior regions (Fig. 2). Aggregating the 2001-2016 average mean summer BSA into 50 m elevation bins, we observed a linear rate of BSA increase with elevation (0.0085 per 50 m elevation bin, r² = 0.99). During years when the QEI-wide mean summer BSA was low (e.g.~~
~~2011), we observed a broad zone of low albedo values (< 0.4) around the margins of the major ice masses (Fig. 2). Conversely,~~
295 ~~in years when the mean summer BSA was high (e.g. 2013), this zone was much less obvious. High data dropout at high elevations on Axel Heiberg Island and over the summit of the Devon Ice Cap in 2014 and 2006 (Table S1), may have produced a negative albedo bias for these regions, since the albedo is typically greater at higher elevations.~~

3.2 Albedo anomalies

3.~~1~~2.1 Mean summer (JJA) BSA anomalies~~Albedo anomalies: 2001 to 2016~~

300 The mean summer BSA anomal~~yies~~, relative to the 2001-16 mean, are presented in Figure 3 and Table 1. For consistency with the regression analysis (Sect. 3.3), BSA anomalies were only computed for pixels having mean summer BSA observations in 11 or more of the 16 years (Sect. 2.3). The period 2001-16 is characterised by a six-year period of positive BSA anomalies (2001-06) followed by a six year period of negative BSA anomalies (2007-12) (Table 1). ~~QEI wide and regional BSA anomalies, relative to the 2001-2016 mean, were positive from 2001 to 2006 and negative from 2007 to 2012 (Table 1, Fig.~~
305 ~~3).~~ Positive BSA anomalies were also observed in 2013 (+0.060) and 2014 (+0.015), while 2015 (-0.022) and 2016 (-0.005) saw a return to negative anomalies (Table 1). ~~For each region shown in Fig. 1, the most negative regionally averaged BSA anomalies occurred in either 2001 or 2012, while the most positive regionally averaged BSA anomalies occurred in either 2004 or 2013 (Table S2).~~ Negative BSA anomalies during 2007-~~20~~12, which indicate a larger absorbed fraction of incoming shortwave radiation relative to the 16-year mean, coincide, and are consistent with, positive summer air and glacier surface
310 temperature anomalies in the QEI from 2007 to 2015 (Mortimer et al., 2016). Higher temperatures increase the rate of snow grain metamorphism which lowers the surface albedo (Wiscombe and Warren, 1980; Colbeck, 1982; Warren 1982), and a lower albedo increases the proportion of solar radiation absorbed at the ice-air interface, providing more energy for surface

10

warming and melt. This positive feedback mechanism may have contributed to the tripling of glacier mass loss from this region between 2004-06 and 2007-09 (Gardner et al., 2011).

315 There was no year in which the BSA anomalies for all glaciated pixels were either all positive or all negative. The lowest amount of spatial variability in mean summer BSA anomalies (Fig. 3) was observed in years when the QEI-wide mean summer BSA anomaly was either extremely positive (2004 and 2013) or extremely negative (2011 and 2012) (~~Fig. 3~~Table 1). In 2004 and 2013 (large positive QEI-wide BSA anomalies), large positive BSA anomalies (> 0.1) were observed ~~mainly~~ at lower elevations around the margins of the ice masses, while BSA anomalies were near zero at higher elevations in the interiors of

320 the ice masses (Fig. 3). In 2011 and 2012 (large negative QEI-wide BSA anomalies), a similar spatial pattern, but with anomalies of opposite~~,~~ sign,~~spatial pattern~~ was observed.~~, with large negative BSA anomalies occurring at low elevations; expect on the Devon Ice Cap in 2012 when BSA anomalies over most of the ice cap were near zero (> -0.0125).~~

~~T~~the largest amount of spatial variability in the mean summer BSA occurred in years when the QEI-wide BSA anomaly was near zero (between ~-0.0048 and +0.0030; Table 1). In 2005, 2006, and 2016, BSA anomalies in a region that includes the

325 eastern half of the Devon Ice Cap, the majority of the Manson Icefield, and the southernmost portion of the Prince of Wales Icefield were often opposite to those observed in the rest of the QEI (Fig. 3). These regions are in close proximity to open water sources in Baffin Bay (Fig. 1) which is largest moisture source for the QEI (Koerner, 1977). Variability in the extent of open water in the QEI's interisland channels has previously been correlated with the variability in summer temperatures (Koerner, 1977) and the 500 hPa geopotential height anomalies in the QEI (Bezeau et al., 2015). Nearby open water sources

330 may serve to moderate the surface albedo variability in this eastern maritime region through more frequent and/or persistent snowfall and riming events in warm summers when the open water extent is large (Koerner, 1977; 1979; Alt, 1978). ~~In years when the QEI-wide BSA anomaly was near zero (between ~-0.0048 and +0.0030; Table 1), BSA anomalies were of opposite sign to those in the rest of the QEI in a region that includes the eastern half of the Devon Ice Cap, the majority of the Manson Icefield, and the southernmost portion of the Prince of Wales Icefield (Fig. 3). In 2005 and 2006 when the QEI-wide BSA~~

335 ~~anomalies were small and positive (0.0035 and 0.0030, respectively), BSA anomalies in this region were negative. Conversely, in 2016 when the QEI-wide BSA anomaly was small and negative (-0.0048), large negative BSA anomalies were observed in this region while only weak negative, or even positive, BSA anomalies occurred elsewhere. This eastern maritime region is located close to open water sources in Baffin Bay (Fig. 1). These areas may moderate surface albedo variability through more frequent and/or persistent snowfall and riming events in warm summers when the open water extent is large (Koerner, 1977;~~

340 ~~1979; Alt, 1978).~~

In 2005 and 2006 (years when the mean summer QEI-wide BSA anomaly was near zero and there was a large amount of spatial variability in the mean summer BSA), ~~large~~ BSA anomalies on the western-most part of Axel Heiberg Island (< -0.05; Fig. 3) were double the magnitude of the QEI-wide BSA anomaly (Table 1) and were of the same sign. A similar feature (large anomaly values of the same sign as the QEI-wide anomaly) was also observed in the LST anomaly record in 2005 (Fig. S7).

345 ~~In years when BSA anomalies in maritime regions of the southeastern QEI were opposite to those in the rest of the QEI, BSA anomalies on the western-most part of Axel Heiberg Island tended to be large (< -0.05; Fig. 3) though of the same sign as the~~

11

~~QEI-wide BSA anomaly (Table 1).~~ Examination of the 500 hPa geopotential height anomalies for 2001-2016 in NCEP/NCAR reanalysis R1 data (Kalnay et al., 1996; https://www.esrl.noaa.gov/psd) ~~reveals~~ shows that in years when the mean summer QEI-wide BSA anomaly was strongly negative (e.g. 2001-~~20~~04) (or positive (e.g. 2007-~~20~~12)) a persistent ridge (trough) was centred over the north and west of the QEI (which includes Axel Heiberg Island) (Fig. 4). These circulation features are likely responsible for the strong negative BSA anomalies observed over Axel Heiberg Island because~~.~~ ~~c~~Clear sky conditions that accompany anticyclonic circulation increase the proportion of incoming shortwave radiation received at the air-ice interface, providing more energy for melt, and driving albedo decline.

~~Finally, when the QEI-wide BSA anomaly was small and positive (<0.03, e.g. 2001 and 2003), BSA anomalies on either side of the north-south trending mountain ranges of eastern Ellesmere and Devon Islands were typically of opposite sign. For example, in 2001, positive BSA anomalies occurred on Devon Ice Cap (southeast QEI) and on the eastern side of the north-south trending mountain range of eastern Ellesmere Island, while negative BSA anomalies occurred in the north and west of the QEI (Fig. 3). We note, however, that there were also instances of instances of positive BSA anomalies at higher elevations in the interior regions of the ice masses on Axel Heiberg Island and northwest Ellesmere Island. In 2003, negative BSA anomalies dominate the south and east of the QEI while BSA anomalies were positive in the northwest of Ellesmere Island and generally negative on Axel Heiberg Island (western QEI). This southeast-northwest spatial pattern is similar to the pattern of LST change described by Mortimer et al. (2016) where LST change was greatest in the north and west of the QEI.~~

3.2.2 Summer monthly BSA anomalies

In addition to the mean summer (JJA) BSA anomalies, the mean June, July, and August BSA anomalies were also examined (Fig. S4-S6) (Sect. 2.3). ~~The spatial pattern of BSA anomalies also varies from month to month (Fig. S4-S6). T~~the sign of the mean July BSA ~~QEI-wide BSA~~ anomaly (Table 2) was always ~~the same as~~consistent ~~as~~with that of the mean summer (JJA) ~~QEI-wide~~ BSA anomaly (Table 1).~~2, Fig. S5).~~ In contrast, the sign of the mean June and August QEI-wide BSA anomaly was often opposite to that of the mean summer BSA anomaly. In June, negative QEI-wide BSA anomalies occurred in 2002 and 2005 when the mean summer QEI-wide BSA anomaly was positive, while positive QEI-wide BSA anomalies occurred in 2007 and 2009 when the mean summer BSA anomaly was negative. Negative QEI-wide BSA anomalies occurred in August 2005 and 2006, when the QEI-wide mean summer anomaly was positive; positive BSA anomalies occurred in August 2010, 2015 and 2016, when the QEI-wide mean summer anomaly was negative. ~~June BSA anomalies were generally characterized by a southeast-northwest spatial pattern.~~

There are also distinct differences in the large-scale spatial patterns of the BSA anomaly between months. In years with strong negative (positive) QEI-wide June BSA anomalies, most of the ice-covered pixels also ~~QEI~~ had negative (positive) anomalies, in this month (Fig. S4). ~~and the largest negative (positive) anomalies were observed at low elevations around the margins of the ice masses in the continental interior (Fig. S4).~~ ~~In contrast, i~~In years with weak negative QEI-wide June BSA anomalies

(e.g. 2002), positive (June BSA) anomalies occurred in the southeast while, negative BSA anomalies occurred in the west and northwest (Fig. 4). The opposite scenario occurred in years with weak positive QEI-wide June BSA anomalies (e.g. 2003).

380   In July (Fig. S5), (the month with the lowest QEI-wide BSA, Table 2), when the mean monthly BSA was typically lowest, BSA anomalies were typically both large (-0.0805 to +0.0843) and less spatially variable than in either June or August (Fig. S4 and S6). However, in some years (e.g. 2005) July BSA anomalies in the southeast maritime region that includes the eastern part of the Devon iIce capC, Manson Icefield and the south-easternmost part of the Prince of Wales Icefield were opposite in sign to those over the rest of the QEI. Nearby open water sources may have moderated the BSA in this region (Sect. 3.2.1).

385   , and the sign of the July QEI-wide BSA anomaly was always the same as that of the mean summer (JJA) QEI-wide BSA anomaly (Table 2, Fig. S5).

Mean August BSA anomalies displayed higher spatial variability than July anomalies, but were typically of similar magnitude (-0.0657 to +0.0836, Table 2). Unlike the June BSA anomalies (Fig. S4), which are characterized by a northwest-southeast spatial pattern, spatial variations in the August BSA anomaly are more local (zonal) in nature (Fig. S6). Cyclonic circulation

390   is much more prevalent over the QEI in August than in June and July (Alt, 1987; Gascon et al., 2013). The zonal nature of the August BSA anomaly likely reflects localized snowfall events related to the passage of individual low-pressure systems, associated with cyclonic circulation conditions. These snowfalls would temporarily raise the surface albedo in affected regions.

3.2 3 Albedo change: 2001–162001 to 2016

3.3.1 Mean summer BSA change

395   To determine whether there was a measurable change in the summer surface albedo over the period 2001-16 we performed a linear regression. Regressions were performed on a pixel-by-pixel basis for all pixels having mean summer BSA observations in at least 11 of the 16 years of observation (Sect. 2.3). The QEI-wide rate of change was taken as the average for these pixels. Between 2001 and 2016 the mean summer (JJA) QEI-wide BSA decreased at a rate of 0.0029 ± 0.0025 yr^{-1} (Table 23, Fig. 54a). As More than 95% of pixels experienced a non-negligible ($> |0.001|$ yr^{-1}, Sect. 2.3) decrease in summer BSA and the

400   total BSA change (-0.046) exceeds the MODIS sensor capabilities (2% in absolute reflectance units for the reflective solar bands (0.41-2.2 µm) (Justice et al., 1998) (Sect. 2.1), suggesting that the mean summer BSA did decline somewhat during this 16-year period. Although the measured change in the QEI-wide mean summer BSA (average correlation coefficient of all pixels) (r = 0.31, p = 0.24) was not statistically significant (r = 0.31, p = 0.24), BSA declines that were significant at the $p \leq$ 0.05 significance level were observed at the pixel level on all ice masses (Fig. 6a). The BSA change reported here is comparable

405   to, although slightly larger, than, that identified for the Greenland Ice Sheet's wet snow zone over the same time period (2001-2016) using similar data (-0.00254 decadeyr^{-1} for MCD43A3 Band 4 (545 – 565 µm)) (Casey et al., 2017). Furthermore, the measured albedo decline exceeds the detection limit of the MODIS C6 calibration accuracy (0.01 decade^{-1}; Lyapustin et al. (2014)), suggesting that BSA did decline somewhat during this 16-year period. There was a larger (but still not significant) decrease in the QEI-wide mean July BSA (-0.0050 ± 0.0031 yr^{-1}, r = 0.38, p = 0.15), while no QEI-wide change was observed

13

Commented [m33]: Rev. 2
RC 26: Page 9, line 272 – Note that it is not only the calibration accuracy that limits the capability to measure trends, but also the sensor design. Please add reference to sensor capabilities (e.g. Ju et al., 1998, doi: 10.1109/36.701075 and/or similar on MODIS instrument design and post-launch capabilities, see https://mcst.gsfc.nasa.gov/publications?f%5Btype%5D=102).
AR 26: Sentence revised for accuracy in both the methods and re sections. Additional references to the appropriate methods section and literature have been included.

410 ~~in either June or August (Table 3, Fig. 5), suggesting that the bulk of the mean summer BSA decline occurred in the month of July. In July, > 93% of pixels exhibited a detectable decrease in BSA and 24% of the measured BSA declines were significant at the p < 0.05 level. The BSA change reported here is comparable to, although slightly larger, than that identified for the Greenland Ice Sheet's wet snow zone over the same time period (2001-2016) using similar data (-0.0254 decade^{-1} for MCD43A3 Band 4 (545 – 565 µm)) (Casey et al., 2017).~~

415 Between 2001 and 2016, the area-averaged mean summer (JJA) incoming solar radiation over ice covered surfaces in the QEI, computed from daily means of NCEP/NCAR R1 Reanalysis data (Kalnay et al., 1996) (http://www.esrl.noaa.gov/psd/data/gridded/), ranged from 346 W m^{-2} (clear-sky downward solar flux) to 299 W m^{-2} (all-sky downward solar flux). Assuming the solar radiation received at the surface was constant over the ~~16~~ 16-year period, our measured BSA reduction (-0.0029 yr^{-1}) translates to a total increase in area-averaged absorbed solar radiation of between 1.1
420 and 1.4 MJ over the 16 year period. For a surface already at the melting point, this would equate~~s~~ to an increase in (area-averaged) summer melt of between 0.38 and 0.44 m w.e. (Cuffey and Paterson, 2010 Table 5.1).

Spatially, large reductions in the mean summer BSA (< -0.005 yr^{-1}) occurred at lower elevations around the margins of the ice masses (where the mean summer BSA is lowest), especially on Axel Heiberg Island, northern Manson Icefield, and on the continental (western) side of the ice masses on Ellesmere Island (Fig. 5a). Many of these BSA declines were significant at the
425 p ≤ 0.05 level (Fig. 6a). Statistically significant BSA declines (~ -0.00357 yr^{-1}, p ≤ 0.05) also occurred in the interior of the Manson Icefield and on the southern half of the Devon Ice Cap (Fig. 5a, 6a). Although BSA declines tended to be larger at lower elevations, slight BSA increases (> 0.001 yr^{-1}, not statistically significant) ~~Detectable (although not statistically significant) BSA increases (> 0.001 yr^{-1})~~ were observed along the lower portions of outlet glaciers (Fig. 6a). ~~and may point to an increased occurrence of summer snowfall events and/or a later removal of the previous year's snowpack (either from higher
430 fall/winter snow accumulation and/or later melt onset).~~ Many of these glaciers are close to open water sources where ~~In addition, in areas close to the oceans,~~ coastal fog may play a role in reducing summer melt, thereby suppressing albedo declines over the lower portions of outlet glaciers (Alt, 1987). ~~These variations likely contributed to the low correlation coefficients along the lower reaches of many outlet glaciers.~~ No ~~detectable~~ measurable change~~s~~ in mean summer BSA ~~was~~ were observed over the high elevation (> ~1500 m a.s.l.; > ~1200 m a.s.l for Sydkap Ice Cap) interior regions of the Devon Ice Cap, Sydkap Ice
435 Cap, Agassiz Ice Cap, Prince of Wales Icefield, or northern Ellesmere Island ice caps, even though strong increases in LST were observed in these locations between 2000 and ~~2015~~ 2016 (Fig. 7). ~~(Mortimer et al., 2016). Figure 6a also shows a large cluster of pixels with significant declines in mean summer BSA (~ -0.00357 yr^{-1}, p ≤ 0.05) in the interior of the Devon Ice Cap.~~

~~The spatial pattern of BSA change in July (the month when BSA decrease was largest) is similar to the spatial pattern of mean
440 summer BSA, with the largest BSA declines occurring at lower elevations (Fig. 5c). In July, BSA trends at the p ≤ 0.05 significance level (Fig. 6c) coincide, in general, with those locations having the largest BSA declines (< -0.0075 yr^{-1}). Statistically significant BSA declines occurred in the continental interiors of all the ice masses on Ellesmere Island, as well as~~

14

on the northern half of Axel Heiberg Island, the southern Prince of Wales Icefield, northern Manson Ice Cap, and southwest Devon Ice Cap.

445 Although no significant QEI-wide BSA change was observed in either June (-0.0017 ± 0.0024 yr⁻¹) or August (-0.0022 ± 0.0036 yr⁻¹), owing to the large amount of spatial variability in the sign and magnitude of BSA change in these months, local areas of consistent BSA change are observed. In June, increases in BSA occurred on the eastern portions of Prince of Wales Icefield and Agassiz Ice Cap, while weak-to-moderate BSA declines (>~ -0.005 yr⁻¹) occurred elsewhere. We note, however, that only 10% of pixels had June mean BSA trends significant at the p ≤ 0.05 level. These pixels are mainly found on the
450 southwest parts of the Devon and Agassiz Ice Caps and in northwest Ellesmere Island (Fig. 6b).
In August, large and statistically significant BSA declines (< -0.00625 yr⁻¹, p ≤ 0.05) occurred on the eastern Devon Ice Cap, Manson Icefield, and southeast Prince of Wales Icefield (Fig. 6d). Moderate August mean BSA declines (< -0.005 yr⁻¹, p ≤ 0.05) occurred on the northern half of northwest Ellesmere Island. August mean BSA increased on the summits of Devon Ice Cap and Sydkap Ice Cap, in the western part of Prince of Wales Icefield, in some eastern and southerly sections of the Agassiz
455 Ice Cap, and on some outlet glaciers in northwest Ellesmere Island and Axel Heiberg Island. These increases, however, were not statistically significant.

3.3.2 Summer monthly BSA change

3.3.2 Summer monthly BSA change: 2001 to 2016

In addition to the mean summer BSA change, trends in the mean monthly (June, July, and August) BSA were also investigated
460 (Sect. 2.3). Maps of the mean monthly BSA change, presented in Figures 5b-d, illustrate differences in the spatial patterns of BSA change for each summer month. There was a larger (but still not significant at the Pp < 0.05 level) decrease in the QEI-wide mean July BSA (-0.0050 ± 0.0031 yr⁻¹, r = 0.38, p = 0.15), whilebut no QEI-wide change was observed in either June or August (Table 3, Fig. 5). This, suggestsing that the bulk of the mean summer (JJA) BSA decline occurred in the month of July. In July, > 93% of pixels exhibited a detectablenon-negligible decrease in BSA (Fig. 5c), and 24% of the measured (July) BSA
465 declines were significant at the p < 0.05 level. The spatial pattern of July BSA change in July(Fig. 5c) (the month when BSA decrease was largest) is similar to that the spatial pattern of mean summer BSA change (Fig. 5a), with the largest BSA declines occurring at lower elevations (Fig. 5c). In this monthJuly, statistically significant (p < 0.05) BSA declinesdecreases occurred in the climatically continental interior sregions of all the ice masses on northern Ellesmere Island, as well as on the northern half of Axel Heiberg Island, the southern Prince of Wales Icefield, northern Manson Ice CapIcefield, and the southwest Devon
470 Ice Cap (Fig. 5c, 6c). In July, BSA trends at the p ≤ 0.05 significance level (Fig. 6c) coincide, in general, with those locations having the largest BSA declines (< -0.0075 yr⁻¹). Statistically significant BSA declines occurred in the continental interiors of all the ice masses on Ellesmere Island, as well as on the northern half of Axel Heiberg Island, the southern Prince of Wales Icefield, northern Manson Ice Cap, and southwest Devon Ice Cap.

Although nothere was no measurable change significantin the QEI-wide BSA change was observed in either June (-0.0017 ± 0.0024 yr^{-1}) or August (-0.0022 ± 0.0036 yr^{-1}), owing to the large amount of spatial variability in the sign and magnitude of BSA changes in these months, localnotable clusters areas of consistent BSA change are observed (Fig. 5b, 5d). In June, increases in BSA occurred on the eastern portions of Prince of Wales Icefield and Agassiz Ice Cap, while weak-to-moderate BSA declines (>~ -0.005 yr^{-1}) occurred elsewhere (Fig. 5b). We note, however, thatIn June, only 10% of pixels had June mean BSA trends that were significant at the p ≤ 0.05 level.. TtThese pixels are found mainly found on the southwestern parts of the Devon and Agassiz Ice Caps, and in northwest Ellesmere Island (Fig. 6b).

In August, large and statistically significant BSA declinesdecreases (< -0.00625 yr^{-1}, p ≤ 0.05) occurred on the eastern Devon Ice Cap, Manson Icefield, and southeast Prince of Wales Icefield (Fig. 5d, 6d). Moderate declines in August mean BSA declines (< -0.005 yr^{-1}, p ≤ 0.05) occurred on the icefields in the northern half of northwest Ellesmere Island. The mean August mean BSA increased on the summits of the Devon Ice Cap and Sydkap Ice Caps, in the western part of the Prince of Wales Icefield, in some eastern and southerly sections of the Agassiz Ice Cap, and on some outlet glaciers in northwest Ellesmere Island and Axel Heiberg Island (Fig. 5d). However, tThese increases, however, were not statistically significant (Fig. 6d).

3.3 4 Principal components Components analysisAnalysis

To explore whether there are any other spatial patterns in the 16-year mean summer BSA record that differ from the long-term (linear) trend, we performed a Principal Components Analysis of the BSA record (Sect. 2.3). The first and second Principal Components (Fig. 78) explain 65% and 12% of the variance in the mean summer BSA record, respectively. The spatial pattern of the First Principal Component (PC1) scores (Fig. 7a8a) is generally consistent with the spatial patterns of summer (JJA, Fig. 5a) and July (Fig. 5c) mean BSA change described previously (Sect. 3.2), Fig. 5a,c). PC1 scores are strongly negative (< -0.005) on western Axel Heiberg Island (large BSA declines), and weakly negative (> -0.001) or even positive at high elevations in the interiors of the ice masses where there was no detectable change in mean summer BSA was observed. Moderately negative (~ -0.002) component scores occur on the western (continental) side of eastern Ellesmere Island's ice masses as well as over much of Manson Icefield and the southeast portion of Prince of Wales Icefield, where large decreases were observed in both summer (JJA) and the July BSA.

For PC1, the highest Empirical Orthogonal Functions (EOFs) (32.8 and 25.9) correspond to the years with the lowest mean summer BSA (2011 and 2012) (Fig. 89). The lowest EOFs (-31.7 and -24.6) correspond to the years with the highest mean summer BSA (2013 and 2004). In addition, the departure from zero is much larger for the minimum component scores than for the maximum component scores (Fig. 7a8a), suggesting that both positive and negative BSA anomalies are likely caused by forcings with the same spatial pattern, albeit with the opposite sign. Investigating possible relationships between surface albedo and known large-scale patterns of atmospheric variability (Arctic Oscillation, Pacific North American Pattern, North Atlantic Oscillation), we found the EOFs for PC1 to be well (negatively) correlated with the mean summer North Atlantic

Oscillation (NAO) index (r = -0.84, p < 0.001, Fig. ~~8~~9), derived by averaging the June-August monthly mean NAO indices for 2001 to 2016 (http:www.cpc.ncep.noaa.gov). This is consistent with the finding of Mortimer et al. (2016) that there was a good agreement between the mean summer LST record and the NAO index in the QEI over the 2000-15 period. ~~From 2007-2012, when both the NAO index and BSA anomalies were negative (Fig. 8),~~ the frequency of anticyclonic circulation over the QEI in summer doubled relative to the 1948-2012 mean (Bezeau et al., 2015). ~~Clear sky conditions that accompany anticyclonic circulation increase the proportion of incoming shortwave radiation received at the air-ice interface, providing more energy for melt and driving albedo decline.~~

~~The spatial pattern of the second Principal Component (PC2) scores (Fig. 7b) resembles that of the August BSA change (Fig. 5d). Large negative component scores (< -0.004) were observed on eastern Devon Ice Cap and Manson Icefield, where large August BSA declines (< -0.0075 yr⁻¹) occurred. Positive component scores were observed in the in southwest Axel Heiberg Island and at lower elevations on northern Ellesmere Island's southwestern ice caps, where the mean August BSA increased (Fig. 5d).~~

The second Principal Component (PC2) had the largest EOFs of any component in 2006, 2010, and 2016. In these years, ~~the mean August BSA anomaly in these regions was of opposite sign to that of the mean summer (JJA) anomaly, and~~ there was poor correspondence between the PC1 EOFs and the JJA NAO index (Fig. ~~8~~9). The spatial pattern of the second Principal Component (PC2) scores (Fig. ~~7~~8b) resembles that of the August BSA change (Fig. 5d). Large negative ~~component~~PC2 scores (< -0.004) were observed on eastern Devon Ice Cap and Manson Icefield, where large August BSA declines (< -0.0075 yr⁻¹) occurred. Positive ~~component~~PC2 scores (Fig. 8b) were observed in ~~the in~~ southwest Axel Heiberg Island and at lower elevations on northern Ellesmere Island's southwestern ice caps, where the mean August BSA increased (Fig. 5d). Unlike PC1, there were no significant correlations between the EOFs of PC2 and known large-scale patterns of atmospheric variability. ~~Examination of the cumulative mass change record for the QEI from the Gravity Recovery and Climate Experiment (GRACE; Wolken et al. (2016), extended to 2016) shows that in the same years (2006, 2010, 2016), once the annual minimum glacier mass was reached, there was a prolonged period of constant but low mass (i.e. no melt or snowfall) before fall/winter accumulation began (inferred from an increase in mass). In other years, there was a sharp transition from the local end-of-summer mass minimum to the period of seasonally increasing mass. There is also good correspondence between the spatial pattern of PC2 scores and the spatial pattern of snow accumulation and ∂¹⁸O values that was inferred for the 1962-1974 period from surface snow samples and shallow firn cores collected in spring 1974 (Koerner, 1979). Areas having large negative PC2 component scores (< -0.004) were characterized by relatively high accumulation rates (Fig. 2 and 3 in Koerner (1979)) and snow that is isotopically warm (Fig. 7 in Koerner (1979)). Areas with positive PC2 component scores had lower snow accumulation rates. The correspondence between the pattern of PC2 component scores (Fig. 6b) to previously reported snow accumulation patterns over the QEI, and the spatial pattern of change in the August mean BSA (Fig. 4d), suggests that anomalously low snow accumulation in August may have influenced the mean summer BSA in those years when PC2 had the largest EOFs (e.g. 2006, 2010, and 2016).~~

17

3.5 Comparison with the mean summer LST

Owing to the positive feedback between albedo and surface temperature we would expect to observe strong increases in surface temperature where albedo declines were large. To investigate the relationship between temperature and albedo over the QEI the 16 year mean summer LST record was compared with the 16 year mean summer BSA record (Sect. 2.3). Due to the 8-day averaging period of the MOD11A2 data used here, the mean monthly BSA were not included in this comparison (Sect. 2.3). Between 2001 and 2016, the mean summer LST (-3.0 ± 1.8°C) increased at a rate of 0.049 ± 0.038 °C yr^{-1} (Table 3). LST increases (Fig. 7b) were greatest at higher elevations where the mean summer LST (Fig. 7a) is lower;. Iin contrast, BSA decreases (Fig. 5a) were largest at lower elevations where the mean summer BSA was lowest (Fig. 2). This observation may be explained by the fact that, at lower elevations where the mean summer LST regularly reached the melting point, there was less potential for warming than at higher elevations (Mortimer et al., 2016).

As expected, the 16-year QEI-wide LST record was negatively correlated (r = -0.86) with the 16 year QEI-wide BSA record. This negative correlation points to a positive ice-albedo feedback that would enhance rates of glacier mass loss from the QEI. Spatially, correlations (derived from linear correlations between the 16 year LST and BSA records for each pixel (Sect. 2.3)) were strongly negative in the north and west toof the QEI (Fig. 10). Weaker (negative) correlations (Fig. 10) occurred on the southwest Devon Ice Cap, and Manson Icefield where LST decreased (Fig. 7b) and BSA increased (Fig. 5a). In these regions, where the mean summer LST is high, the weak correlations between LST and BSA may reflect the fact that the albedo continues to decline once the surface temperature has reached the melting point. We note, however, that the large amount of missing data limits our ability to discern broad spatial patterns of the relationship between LST and BSA in the QEI.

4 Discussion

4.1 Summer and monthly BSA

Between 2001 and 2016 Our results show that the bulk of the measured mean summer BSA declines in the mean summer QEI albedo occurred in July (Sect. 3.2)., whichThis finding is consistent with previous work (e.g. Alt, 1987; Gardner and Sharp, 2007) that found variability in July near-surface air temperatures to be the primary influence on inter-annual variability in annual QEI mass balance. Variability in July air temperatures has, in turn, been associated with the variations in the strength, position, and geometry of the July circumpolar vortex (Gardner and Sharp, 2007). Extreme high melt years in the QEI are associated with the intrusion of a steep ridge at all levels in the troposphere and the absence of the North American trough, making the QEI thermally homogeneous with continental North America (Alt, 1987). Between 2001 and 2016, in warm years with low (e.g. 2007-2012) (high (e.g. 2001-2004)) albedos, there was a persistent ridge (trough) in the 500 hPa geopotential height surface centered over the north and west of the QEI (Fig. 4; Sect. 3.1.1;). This configuration appears to be tied to the increased warming and albedo declines observed in the central western part of the QEI from 2007 to 2012. For example, strong

warming and albedo declines over Axel Heiberg Island and north-central Ellesmere Island coincided with a ridge of high pressure centered over the north and west of the QEI that was often observed in years when the NAO index was negative (Fig. 9).

Differences in the ~~sS~~patial ~~variations~~patterns of ~~in~~ the monthly BSA change (Fig. 5b–d) ~~also~~ reflect the ~~different~~dominant atmospheric circulation patterns that occur over the QEI during the ~~course of~~ summer months. In the QEI, anticyclonic circulation tends to dominate in the months of June and July, while cyclonic circulation often occurs in August (Alt, 1987; Gascon et al., 2013).

In ~~In contrast to~~ June and July, ~~when~~ the largest BSA declines occurred in the ~~west~~climatically continental interiors of the ice masses on Ellesmere and Devon Islands, as well as on Axel Heiberg Island (Fig. 5). In these months, the mountains on eastern Ellesmere and Devon Islands act as a barrier to moisture transport from the east limiting (solid) precipitation (which can temporarily raise the surface albedo) on the western (lee) side of the eastern ice masses (Koerner, 1979). Adiabatic heating of descending air masses on the western (lee) side of the eastern ice masses results in warm dry air which promotes warming, melting, and enhance~~d~~ albedo declines ~~of the QEI, BSA declines in August were largest at low elevations in the maritime regions of eastern Devon Ice Cap, Manson Icefield, and the southwestern Prince of Wales Icefield (Fig. 5).~~ In contrast, in August, when ~~As mentioned in Section 3.2.1, August weather in the QEI tends to be dominated by~~ cyclonic circulation is common~~t~~ (Sect. 3.2.1) (Alt, 1987; Gascon et al., 2013) BSA declines were largest at low elevations in the maritime regions of eastern Devon Ice Cap, Manson Icefield, and the southwestern Prince of Wales Icefield (Fig. 5d).~~.~~ Low pressure systems which track from the southwest to the north and northeast are common in August, and they advect warm moist air into the Arctic from the south (Alt, 1987; Gascon et al., 2013). In the eastern QEI, orographic uplift of air masses tracking from the southwest, and subsequent adiabatic heating of these air masses when they descend on the eastern sides of ice masses, would bring warm dry air to the eastern (lee) side of the mountains in the eastern QEI, promoting both warming and albedo decline in these regions in August.

During the 2001-16 period, the mean summer QEI-wide BSA record was strongly tied to the summer NAO index (Sect. 2.4). ~~Inter-annual variations in the QEI mean summer LST anomalies have previously been linked to variations in the NAO index (Mortimer et al., 2016). Here we find that the 16-year record of summer BSA is also strongly tied to the summer NAO index (Sect. 3.3). In years with strong negative (positive) BSA anomalies and positive (negative) LST anomalies (e.g. positive: 2007-2012, negative: ; 2013; see Mortimer et al. (2016)) the NAO index was negative (positive).~~ During the 2007-2012 period when the NAO index was negative (Fig. 8), there was an increase in the frequency of ~~A~~anticyclonic circulation~~, compared to the 1948-2012 mean (Bezeau et al., 2015). Similarly, over the Greenland Ice Sheet, strong anticyclonic ridging, associated with clear skies and the advection of warm air from the south~~, was ~~found~~ shown to co-vary with the NAO index over the Greenland Ice Sheet, immediately to the east of the QEI, ~~over the period~~ since ~2001 (Rajewicz and Marshall, 2014). On the Greenland Ice Sheet, clear sky conditions and the advection of warm air from the south which accompany anticyclonic ridging (Rajewicz and Marshall, 2014), similar to that observed in the QEI in June and July (Alt, 1987; Gascon et al., 2013; Bezeau et al., 2015), ~~These conditions~~ were found to enhance the strength of the ice-albedo feedback ~~on the Greenland Ice Sheet during~~

19

frombetween 2009— and 2011, which resulting resulted in higher rates of melt and glacier mass loss (Box et al., 2012). Although a similar phenomenon is likely to have occurred in the QEI, we find that in some years (2006, 2010, 2016) there was poor correspondence between the mean summer BSA record and the NAO index (Fig. 89), suggesting that an additional forcing may be influencing the spatial and temporal variability of glacier surface albedo in the QEI.

In 2006, 2010, and 2016, the spatial pattern of BSA anomalies (Fig. 3) closely resembles that of the mean August BSA change (Fig. 5d), which, in turn, closely resembles the spatial pattern of PC2 component scores (Fig. 8b)

There is also good correspondence between the spatial pattern of PC2 scores and Tthe spatial pattern of snow accumulation (Fig. 2 and 3 in Koerner 1979) and $\partial^{18}O$ values(Fig. 7 in Koerner 1979) that waswere inferred by Koerner (1979) for the 1962-19743 period from surface snow samples and shallow firn cores collected in spring 1974. (Koerner, 1979). These spatial patterns (of snow accumulation and $\partial^{18}O$) closely resemble the spatial pattern of PC2 scores (Fig. 8b). Specifically, aAreas having large negative PC2 component scores (< -0.002, Fig. 8b4) of the 16-year mean summer BSA record (Sect. 3.4) were characterized by relatively high accumulation rates (Fig. 2 and 3 in Koerner (1979)) and snow that is isotopically warm (Fig. 7 in Koerner (1979)). while aAreas with positive PC2 component scores had lower snow accumulation rates. This similarity points to a possible role of precipitation in affecting the mean summer BSA in some years. The correspondence between the pattern of PC2 component scores (Fig. 68b), to previously reported snow accumulation patterns over the QEI, and and the spatial pattern of the mean August change in the August mean BSA change (Fig. 45d), suggests that anomalously low snow accumulation in August may have influenced the mean summer BSA in those years when PC2 had the largest EOFs (e.g. 2006, 2010, and 2016). To investigate the relationship between the albedo record and variability in precipitation we Eexaminationed of the cumulative mass change record for the QEI from the Gravity Recovery and Climate Experiment (GRACE; Wolken et al. (2016), extended to 2016 (B. Wouters, personal communication, 2017)). The record shows that in 2006, 2010, 2016 (the years when PC2 of the 16-year mean summer BSA record had the largest EOFs of any Principal Component, Sect. 3.4), once the annual minimum glacier mass was reached, there washas been was a prolonged period of constant but low mass (i.e. no melt or snowfall) before fall/winter accumulation began (inferred from an increase in mass). In other years, there was a sharp transition from the local end-of-summer mass minimum to the period of seasonally increasing mass.

. In these years, delayed snowfall onset and limited melt in August were inferred from the GRACE mass change record. This could indicate that in some years during the 2001-2016 period, variability in August snowfall, in addition to that tied to the NAO, may have influenced the mean summer BSA.

Spatial variations in the monthly BSA reflect the different atmospheric circulation patterns that occur over the QEI during the course of the summer. In the QEI, anticyclonic circulation tends to dominate in the months of June and July, while cyclonic circulation often occurs in August (Alt, 1987; Gascon et al., 2013). Investigation of the surface energy balance of the Devon Ice Cap between 2007 and 2010 found increases in summer (JJA) melt energy were associated with an increase in net shortwave radiation in June and July, and with an increase in net longwave radiation in August (Gascon et al., 2013). Strong, persistent anticyclonic circulation maximizes the incoming shortwave radiation received at the air-ice interface, and a lower albedo increases the proportion of incoming solar radiation that is absorbed, providing more energy for warming and melt.

Our results show that the bulk of the decline in mean summer QEI albedo occurred in July (Sect. 3.2), which is consistent with previous work (e.g. Alt, 1987; Gardner and Sharp, 2007) that found variability in July near-surface air temperatures to be the primary influence on inter-annual variability in annual QEI mass balance. Variability in July air temperatures has, in turn, been associated with the variations in the strength, position, and geometry of the July circumpolar vortex (Gardner and Sharp, 2007). Extreme high melt years in the QEI are associated with the intrusion of a steep ridge at all levels in the troposphere and the absence of the North American trough, making the QEI thermally homogeneous with continental North America (Alt, 1987). Between 2001 and 2016, in warm years with low (e.g. 2007-2012) (high (e.g. 2001-2004)) albedos, there was a persistent ridge (trough) in the 500 hPa geopotential height surface centered over the north and west of the QEI (Fig. 4; Sect. 3.1.1;). This configuration appears to be tied to the increased warming and albedo declines observed in the central western part of the QEI from 2007 to 2012. For example, strong warming and albedo declines over Axel Heiberg Island and north-central Ellesmere Island coincided with a ridge of high pressure centered over the north and west of the QEI that was often observed in years when the NAO index was negative (Fig. 9).

In contrast to June and July, when the largest BSA declines occurred in the west of the QEI, BSA declines in August were largest at low elevations in the maritime regions of eastern Devon Ice Cap, Manson Icefield, and the southwestern Prince of Wales Icefield (Fig. 5). As mentioned in Section 3.2.1, August weather in the QEI tends to be dominated by cyclonic circulation (Alt, 1987; Gascon et al., 2013). Low pressure systems which track from the southwest to the north and northeast are common in August, and they advect warm moist air into the Arctic from the south. In the eastern QEI, orographic uplift of air masses tracking from the southwest, and subsequent adiabatic heating of these air masses when they descend on the eastern sides of ice masses, would bring warm dry air to the eastern (lee) side of the mountains in the eastern QEI, promoting both warming and albedo decline in these regions in August.

Differences in the dominant atmospheric circulation patterns over the course of the summer season are responsible, at least in part, for where and in which month the largest albedo declines occur. Albedo lowering increases the proportion of incoming solar radiation absorbed at the air-ice interface, and thus the energy available to drive further melt and surface albedo decline. Knowing where and when albedo changes are likely to occur in future is, therefore, important for predicting future rates of mass loss from the QEI ice caps. Recent investigations of atmospheric circulation patterns over the QEI (e.g. Gardner and Sharp, 2007) focused on characterization of July temperature and atmospheric conditions, since July is usually the month when melt rates peak. Our results suggest, however, that changes occurring during the month of August are also important, especially as the length of the melt season continues to increase.

Although large-scale circulation patterns appear to explain much of the broad spatial pattern (and seasonal variability) of BSA change, the physiography of the QEI introduces considerable local variation into the way these changes are expressed. Variations in the magnitudes of both inter-annual variability and longer-term changes in annual precipitation, summer melt duration, and melt intensity have previously been associated with distance from moisture sources (Koerner, 1979; Alt, 1987; Wang et al., 2005). Snow accumulation rates in the QEI tend to decrease from east to west, and Baffin Bay is the largest moisture source for the eastern QEI (Koerner, 1979). Summer snowfall events temporarily raise the surface albedo, while

21

locally higher fall and winter snow accumulation can delay the exposure of bare ice and firn in the following summer relative to areas with lower accumulation rates. However, although BSA decreases were generally larger in the north and west, equally large decreases occurred at low elevations on Manson Icefield and southeast Prince of Wales Icefield in the eastern QEI. These large BSA decreases at low elevations in the eastern QEI may arise from a decoupling of high and low elevation temperatures in low melt years. For example, Alt (1978) found that, in some years when there was very little melt near the summit of the Devon Ice Cap, the Sverdrup Glacier (lower elevation) experienced very high melt rates. Further, Wang et al. (2005) attributed comparatively high melt rates observed at low elevations on the Prince of Wales Icefield in 2002 to a decoupling of the temperature regimes experienced at high and low elevations, similar to that described by Alt (1978).

4.2 Relationship between albedo change and temperature

During the period 2001-2016, mean summer QEI-wide LST (16-yr average: -3.25 ± 1.73 °C) increased at a rate of 0.046 ± 0.036 °C yr^{-1} (Table 3). The spatial pattern of LST increase (Fig. S7b) is opposite to the pattern of mean summer BSA change, in that BSA decreases were largest at lower elevations where the mean summer BSA was lowest (Fig. 5a), while LST increases were greatest at higher elevations where the mean summer LST is lower. This observation may be explained by the fact that, at lower elevations, where the mean summer LST regularly reached the melting point, there was less potential for warming than at higher elevations (Mortimer et al., 2016). Investigation of the spatial pattern of the relationship between LST and BSA (derived from linear correlations between the 16 year LST and BSA records for each pixel (Sect. 2.3)), shows that, as expected, LST and BSA were negatively correlated over most of the QEI (~99.7% of pixels; Fig. 9). This negative correlation (average correlation coefficient of all pixels: r = -0.64, p < 0.01) points to a positive ice-albedo feedback which would promote enhanced rates of glacier mass loss from the QEI. In general, correlations were stronger in the north and west of the QEI than in the south and east, with the exception of the northwest Devon Ice Cap (southeast QEI) where large negative correlation coefficients (r < -0.8) were also observed.

The nature of the relationship between LST and BSA varies both within and between regions (Fig. 9). In the eastern QEI [Agassiz Ice Cap, Prince of Wales Icefield, and Devon Ice Cap], correlations tended to be stronger on the western continental side of the north-south running mountain range (where BSA declines were also large) than on the eastern maritime slopes. There were, however, some exceptions to this pattern, most notably a low elevation region near Cadogan Inlet (Fig. 9a, black box), eastern Prince of Wales Icefield, where large negative correlations (r < -0.8) were observed and BSA and LST changes were both small. The strong negative correlations in the continental interior are likely attributable to the presence of the north-south trending mountain range in eastern Ellesmere and Devon Islands. In the continental interior of eastern Devon and Ellesmere Islands, warming of air and glacier surface temperatures resulted in albedo decreases, leading to further surface warming. Koerner (1979) attributed the existence of a dry area with low amounts of snow accumulation centered on western Ellesmere Island to the precipitation-shadowing effect of the mountains to the east. In June and July when circulation is primarily anticyclonic, the presence of a barrier to moisture transport from the east limits precipitation on the western (lee)

22

side of the eastern ice masses, while adiabatic heating of descending air masses results in warm dry air which promotes warming and melting, and enhances albedo decline, in the west.

705   The strength of the relationship between LST and BSA also varies with elevation. Correlations tended to be weaker and more variable at high elevations, although there are also several instances of low correlations at low elevations, for instance on southeast Devon Ice Cap and Manson Icefield. At lower elevations, where the mean summer LST is high (Fig. S7a), weaker correlations between temperature and albedo may reflect the fact that the albedo continues to decline once the surface temperature has reached the melting point. At high elevations (above ~1500 m a.s.l., Sect. 3.2) BSA decreases were small or

710   non-existent, and the correlation between LST and BSA was both modest and highly variable (Fig. 9). Moderate negative correlations (r > -0.6) and some instances of positive correlations, were observed at high elevations on Prince of Wales Icefield and Agassiz Ice Cap. On northwest Ellesmere Island where correlations were generally strongly negative, high elevation regions had more moderate correlations and some instances of positive correlations between LST and BSA were also observed. LST increases were largest at high elevations (Fig. S7b) and melt occurred at all elevations and at all locations in the QEI at

715   some point during the 2000-2015 period (Mortimer et al., 2016). Since the rate of grain metamorphism increases with the temperature and water content of snow, even warmer summer temperatures may be needed to promote large scale albedo decline in permanently snow-covered high elevation areas. Alternatively, higher air temperatures in such regions may promote increased summer snowfall and more frequent riming events, which temporarily raise the surface albedo and limit long term albedo decline. We note that in many high elevation regions, where BSA changes were either small or not observed and

720   correlations between LST and BSA were weak and highly variable, PC1 had positive component scores (compared with negative scores elsewhere). Although PC1 was strongly correlated with the summer NAO index (Sect. 3.3), the occurrence of positive component scores in these high elevation regions (compared with large negative scores elsewhere) may point to an additional mechanism that is affecting the albedo record in these regions. Variability in the extent of open water in the QEI's inter-island channels has previously been correlated with variability in summer temperatures and 500 hPa geopotential height

725   anomalies in the QEI (Koerner, 1977; Bezeau et al., 2015). Increased open water extent during warm years promotes atmospheric convection, which strengthens the advection of warm moist air masses into Baffin Bay (Koerner, 1979). In the eastern QEI, the high elevation regions of eastern Ellesmere and Devon Islands act as a barrier to this increased moisture transport (Koerner, 1979). As a result, precipitation is deposited on the eastern maritime slopes, where it temporarily increases the surface albedo. This scenario provides a plausible explanation for lower rates of BSA decline and poor correspondence

730   between LST and BSA changes at higher elevations in the eastern QEI. A similar set of processes may also be occurring at high elevations on northern Ellesmere Island where the Arctic Ocean is the primary moisture source.

5 Conclusions

This study presents the first complete picture of mean summer surface albedo variations over all glaciated surfaces in the QEI during the period 2001-2016. Mean summer shortwave broadband black-sky albedo decreased at a rate of 0.0029 ± 0.0025 yr$^-$

23

[1] over the 16-year period. Strong negative BSA anomalies from 2007-~~20~~12 suggest that the bulk of the observed albedo decline occurred during this six-year period. Large albedo declines occurred in July (-0.0050 ± 0.0031 yr^{-1}); while no change in BSA occurred in either June or August, indicating that the bulk of the mean summer BSA decrease is concentrated in July~~,~~ when strong anticyclonic circulation occurs. The 16-year history of mean summer BSA changes is strongly tied to variations in the summer NAO index, except in the years 2006, 2010, and 2016 when changes in the mean summer BSA appear to be dominated by the effect of changes in the mean August BSA. Albedo declines were largest at low elevations around the margins of the ice masses and the 16-year record of mean summer BSA was negatively correlated with the 16 year record of mean summer LST ~~(which increased at a rate of 0.046 ± 0.036 °C yr⁻¹ during the 2001-2016 period), indicating~~ suggesting the ~~presence existence~~ of a positive ice-albedo feedback ~~in a warming climate~~ that would enhance rates of glacier mass loss from the QEI in a warming climate.

Albedo declines increase the proportion of incoming solar radiation absorbed at the air-ice interface, and thus the energy available to drive melt, warming, and further surface albedo decline. Warmer temperatures, in turn, increase the rate of snow grain metamorphism which lowers the albedo. Air and surface temperatures affect the removal (timing and extent) of the seasonal snowpack which exposes lower albedo firn and/or glacier ice, while melting glacier ice releases impurities that further reduce its albedo. Given that temperature and albedo are inextricably linked, ~~Differences in the dominant atmospheric circulation patterns over the course of the summer season are responsible, at least in part, for where and in which month the largest albedo declines occur. Albedo lowering increases the proportion of incoming solar radiation absorbed at the air-ice interface, and thus the energy available to drive further melt and surface albedo decline. K~~knowing where and when albedo changes are likely to occur in future is, therefore, important for predicting future rates of mass loss from the QEI ice caps. Recent investigations of atmospheric circulation patterns over the QEI (e.g. Gardner and Sharp, 2007) focused on characterization of July temperature and atmospheric conditions, since July is usually the month when melt rates peak. Our results suggest, however, that changes occurring during the month of August are also important, especially as the length of the melt season continues to increase.

Commented [CM37]: Rev. 1
RC: Though they point out that albedo and LST are negatively correlated for the QEI, they do not discuss that relationship as cause-and-effect in either the Abstract or the Conclusion. The relationship between albedo and LST is discussed in Section 4.2 but I would have liked that discussion to have been better integrated throughout the paper.
AC: Additional text regarding the relationship between temperature and albedo has been included in the conclusion.

24

References

Ackerman, S. A., Strabala, K. I., Menzel, P. W., Frey, R. A., Moeller, C. C., and Gumley, L. E.: Discriminating clear sky from clouds with MODIS, J. Geophys. Res., 103(D24), 32141–32157, doi:10.1029/1998JD200032, 1998.

Alexander, P. M., Tedesco, M., Fettweis, X., van de Wal, R. S. W., Smeets, C. J. P. P., and van den Broeke, M. R.: Assessing spatiotemporal variability and trends in modeled and measured Greenland Ice Sheet albedo (2000-2013), The Cryosphere, 8(6), 2293-2312, doi: 10.5194/tc-8-2293-2014, 2014.

Alt, B. T.: Synoptic climate controls of mass-balance variations on Devon Island Ice Cap, Arct. Alp. Res., 10(1), 61–80, doi:10.2307/1550657, 1978.

Alt, B. T.: Developing synoptic analogs for extreme mass balance conditions on Queen Elizabeth Island ice caps, Journal of Applied Climate, 26(12), 1605-1623, doi: 10.1175/1520-0450(1987)026<1605:DSAFEM>2.0.CO;2, 1987.

Arendt, A., et al.: Randolph Glacier Inventory Vers. 3.0: *a dataset of Global Glacier Outlines*. Global Land Ice Measurements from Space, Boulder, CO. Digital media: http//www.glims.org/RGI/rgi32_dl.html, 2013̶2.

Barnes, W. L., Pagano, T.S., and Salomonson V.V.: Prelaunch characteristics of the Moderate Resolution Imaging Spectroradiometer (MODIS) on EOS-AM1, IEEE Transactions on Geoscience and Remote Sensing, 36(4), 1088-1100, doi: 10.1109/36.700993, 1998.

Bezeau, P., Sharp, M. and Gascon, G.: Variability in summer anticyclonic circulation over the Canadian Arctic Archipelago and west Greenland in the late 20th/early 21st centuries and its effects on glacier mass balance, Int. J. Climatol, 35(4), 540-557, doi:10.1002/joc.4000, 2015.

Box, J. E., Fettweis, X., Stroeve, J. C., Tedesco, M., Hall, D. K., and Steffen, K.: Greenland ice sheet albedo feedback: thermodynamics and atmospheric drivers, The Cryosphere, 6(4), 821-839, doi: 10.5194/tc-6-821-2012, 2012.

Box, J. E., van As D., and Steffen, K.: Greenland, Canadian and Icelandic land ice albedo grids (2000-2016), Geological Survey of Denmark and Greenland Bulletin, 38, 69-72, 2017.

Braithwaite, R. J.: Mass balance characteristics of arctic glaciers, Ann. Glaciol., 42, 225-229, doi: 10.3189/17275640578182899, 2005.

Casey, K. A., Polashenski, C. M., Chen, J., and Tedesco, M.: Impact of MODIS sensor calibration updates on Greenland Ice Sheet surface reflectance and albedo trends, The Cryosphere, 11, 1781-1795, doi: 10.5194/tc-11-1781-2017, 2017.

Clarke, A. D., and Noone, K. J.: Soot in the Arctic snowpack: a cause for perturbations in radiative transfer, Atmospheric Environment, 19(12), 2045-2053, doi: 10.1016/0004-6981(85)90113-1, 1985.

Colbeck, S. C.: An overview of seasonal snow metamorphism, Rev. Geophys., 20(1), 45-61, doi: 10.1029/RG020i001p00045, 1982.

Conway, H., Gades, A., and Raymond, C. F.: Albedo of dirty snow during conditions of melt, Water Resour. Res, 32(6), 1716-1718, doi: 10.1029/96WR00712, 1996.

Cuffey, K. M., and Paterson, W. (Eds.): The physics of glaciers, 4th edn. Butterworth-Heinemann, Oxford, 2010.

Doherty, S. J., Warren, S. G., Grenfell, T. C., Clarke, A. D., and Brandt, R. E.: Light absorbing impurities in Arctic snow, Atmos. Chem Phys, 10(23), 11647-11680, doi: 10.5194/acp-10-11647-2010, 2010.

Flanner, M. G., Zender, C. S., Randerson, J. T., and Rasch, P. J.: Present-day climate forcing and response from black carbon in snow, J. Geophys. Res., 112, D11202, doi:10.1029/2006JD008003, 2007.

Fountain, A.G., Tranter, M., Nylen, T. H., and Muller, D. R.: Evolution of cryoconite holes and their contribution to meltwater runoff from glaciers in the McMurdo Dry Valleys, Antarctica, J. Glaciol, 50(168), 35-45, doi: 10.3189/172756504781830312, 2004.

Franz, B.A., Kwiatkowska, E.J., Meister, G. and McClain, C.R.: Moderate Resolution Imaging Spectroradiometer on Terra: limitations for ocean color applications, Journal of Applied Remote Sensing, 2(1), 023525, doi: 10.1117/1.2957964, 2008.

Gardner, A. S., and Sharp, M.: Influence of the Arctic circumpolar vortex on the mass balance of Canadian High Arctic glaciers, J. Clim., 20(18), 4586-4598, doi10.1175JCLI4268.1, 2007.

Gardner, A. S., Moholdt, G., Wouters, B., Wolken, G. J., Burgess, D. O., Sharp, M. J., Braun, C., Labine, C.: Sharply increased mass loss from glaciers and ice caps in the Canadian Arctic Archipelago, Nature, 473(7347), 357-360, doi: 10.1038/nature10089, 2011.

Gardner, A. S., Moholdt, G., Cogley, G., Wouters, B., Arendt, A. A., Wahr, J., Berthier, E., Hock, R., Pfeffer, W. T., Kaser, G., Ligtenberg, S. R. M., Bolch, T., Sharp, M., Hagen, J. O., van den Broeke, M. R., and Paul, F.: et al.: A reconciled estimate of glacier contributions to sea level rise: 2003 to 2009, Science, 340(6134), 852-857, doi:10.1126/science.1234532, 2013.

Gascon, G., Sharp, M., and Bush, A.: Changes in melt season characteristics on Devon Ice Cap, Canada, and their association with the Arctic atmospheric circulation, Ann. Glaciol., 54, 101–110, doi:10.3189/2013AoG63A601, 2013.

Guenther, B., Barnes, W., Knight, E., Barker, J., Harnden, J., Weber, R., Roberto, M., Godden, G., Montgomery, H., and Abel, P.: MODIS calibration: a brief review of the strategy for the at-launch calibration approach, Journal of Atmospheric and Oceanic Technology, 13(2), 274-285. doi: 10.1175/1520-0426(1996)013<0274:MCABRO>2.0.CO;2, 1996.

26

Guenther, B. Godden, G. D., Xiong, X., Knight, E.J., Qiu, S. Y., Montgomery, H., Hopkins, M. M., Khayat, M. G., and Zhidong Hao, Z.: Prelaunch algorithm and data format for the Level 1 calibration products for the EOS-AM1 Moderate Resolution Imaging Spectroradiometer (MODIS), IEEE Transactions on Geoscience and Remote Sensing, 36(4), 1142-1151, doi: 10.1109/36.701021, 1998.

825 Hall, D. K., Riggs, G. A., Salomonson V. V. DiGirolamo N. E., Bayr K. J.: MODIS snow-cover products, Remote Sens. Environ., 83(1), 181-194, doi: 10.1016/S0034-4257(02)00095-0, 2002.

Hall, D. K., Box, J. E., Casey, K. A., Hook, S. J., Shuman, C. A., and Steffen, K.: Comparison of satellite-derived and in-situ observations of ice and snow surface temperatures over Greenland, Remote Sens. Environ., 112(10), 3739-3749, doi: 10.1016/j.rse.2008.05.007, 2008ba.

830 Hall, D. K., Williams, R. S., Luthcke, S. B., and DiGirolamo, N. E.: Greenland ice sheet surface temperature, melt and mass loss: 2000–2006, J. Glaciol., 54(184), 81–93, doi:10.3189/002214308784409170, 2008a2008b.

Hall, D. K., Box, J. E., Casey, K. A., Hook, S. J., Shuman, C. A., and Steffen, K.: Comparison of satellite-derived and in-situ observations of ice and snow surface temperatures over Greenland, Remote Sens. Environ., 112(10), 3739-3749, doi: 10.1016/j.rse.2008.05.007, 2008b.

835 Hall, D. K., Comiso, J. C., DiGirolamo, N. E., Shuman, C. A., Key, J. R., and Koenig, L. S.: A satellite-derived climate-quality data record of the clear-sky surface temperature of the Greenland ice sheet, J. Clim., 25, 4785-4798, doi: 10.1175/JCLI-D-11-00365.1, 2012.

He, T., Lian, S. L., and Song, D. X.: Analysis of global land surface albedo climatology and spatial-temporal variation during 1981-2010 from multiple satellite products, J. Geophys. Res.-Atmos., 119(17), 10281-10298, doi: 10.1002/2014/JD021667, 840 2014.

Jin, Y., Schaaf, C. B., Woodcock, C. E., Gao, F., Li, X., and Strahler, A. H.: Consistency of MODIS surface BRDF/Albedo retrievals: 1. Algorithm performance, J. Geophys. Res. 108(D5), 4158, doi: 10.1029/2002JD002803, 2003.

Justice, C.O., Vermote, E., Townshend, J.R.G., Defries, R., Roy, D. P., Hall, D. K., Vincent V. Salomonson V. V. et al.: The Moderate Resolution Imaging Spectroradiometer (MODIS): Land remote sensing for global change research, IEEE 845 Transactions on Geoscience and Remote Sensing, 36(4), 1228-1249, doi: 10.1109/36.701075, 1998.

Kalnay, E., Kanamitsu, M., Kistler, R., Collins, W., Deaven, D., Gandin, L., Iredell, M., Saha, S., White, G., Woollen, J., Zhu, Y., Leetmaa, A., Reynolds, R., Chelliah, M., Ebisuzaki, W., Higgins, W., Janowiak, J., Mo, K.C., Ropelewski, C., Wang, J., Jenne, R., and Joseph, D.: The NCEP/NCAR 40 year reanalysis project, Bull. Am. Meteorol. Soc., 77(3), 437–471, doi:10.1175/1520-0477(1996) 077<0437:TNYRP>2.0.CO;2, 1996.

King, M. D., Platnick, S., Yang, P., Arnold, G. T., Gray, M. A., Ridei, J. C., Ackerman, S. A., and Liu, K. N.: Remote Sensing of Liquid Water and Ice Cloud Optical Thickness and Effective Radius in the Arctic: Application of Airborne Multispectral MAS Data, J. Atmos. Ocean. Technol., 21(6), 857–875, doi:10.1175/1520-0426(2004)021<0857:RSOLWA>2.0.CO;2, 2004.

Koenig, L. S., and Hall, D. K.: Comparison of satellite, thermochron and station temperatures at Summit, Greenland, during the winter of 2008/09, J. Glaciol., 56(198), 735-741, (doi: 10.3189/002214310793146269), 2010.

Koerner, R. M.: Devon Island ice cap: core stratigraphy and paleoclimate, Science, 196(4285), 15-18, doi: 10.1126/science.196.4285.15, 1977.

Koerner, R. M.: Accumulation, ablation, and oxygen isotope variations on the Queen Elizabeth Islands ice caps, Canada, J. Glaciol., 22(86), 25-41, 1979.

Koerner, R. M.: Mass balance of glaciers in the Queen Elizabeth Islands, Nunavut, Canada, Ann. Glaciol., 42, 417–423, doi:10.3189/172756405781813122, 2005.

Kwiatkowska, E. J., Franz, B. A., Meister, G., McClain, C. R., and Xiong, X.: Cross calibration of ocean-color bands from Moderate-Resolution Imaging Spectroradiometer on Terra platform, Applied Optics, 47(36), 6796–6810, doi:10.1364/AO.47.006796, 2008.

Land Processes Distributed Active Archive Center (LP DAAC), MODIS Level 3 Global 1 km Grid SIN Version 56. NASA EOSDIS Land Processes DAAC, USGS Earth Resources Observation and Science (EROS) Center, Sioux Falls, South Dakota (https://lpdaac.usgs.gov), dataset accessed September 2014 October 2015 2017 and June 2017 at http://e4ftl01.cr.usgs.gov.

Lenaerts, J. T. M., van Angelen, J.H., van den Broeke, M. R., Gardner, A. S., Wouters, B., and van Meijgaard, E.: Irreversible mass loss of Canadian Arctic Archipelago glaciers, Geophys. Res. Lett., 40(5), 870–874, doi:10.1002/grl.50214, 2013.

Liu, J., Schaaf, C. B., Strahler, A. H., Jiao, Z., Shuai, Y., Zhang, Q., Román, M., Augustine, J. A., and Dutton, E. G.: Validation of Moderate Resolution Imaging Spectroradiometer (MODIS) albedo retrieval algorithm: Dependence of albedo on solar zenith angle, J. Geophys. Res.-Atmos., 114, D01106, doi:10.1029/2008JD009969, 2009.

Lucht, W., Schaaf, C. B., and Strahler, A. H.: An algorithm for the retrieval of albedo from space using semiempirical BRDF models, IEEE Transactions on Geoscience and Remote Sensing, 38, 977-998, 2000.

Lyapustin, A., Wang, Y., Xiong, X., Meister, G., Platnick, S., Levy, R., Franz, B., Korkin, S., Hilker, T., Tucker, J., Hall, F., Sellers, P., Wu, A., and Angal, A.: Scientific impact of MODIS C5 calibration degradation and C6+ improvements, Atmos. Meas. Tech., 7(12), 4353-4365, doi:10.5194/amt-7-4353-2014, 2014.

Mortimer, C. A., Sharp, M., and Wouters, B.: Glacier surface temperatures in the Canadian high arctic, 2000-2015, J. Glaciol., 62(23), 963-975, doi: 10.1017/jog.2016.80, 2016.

Pan C., Xiong, X., Che, N.: MODIS pre-launch characterization of reflective solar bands response vs. Scan angle, Proc. SPIE – Earth Observeing Systems XII, Optical Engineering Applications, 66770R, doi:10.117/12.730573, 2007.

Pfeffer, W. T., Arendt, A. A., Bliss, A., Bloch, T., Cogley, J. G., Gardner, A. S., Hagen, J. O., Hock, R., Kaser, G., Kienholz, C., Miles, E. S., Moholdt, G., Molg, N., Paul, F., Radic, V., Rastner, P., Raup, B., Rich, J., Sharp, M. J., and The Randolph Consortium: The Randolph Glacier Inventory: a globally complete inventory of glaciers, J. Glaciol., 60(221), 537-552, doi:10.3189/2014JoG13J176, 2014.

Polashenski, C. M., Dibb, J. E., Flanner, M. G., Chen, J. Y., Courville, Z. R., Lai, A. M., Schauer, J. J., Shafer, M. M., and Bergin, M.: Neither dust nor black carbon causing apparent albedo decline in Greenland's dry snow zone: Implications for MODIS C5 surface reflectance, Geophys. Res. Lett., 42(12), 9319-9327, doi: 10.1002/2015GL065912, 2015.

Rajewicz, J., and Marshall, S. J.: Variability and trends in anticyclonic circulation over the Greenland ice sheet, 1948-2013, Geophys. Res. Lett., 41(8), 2842-2850, doi:10.1002/2014GL059255, 2014.

Salomon, J. G., Schaaf, C. B., Strahler, A. H., Gao, F., and Jin, Y.: Validation of the MODIS Bidirectional Reflectance Distribution Function and Albedo retrievals using combined observations from the Aqua and Terra platforms, IEEE Transactions on Geoscience and Remote Sensing, 44(6), 1555-1565, 2006.

Schaaf, C. B., Gao, F., Strahler, A. H., Lucht, W., Li, X., Tsang, T., Strugnell, N. C., Zhang, X., Jin, Y., Muller, J. P., Lewis, P., Barnsley, M., Hobson, P., Disney, M., Roberts, G., Dunderdale, M., Doll, C., d'Entremont, R. P., Hu, B., Liang, S., Privette, J. L., and Roy, D.: First operational BRDF, albedo nadir reflectance products from MODIS, Remote Sens. Environ., 83(1), 135-148, doi: 10.1016/S0034-4257(02)00091-3, 2002.

Schaaf, C. B., Wang, Z., and Strahler, A. H.: Commentary on Wang and Zender – MODIS snow albedo bias at high solar zenith angles relative to theory and in situ observations in Greenland, Remote Sens. Environ., 115(5), 1296-1300, doi: 10.1016/j.rse.2011.01.002, 2011.

Schaaf, C., and Wang, Z.: MCD43A3 MODIS/Terra+Aqua BRDF/Albedo Daily L3 Global - 500m V006. NASA EOSDIS Land Processes DAAC. dataset accessed November 2016 at doi:10.5067/MODIS/MCD43A3.006, 2015.

Sharp, M., Burgess, D. O., Cogley, J. G., Ecclestone, M., Labine, C., and Wolken, G. J.: Extreme melt on Canada's Arctic ice caps in the 21st century, Geophys. Res. Lett., 38(11), L11501, doi:10.1029/2011GL047381, 2011.

Strabala, K. I., Ackerman, S. A., and Menzel, W. P.: Cloud Properties inferred from 8-12 μm Data, J. Appl. Meteor., 33(2), 212-229, doi:10.1175/15200450(1994)033<0212:CPIFD>2.0.C;2, 1994.

Commented [m38]: Rev. 1
RC 14 Line 601: should read IEEE instead of IEE
AR 14 Reference corrected

Stroeve, J. C., Box, J., Gao, F., Liang, S., Nolin, A., and Schaaf, C.: Accuracy assessment of the MODIS 16-day albedo product for snow: Comparison with Greenland in situ measurements, Remote Sens. Environ., 94(1), 46-60, doi: 10.1016/j.rse.2004.09.001, 2005.

Stroeve, J. C., Box, J., and Haran, T.: Evaluation of the MODIS (MOD10A1) daily snow albedo product over the Greenland
910   Ice Sheet, Remote Sens. Environ., 105(2), 155-171, doi: 10.1016/j.rse.2006.06.009, 2006.

Stroeve, J., Box, J. E., Wang, Z., Schaaf, C., and Barret, A.: Re-evaluation of MODIS MCD43 Greenland albedo accuracy and trends, Remote Sens. Environ., 138, 199-214, doi: 10.1016/j.rse.2013.07.023, 2013.

Strugnell, N., and Lucht, W.: Continental-scale albedo inferred from AVHRR data, land cover class and field observations of typical BRDFs, J. Clim, 14(7), 1360-1376, doi: 10.1175/1520-0442(2001)014<1360:AATICS>2.0.CO;2, 2001.

915   Sun, J., Xiong, X., Guenther, B., and Barnes, W.: Radiometric stability monitoring of the MODIS reflective solar bands using the Moon, Metrologia, 40(1), S85, doi: 10.1088/0026-1394/40/1/319, 2003.

Sun, J., Xiong, X., Angal, A., Chen, H., Wu, A., and Geng, X.: Time-dependent response versus scan angle for MODIS reflective solar bands, IEEE Transactions on Geoscience and Remote Sensing, 52(6), 3159-3174, doi: 10.1109/TGRS.2013.2271448, 2014.

920   Tedesco, M., Doherty, S., Fettweis, X., Alexander, P., Jeyaratnam, J., and Stroeve, J.: The darkening of the Greenland ice sheet: trends, drivers, and projections (1981-2100), The Cryosphere, 10, 477-496, doi: 10.5194/tc-10-477-2016, 2016.

Toller, G., Xiong, X., Sun, J., Wenny, B. N., Geng, X., Kuyper, J., Angal, A., Chen, H., Madhavan, S., and Wu, A.: Terra and Aqua moderate-resolution imaging spectroradiometer collection 6 level 1B algorithm, J. Appl. Remote Sens., 7(1), 073557-073557, doi: 10.1117/1.JRS.7.073557, 2013.

925   van den Broeke, M. R., Smeets, C. J. P. P., and Rvan de Wal, R. S. W.: The seasonal cycle and interannual variability of surface energy balance and melt in the ablation zone of the west Greenland ice sheet, The Crysophere, 5(2), 377-390, doi: 10.5194/tc-5-377-2011, 2011.

Vermote, E. F., Kotchenova, S. Y., and Ray, J. P.: MODIS surface reflectance user's guide. MODIS Land Surface Reflectance Science Computing Facility, version 1, 2011.

930   Vincent, L. A., Zhang, X., Brown, R. D., Feng, Y., Mekis, E., Milewska, E. J., Wan, H., and Wang, X. L.: Observed trends in Canada's climate and influence of low-frequency variability modes, Journal of Climate, 28, 4545-4560, doi: 10.1175/JCLI-D-14-00697.1, 2015.

Wan, Z., Zhang, Y., Zhang, Q., and Li, Z. L.: Validation of the land-surface temperature products retrieved from Terra Moderate Resolution Spectroradiomerter data, Remote Sens. Environ., 83(1-2), 163-180, doi: 10.1016/S0034-4257(02)00093-935 7, 2002.

Wang L., Sharp, M., Rivard, B., Marshall, S., and Burgess, D.: Melt season duration on Canadian Arctic ice caps, 2000-2004, Geophys. Res. Lett., 32(19), L19502, doi: 10.1029/2005GL023962, 2005.

Wang, Z., Schaaf, C. B., Chopping, M. J., Strahler, A. H., Wang, J., Román, M. O., Rocha, A. V., Woodcock, C. E., and Shuai, Y.: Evaluation of Moderate-resolution Imaging Spectroradiometer (MODIS) snow albedo product (MCD43A) over tundra, 940 Remote Sens. Environ., 117, 264-280, doi: 10.1016/j.rse.2011.10.002, 2012.

Wanner, W., Strahler, A. H., Hu, B., Lewis, P., Muller, J. P., Li, X., Schaaf, C. L. B., and Barnsley, M. J..: Global retrieval of bidirectional reflectance and albedo over than from EOS MODIS and MISR data: theory and algorithm, J. Geophys. Res. 102(D14), 17143-17162, doi: 10.1029/96JD03295, 1997.

Warren, S. G.: Optical properties of snow, Reviews of Geophysics, 20(1), 67-89, doi:10.1029/RG020i001p00067, 1982.

945 Warren, S. G., and Wiscombe, W. J.: A model for the spectral albedo of snow. II Snow containing atmospheric aerosols, J. Atmos. Sci., 37(12), 2734-2745, doi: 10.1175/15200469(1980)037<2734: AMFTSA>2.0.CO;2, 1980.

Wenny, B. N., Sun, J., Xiong, X., Wu, A., Chen, H., Angal, A., Choi, T., Madhavan, S., Geng, X., Kuyper, J., and Tan, L.: MODIS calibration algorithm improvements developed for Collection 6 Level-1B, Proc. SPIE – Earth Observing Systems XV, 78071F, doi: 10.1117/12.860892, 2010.

950 Wiscombe, W. J., and Warren, S. G.: A model for the spectral albedo of snow. I: Pure snow, J. Atmos. Sci., 37(12), 2712-2732, doi: 10.1175.1520-0469(1980)037<2712:AMFTSA>2.0.CO;2, 1980.

Wolken, G., Sharp, M., Andreassen, L.M., Arendt, A., Burgess, D., Cogley, J.G., Copland, L., Kohler, J., O'Neel, S., Pelto, M., Thomson, L., and Wouters, B.: [Arctic] Glaciers and ice caps outside Greenland [in "State of the Climate 2015"], Bull. Am. Meteorol. Soc., 97(8), S142-S145, 2016.

955 Xiong, X., Esposito, J., Sun, J., Pan, C., Guenther, B., and Barnes, W. L.: Degradation of MODIS optics and its reflective solar bands calibration, In Proc. SPIE – Sensors, Systems, and Next-Generation Satellites V, 4540, 62-70. Doi: 10.1117/12.450646, 2001.

Xiong, X., Eriyes, H., Xiong, S., Xie, X., Esposito, J., Sun, J., and Barnes, W.: Performance of Terra MODIS solar diffuser and solar diffuser stability monitor, In Proc. SPIE - Earth Observing Systems X, 58820S doi: 10.1117/12.615334, 2005.

31

960 Xiong, X., and Barnes, W.: An overview of MODIS radiometric calibration and characterization, Advances in Atmospheric Sciences, 23(1), 69-79, doi: 10.1007/s00376-006-0008-3, 2006.

Table 1: Clear-sky BSA and LST; 1 standard deviation. Anomalies are with respect to the 2001-2016 mean.

Year	BSA mean	BSA mean anomaly*	LST mean	LST mean anomaly*
2001	0.631 ± 0.106	0.0226 ± 0.0458	-3.7 ± 2.0 -3.9 ± 1.9	-0.73 ± 0.70 -0.65 ± 0.63
2002	0.633 ± 0.124	0.0316 ± 0.0320	-3.5 ± 2.2 -3.7 ± 2.1	-0.51 ± 0.68 -0.43 ± 0.66
2003	0.627 ± 0.109	0.0292 ± 0.0329	-3.3 ± 1.9 -3.9 ± 1.8	-0.65 ± 0.51 -0.65 ± 0.49
2004	0.655 ± 0.112	0.0517 ± 0.0318	-4.0 ± 2.4 -4.2 ± 2.3	-1.07 ± 0.80 -1.00 ± 0.73
2005	0.605 ± 0.132	0.0035 ± 0.0282	-2.3 ± 1.7 -2.6 ± 1.7	0.69 ± 0.38 -0.67 ± 0.40
2006	0.608 ± 0.120	0.0030 ± 0.0282	-3.9 ± 2.5 -4.2 ± 2.3	-0.94 ± 0.88 -0.95 ± 0.80
2007	0.586 ± 0.125	-0.0167 ± 0.0282	-1.9 ± 1.6 -2.2 ± 1.6	1.06 ± 0.48 -1.00 ± 0.44
2008	0.588 ± 0.119	-0.0117 ± 0.0212	-2.4 ± 1.4 -2.7 ± 1.4	0.57 ± 0.53 -0.54 ± 0.52
2009	0.586 ± 0.115	-0.0177 ± 0.0220	-2.4 ± 1.7 -2.8 ± 1.7	0.53 ± 0.41 -0.46 ± 0.44
2010	0.601 ± 0.112	-0.0021 ± 0.0307	-2.1 ± 1.7 -2.5 ± 1.7	0.86 ± 0.51 -0.77 ± 0.49
2011	0.539 ± 0.127	-0.0651 ± 0.0326	-2.0 ± 1.3 -2.3 ± 1.3	0.93 ± 0.67 -0.90 ± 0.61
2012	0.550 ± 0.126	-0.0516 ± 0.0309	-2.1 ± 1.4 -2.4 ± 1.4	0.92 ± 0.65 -0.87 ± 0.64
2013	0.668 ± 0.086	0.0604 ± 0.0431	-5.2 ± 2.3 -5.4 ± 2.2	-2.26 ± 0.87 -2.14 ± 0.85
2014	0.614 ± 0.109	0.0153 ± 0.0245	-3.2 ± 1.9 -3.4 ± 1.8	-0.18 ± 0.50 -0.18 ± 0.50
2015	0.578 ± 0.124	-0.0223 ± 0.0248	-2.6 ± 1.7 -2.8 ± 1.7	0.37 ± 0.42 -0.37 ± 0.46
2016	0.600 ± 0.120	-0.0048 ± 0.0334	-2.5 ± 1.9 -2.8 ± 1.8	0.43 ± 0.66 -0.42 ± 0.68
2001-16*	0.599 ± 0.115	–	-3.0 ± 1.8 -3.2 ± 1.7	–

*pixels having mean summer (JJA) BSA observations in at least 11 of a possible 16 years (see Sect. 2.3)

Commented [m39]: Values revised using the C6 instead of C5 LST data.

32

Table 2: Clear-sky mean summer monthly BSA^ and BSA^ anomaly relative to the 2001-16 mean for the QEI ice cover; ± 1 standard deviation.

Year	June	July	August	June anomaly*	July anomaly*	August anomaly*
2001	0.722 ± 0.084	0.584 ± 0.127	0.597 ± 0.123	0.0359 ± 0.0502	0.0285 ± 0.0585	0.0153 ± 0.0572
2002	0.680 ± 0.108	0.615 ± 0.135	0.608 ± 0.145	-0.0005 ± 0.0424	0.0595 ± 0.0435	0.0270 ± 0.0466
2003	0.684 ± 0.085	0.561 ± 0.139	0.658 ± 0.127	0.0003 ± 0.0231	0.0029 ± 0.0340	0.0836 ± 0.0768
2004	0.714 ± 0.085	0.620 ± 0.126	0.632 ± 0.133	0.0317 ± 0.0285	0.0638 ± 0.0465	0.0501 ± 0.0472
2005	0.676 ± 0.099	0.572 ± 0.139	0.573 ± 0.143	-0.0064 ± 0.0300	0.0150 ± 0.0364	-0.0116 ± 0.0468
2006	0.712 ± 0.087	0.615 ± 0.129	0.568 ± 0.137	0.0255 ± 0.0316	0.0602 ± 0.0440	-0.0166 ± 0.0431
2007	0.692 ± 0.090	0.544 ± 0.141	0.536 ± 0.155	0.0099 ± 0.0228	-0.0143 ± 0.0339	-0.0518 ± 0.0494
2008	0.660 ± 0.104	0.533 ± 0.148	0.576 ± 0.118	-0.0220 ± 0.0298	-0.0226 ± 0.0353	-0.0050 ± 0.0345
2009	0.690 ± 0.089	0.536 ± 0.132	0.533 ± 0.142	0.0085 ± 0.0258	-0.0212 ± 0.0310	-0.0544 ± 0.0383
2010	0.668 ± 0.091	0.528 ± 0.136	0.606 ± 0.136	-0.0143 ± 0.0230	-0.0289 ± 0.0331	0.0188 ± 0.0656
2011	0.628 ± 0.101	0.480 ± 0.147	0.521 ± 0.148	-0.0557 ± 0.0347	-0.0770 ± 0.0400	-0.0657 ± 0.0517
2012	0.628 ± 0.112	0.478 ± 0.146	0.559 ± 0.137	-0.0532 ± 0.0395	-0.0805 ± 0.0399	-0.0243 ± 0.0532
2013	0.724 ± 0.072	0.640 ± 0.107	0.628 ± 0.109	0.0402 ± 0.0406	0.0843 ± 0.0517	0.0466 ± 0.0637
2014	0.698 ± 0.080	0.572 ± 0.128	0.584 ± 0.136	0.0167 ± 0.0277	0.0148 ± 0.0335	0.0026 ± 0.0495
2015	0.677 ± 0.103	0.490 ± 0.143	0.587 ± 0.147	-0.0033 ± 0.0282	-0.0675 ± 0.0400	0.0026 ± 0.0457
2016	0.675 ± 0.089	0.545 ± 0.146	0.589 ± 0.146	-0.0066 ± 0.0280	-0.0146 ± 0.0354	0.0049 ± 0.0652
2001-2016*	0.680 ± 0.089	0.551 ± 0.131	0.579 ± 0.127	−	−	−

970 ^average of all pixels in each region having at least 11 (10 for June) of a possible 31 (30 for June) observations.

*pixels having June BSA observations in at least 11 of a possible 16 years.

Table 3: 2001–2016 BSA and LST change for glaciated regions of the QEI (Fig. 1); ± 1 standard deviation.

Year	QEI	Agassiz IC	Axel Heiberg I	Devon I & Coburg I	Manson IF	Meighen IC	Northwest Ellesmere I	Prince of Wales IF	Sydkap IC
JJA Mean BSA (yr⁻¹)	-0.0029 ± 0.0025	-0.0021 ± 0.0022	-0.0041 ± 0.0031	-0.0034 ± 0.0021	-0.0043 ± 0.0026	-0.0055 ± 0.0025	-0.0024 ± 0.0025	-0.0028 ± 0.0021	-0.0036 ± 0.0030
June Mean BSA (yr⁻¹)	-0.0017 ± 0.0024	-0.002 ± 0.0023	-0.0027 ± 0.0027	-0.0019 ± 0.0016	-0.0017 ± 0.0028	-0.0046 ± 0.0017	-0.0011 ± 0.0026	-0.0020 ± 0.0024	-0.0028 ± 0.0022
July Mean BSA (yr⁻¹)	-0.0050 ± 0.0031	-0.0044 ± 0.0026	-0.0077 ± 0.0035	-0.0040 ± 0.0024	-0.0054 ± 0.0028	-0.0081 ± 0.0027	-0.0048 ± 0.0032	-0.0049 ± 0.0028	-0.0064 ± 0.0031
August Mean BSA (yr⁻¹)	-0.0022 ± 0.0036	-0.0010 ± 0.0027	-0.0024 ± 0.0039	-0.0043 ± 0.0036	-0.0057 ± 0.0043	-0.0050 ± 0.0041	-0.0014 ± 0.0032	-0.0016 ± 0.0030	-0.0018 ± 0.0049
JJA LST (°C yr⁻¹)	0.05 ± 0.04	0.05 ± 0.03	0.07 ± 0.04	0.04 ± 0.03	0.02 ± 0.02	0.07 ± 0.06	0.06 ± 0.03	0.04 ± 0.03	0.04 ± 0.03

Table 3: QEI-wide (regionally-averaged) BSA and LST change for the period 2001-16; ± 1 standard deviation.

JJA Mean BSA (yr⁻¹)	June Mean BSA (yr⁻¹)	July Mean BSA (yr⁻¹)	August Mean BSA (yr⁻¹)	JJA LST (°C yr⁻¹)
-0.0029 ± 0.0025	-0.0017 ± 0.0024	-0.0050 ± 0.0031	-0.0022 ± 0.0036	+0.049 ± 0.038

Commented [m40]: Table revised because regions no long[er] referenced in text.

Figure 1: Glaciated regions of the Queen Elizabeth Islands~~, . Arctic Canada.~~ Base Image: Moderate Resolution Imaging Spectroradiometer, 4 July 2011. ~~Top-right I~~nset: red polygon shows location of Queen Elizabeth Islands, Arctic Canada. ~~Bottom-left inset: the eight regions used in this study.~~

1000

Figure 2: Mean summer clear-sky shortwave broadband black-sky albedo ~~for~~ over **the QEI** ice caps**. White areas outside of the ice caps indicate non-glaciated ice cover.**

1005

Figure 3: Mean summer clear-sky shortwave broadband albedo anomaly ~~for~~ over the QEI ice caps relative to the 2001-~~20~~16 mean. White areas outside of the ice caps indicate non-glaciated ice cover.

NCEP/NCAR Reanalysis 500 hPa geopotential heigh anomaly(m) relative to 1981-2010

(a)

(b)

2001-2004 composite 500 hPa height anomaly (m)

20 15 10 5 0 -5 -10 -15 -20

2007-2012 composite 500 hPa height anomaly (m)

65 55 40 25 10 -10 -25 -40 -50 -70

NCEP/NCAR Reanalysis 500 hPa geopotential heigh anolamy (m) relative to 1981-2010

(a)

(b)

2001-2004 composite 500 hPa height anomlay (m)

20 15 10 5 0 -5 -10 -15 -20

2007-2012 composite 500 hPa height anomaly (m)

65 55 40 25 10 -10 -25 -40 -50 -70

Figure 4: Mean summer (JJA) composite NCEP/NCAR Reanalysis 500 hPa geopotential height anomaly for (a) a period of large negative BSA anomalies (2001-2004) and (b) a period of large positive BSA anomalies (2007-2012). Source: https://www.esrl.noaa.gov/psd.

Commented [m44]: Rev. 2
RC 33: Figure 4 – Figure text, misspelled word 'anomaly' in two locations, please correct.
AR 33: Figure 4 correct for two erroneous spellings of 'anomaly'

Figure 5: Linear rate of change (yr⁻¹) in (a) mean summer (JJA), (b) June, (c) July, and (b) August, clear-sky shortwave broadband black-sky albedo for 2001-~~2016~~16 ~~for~~ over the QEI ice caps. Background image: MODIS 4 July 2011~~,~~. ~~b~~Brown indicates non-glaciated land cover.

1020

Figure 6: p-value of the linear regression (Fig.4) of (a) mean summer (JJA), (b) June, (c) July, and (~~bd~~) August, clear-sky shortwave broadband black-sky albedo for the period 2001-~~20~~16 ~~for~~ over the QEI ice caps. Background image: MODIS 4 July 2011~~.,~~ ~~b~~Brown indicates non-glaciated land cover.

1025

Figure 7: QEI (a) 16 year average mean summer land surface temperature (°C) and (b) linear rate of change of mean summer LST (°C yr⁻¹) for the period 2001-16 over the QEI ice caps. Background image: MODIS 4 July 2011., bBrown indicates non-glaciated land cover.

Figure 78: Component scores for the first two Principal Components of the mean summer clear-sky BSA (Fig. 2) ~~for~~ over the QEI ice caps. Background image: MODIS 4 July 2011~~.,~~ ~~Bb~~rown indicates non-glaciated land cover.

1035

Figure 89: (a) mean summer (JJA) clear-sky shortwave broadband black-sky albedo (left-hand axis) and the mean summer (JJA) NAO index (right-hand axis) for 2001-2016. (b) Empirical Orthogonal Functions (EOF) for the First and Second Principal Components of the 16 year mean summer BSA record (left-hand axis), and the mean summer (JJA) NAO index (right-hand axis) for 2011-2016 (Sect. 3.4).

Figure 910: (a) Pearson Correlation Coefficient (r) and (b) p-value for linear regression of the 16 year BSA and LST record. ~~Black box shows location of Cadogan Inlet (Sect. 4.2).~~ Background image: MODIS 4 July 2011~~.~~, ~~Bb~~rown indicates non-glaciated land cover.